MICROCOPY RESOLUTION TEST CHART
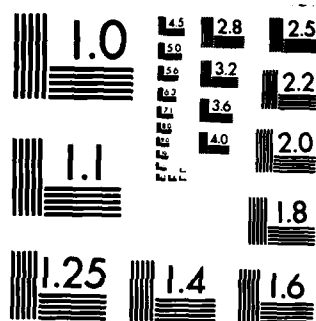NATIONAL BUREAU OF STANDARDS-1963-A

NAVAL POSTGRADUATE SCHOOL
Monterey, California

THESIS

FILM CONDENSATION OF STEAM ON
EXTERNALLY FINNED HORIZONTAL TUBES

by

Frederick A. Flook

March 1985

Thesis Advisor: P. J. Marto

85 06 17 097

NAVAL POSTGRADUATE SCHOOL
Monterey, California

Commodore Robert H. Shumaker   David A. Schrady
Superintendent   Provost

Reproduction of all or part of this report is authorized.

Released as a
Technical Report by:

John N. Dyer
Dean of Science and
Engineering

REPORT DOCUMENTATION PAGE		READ INSTRUCTIONS BEFORE COMPLETING FORM
1. REPORT NUMBER NPS 69-85-002	2. GOVT ACCESSION NO. A155642	3. RECIPIENT'S CATALOG NUMBER
4. TITLE *(and Subtitle)* Film Condensation of Steam on Externally Finned Horizontal Tubes		5. TYPE OF REPORT & PERIOD COVERED Master's Thesis March 1985
		6. PERFORMING ORG. REPORT NUMBER
7. AUTHOR*(s)* Frederick A. Flook		8. CONTRACT OR GRANT NUMBER*(s)* Agreement No. MEA82-03567
9. PERFORMING ORGANIZATION NAME AND ADDRESS Naval Postgraduate School Monterey, California 93943		10. PROGRAM ELEMENT, PROJECT, TASK AREA & WORK UNIT NUMBERS
11. CONTROLLING OFFICE NAME AND ADDRESS Naval Postgraduate School Monterey, California 93943		12. REPORT DATE March 1985
		13. NUMBER OF PAGES 146
14. MONITORING AGENCY NAME & ADDRESS*(If different from Controlling Office)* National Science Foundation Washington, DC 20550		15. SECURITY CLASS. *(of this report)* Unclassified
		15a. DECLASSIFICATION/DOWNGRADING SCHEDULE

16. DISTRIBUTION STATEMENT *(of this Report)*

Approved for public release; distribution unlimited

17. DISTRIBUTION STATEMENT *(of the abstract entered in Block 20, if different from Report)*

18. SUPPLEMENTARY NOTES

19. KEY WORDS *(Continue on reverse side if necessary and identify by block number)*

Steam, Condensation, Filmwise, Tube, External Fin,
Heat-Transfer Coefficient, Enhancement

20. ABSTRACT *(Continue on reverse side if necessary and identify by block number)*

Filmwise condensation measurements of steam were made on horizontal finned tubes under vacuum and near-atmospheric conditions. Data were obtained for copper tubes with fins of rectangular, triangular, trapezoidal, and parabolic cross sections, and for a commercially-available finned tube. A stainless steel finned tube was also tested to investigate the effect of thermal conductivity.

#20 - ABSTRACT - (CONTINUED)

Maximum enhancements of about 4.8 were obtained under vacuum conditions, and about 6.9 at atmospheric pressure, compared to a smooth tube having an outside diameter equal to the root diameter of the finned tubes. The optimum fin spacing was found to be about 2.0 mm for rectangularly-shaped fins with a fin thickness of 1.0 mm, and a fin height of 0.5 and 1.5 mm. Fins with a parabolic shape were shown to perform better than fins of rectangular shape, and fins were shown to degrade the performance of stainless steel tubes. The effects of vapor shear were shown to have only a small influence on the steam-side heat-transfer coefficient. A theoretical model proposed by Webb et al. [25] was found to underpredict the experimental data. Several suggestions to modify this model are described.

Film Condensation of Steam on
Externally Finned Horizontal Tubes

by

Frederick A. Flook
Lieutenant, United States Navy
B.S.M.E., Colorado State University, 1977

Submitted in partial fulfillment of the
requirements for the degree of

MASTER OF SCIENCE IN MECHANICAL ENGINEERING

from the

NAVAL POSTGRADUATE SCHOOL
March 1985

Author: _____
Frederick A. Flook

Approved by: _____
P. J. Marto, Thesis Advisor

_____
A. S. Wanhiarachchi, Co-Advisor

_____
Paul J. Marto, Chairman,
Department of Mechanical Engineering

_____
John N. Dyer,
Dean of Science and Engineering

3

ABSTRACT

Filmwise condensation measurements of steam were made on
horizontal finned tubes under vacuum and near-atmospheric
conditions. Data were obtained for copper tubes with fins
of rectangular, triangular, trapezoidal, and parabolic cross
sections, and for a commercially-available finned tube. A
stainless steel finned tube was also tested to investigate
the effect of thermal conductivity.

Maximum enhancements of about 4.8 were obtained under
vacuum conditions, and about 6.9 at atmospheric pressure,
compared to a smooth tube having an outside diameter equal
to the root diameter of the finned tubes. The optimum fin
spacing was found to be about 2.0 mm for rectangularly
shaped-fins with a fin thickness of 1.0 mm, and fin height
of 0.5 and 1.5 mm. Fins with a parabolic shape were shown
to perform better than fins of rectangular shape, and fins
were shown to degrade the performance of stainless steel
tubes. The effects of vapor shear were shown to have only a
small influence on the steam-side heat-transfer coefficient.
A theoretical model proposed by Webb et al. [25] was found
to underpredict the experimental data. Several suggestions
to modify this model are described.

4

TABLE OF CONTENTS

5

6

LIST OF TABLES

LIST OF FIGURES

9

NOMENCLATURE

a	– Experimentally Determined Constant
A_{bt}	– Surface Area of Tube Between Fins
A_{eff}	– Effective Area of a Finned Tube
A_f	– Total Surface Area of a Finned Tube
A_{ft}	– Fin Surface Area
A_i	– Water-Side Tube Surface Area
A_o	– Surface Area of a Smooth Tube
A_p	– Profile Area of Fin Over Fin Cross Section
A_{sf}	– Smooth Tube Area Based on the Fin Diameter
b	– Experimentally Determined Constant
B	– Constant Used in the Sieder-Tate-Type Equation
c	– Experimentally Determined Constant
C	– Leading Coefficient for the Sieder-Tate-Type Equation
C_1	– Constant of Proportionality
d	– Experimentally Determined Constant
D_e	– Equivalent Tube Diameter
D_f	– Fin Diameter
D_i	– Inside Tube Diameter
D_o	– Root Diameter of Finned Tube (Between Fins)
D_w	– Wire Diameter

10

e	— Fin Height
F	— Property Function
g	— Acceleration of Gravity
G	— Condensate Flow Rate
G_f	— Rate of Condensate Formation
$\bar{h}$	— Steam-Side Heat-Transfer Coefficient
h_b	— Steam-Side Heat-Transfer Coefficient Through the Flooded Tube Surface (Webb et al. Model)
h_{BK}	— Beatty and Katz Steam-Side Heat-Transfer Coefficient
h_f	— Steam-Side Heat-Transfer Coefficient for the Fin Surface (Webb et al. Model)
h_{fg}	— Specific Enthalpy of Vaporization
h_i	— Water-Side Heat-Transfer Coefficient
h_ℓ	— Steam-Side Heat-Transfer Coefficient for the Lower (Flooded) Tube Surface (Owen et al. Model)
h_{oe}	— Experimentally Determined Steam-Side Heat-Transfer Coefficient
h_{ow}	— Average Steam-Side Heat-Transfer Coefficient Predicted by the Webb et al. Model
h_r	— Steam-Side Heat-Transfer Coefficient for the Unflooded Tube Area Between Fins (Webb et al. Model)
h_u	— Steam-Side Heat-Transfer Coefficient for the Upper (Unflooded) Portion of the Tube (Owen et al. Model)

11

k_{eff}	– Effective Thermal Conductivity
k_f	– Thermal Conductivity of Condensate
k_m	– Thermal Conductivity of Tube/Fin Metal
$\dot{m}$, $\dot{m}_r$	– Condensation Rate
Nu	– Nusselt Number
P_A, P_B, P_C	– Pressure at Points A, B, and C in Figure 2.1
ΔP_{AB}, ΔP_{CB}	– Pressure Difference Between Points A and B, and Between Points C and B in Figure 2.1
P_{ℓ}	– Wetted Perimeter of Fin Cross Section
Pr	– Prandtl Number
P_v	– Vapor Pressure
q	– Heat Flux
Q	– Total Heat-Transfer Rate
r	– Radius of Curvature
r_1, r_2	– Arbitrary Radius of Curvature
r_A, r_B, r_C	– Radius of Curvature of the Condensate Film at Points A, B, and C in Figure 2.1
Re	– Reynolds Number
Re_f	– Film Reynolds Number
Re_{tp}	– Two-Phase Reynolds Number
R_w	– Wall Thermal Resistance
s	– Fin Spacing
S_m	– Length of Convex Surface of Fin Condensate Film

t	— Fin Thickness
t_b	— Fin Base Thickness
t_t	— Fin Tip Thickness
ΔT	— Vapor-Side Temperature Drop
U_o	— Overall Heat-Transfer Coefficient Based on A
V_s	— Steam Velocity
z	— Axial Coordinate
Z	— Dimensionless Depth of Condensate Between Fins
α	— Fin Semivertex Angle
β	— Coefficient to be Determined by Iteration
δ_r	— Average Condensate Film Thickness
ϕ	— Ratio of Tube Side Heat Flux with Fins to Tube Side Heat Flux with Fins of Zero Thickness
Φ	— Condensation Efficiency
θ_m	— Rotation Angle of Normal to Condensate Film Surface
ξ	— A Measure of the Fin Aspect Ratio
η	— Fin Efficiency
η_o	— Overall Efficiency
ψ	— Condensate Retention Angle
ρ_f	— Density of Condensate
ρ_v	— Density of Vapor
σ	— Surface Tension of Condensate
μ_c	— Viscosity of Cooling Water at Bulk Temperature

μ_f - Viscosity of Condensate at Film Temperature

μ_w - Viscosity of Cooling Water at Inner Wall Temperature

ACKNOWLEDGEMENTS

The author would like to take this opportunity to thank his advisor, Professor P. J. Marto for his support and guidance throughout this thesis effort.

Special thanks are extended to Dr. A. S. Wanniarachchi without whose patience, expertise, and guidance, this paper would not be possible.

The author would also like to thank Mr. Tom McCord and his machine shop crew for their timely and professional support.

I. INTRODUCTION

A. BACKGROUND

As costs for material and energy continue to rise, the need for smaller, more efficient heat exchangers continues to grow. For those applications involving marine vehicles, size and weight limitations dictate the use of small, highly-efficient heat exchangers. Reducing the size and weight of steam condensers used aboard U. S. Navy ships for propulsion and electrical power generation would result in lower material costs, and help to aleviate the cramped conditions so typical of machinery spaces. Thus, there is a strong motivation for continued study in this area.

The effectiveness of condensers is limited by the water-side, vapor-side, and wall thermal resistances of the condenser tubes. Reducing any one of these will contribute to increased heat-transfer performance, and smaller physical size of condensers. Methods of enhancing the vapor-side coefficient include the use of "roped" tubes, fluted tubes, drainage strips attached on the tubes, finned tubes, and coatings applied to enhance dropwise condensation. This thesis concentrates soley on finned tubes.

Since the late 1940s, externally-finned tubes have been used to increase the vapor-side heat-transfer coefficient of tubes used in refrigeration systems; but condensers used in steam systems, such as shipboard propulsion plants, continue to use smooth tubes. The high surface tension of water, which leads to its tendency to flood the area between fins, has resulted in a widely-held belief that such tubes are inappropriate for use in steam systems. Recent studies [1,2], however, have shown that finned tubes can significantly enhance the heat-transfer rates in such systems.

16

The theoretical treatment of condensation on finned tubes is extremely complex due to the large number of variables and physical mechanisms involved. The interaction of gravitational and surface-tension forces lead to complex three-dimensional flow patterns, which are further dependent on fin spacing, height, and thickness. Other variables include heat flux, vapor shear, tube diameter, fin shape and fluid properties just to name a few. In view of the above, any theoretical models will require numerous simplifying assumptions, and require complex computer solutions involving implicit numerical techniques [3]. To confirm the validity of theoretical models, reliable experimental data which cover a wide range of relevant parameters must be obtained. The availability of such data may then lead to the development of fairly simple experimental correlations, which could be used in the design stage to predict the heat-transfer performance of finned tubes.

This thesis effort is a continuation of research being conducted at the Naval Postgraduate School (NPS) under a grant from the National Science Foundation. The basic test apparatus used to collect experimental data was built by Krohn [4]. Graber [5] provided the majority of instrumentation, and took preliminary data as the system experienced problems with non-condensing gases and partial dropwise condensation on copper tubes. Poole [6] made further improvements on the apparatus as well as on the instrumentation and, most importantly, assured a leak-free apparatus. Unfortunately, he did not have sufficient time to produce useful data, mostly due to the considerable time spent in systematically locating and fixing leaks, and due to the partial dropwise condensation problem that had not been solved. Using this system, Georgiadis [7] was finally able to obtain complete filmwise condensation on copper tubes. He took data on a number of finned tubes with fins of

rectangular shape, as well as on smooth tubes. The repeatability of data obtained by Georgiadis demonstrated the accuracy of the test apparatus and associated instrumentation which was used essentially without modification for this investigation.

The overall objectives of the present program at NPS includes the testing of: (a) tubes with rectangularly-shaped fins to find the best fin spacing, thickness, and height, (b) tubes with various fin shapes to find the best geometry that will maximize heat transfer, (c) tubes with different tube-metal thermal conductivity, and (d) the effect of vapor shear on finned tubes. Georgiadis [7] tested a total of 25 tubes, which were divided into five fin spacings (0.5, 1.0, 1.5, 2.0 and 4.0 mm), five fin thicknesses (0.5, 0.75, 1.0, 1.25, and 1.5 mm), and two fin heights (1.0 and 2.0 mm). At the conclusion of Georgiadis' test program, eight new tubes with fin heights of 0.5 and 1.5 mm, fin spacings of 1.0, 1.5, 2.0, and 4.0 mm, and a fin thickness of 1.0 mm, remained to be tested to complete the sequence of tubes with rectangularly-shaped fins. The testing of these tubes and additional tubes toward objectives (b), (c), and (d) were the primary goals of this thesis effort as listed in the next section.

B. OBJECTIVES

The main objectives of this thesis are as follow:

1. Take data on tubes with rectangularly-shaped fins of various fin spacings and fin heights to augment previous data [7],

2. Take data on tubes with fins of different shapes (triangular, trapezoidal, parabolic, etc.),

3. Take data on commercially-available finned tubes,

18

4. Take data on the "optimum," rectangularly-shaped finned tube at different vapor velocities,

5. Take data on a stainless steel tube with "optimum," rectangularly-shaped fins, and

6. Develop a preliminary correlation based on data for tubes with rectangularly-shaped fins.

II. THEORETICAL TREATMENT OF CONDENSATION ON HORIZONTAL FINNED TUBES

A. FILM CONDENSATION

When filmwise condensation of a vapor takes place on smooth tubes, a thin layer of condensate is formed which thickens with increasing distance around the perimeter of the tube. This condensate layer creates a thermal resistance, which can limit the heat-transfer performance of the tube. This film thickness and its thermal resistance can be reduced by the use of external, radial fins which, in addition to a surface area increase, promote surface-tension effects.

In 1984, Yau et al. [1] measured the enhancement provided by copper finned tubes over smooth tubes for film-wise condensation of steam. Similar experiments by Wanniarachchi et al. [2] also in 1984 confirmed that the observed enhancements were greater than could be explained by the increased surface area alone. This additional enhancement may be a result of the surface-tension forces which act to thin the condensate film. Figure 2.1 schematically depicts this phenomenon.

The effect of surface tension on pressure at the interface between a liquid and vapor is inversely proportional to the radius of curvature of the interface. If a surface has two radii of curvature at right angles (i.e., r_1 and r_2), it can be shown that:

$$\Delta P = \sigma \left[\frac{1}{r_1} + \frac{1}{r_2} \right] \tag{2.1}$$

20

where

σ = surface tension of condensate, and

ΔP = the pressure difference.
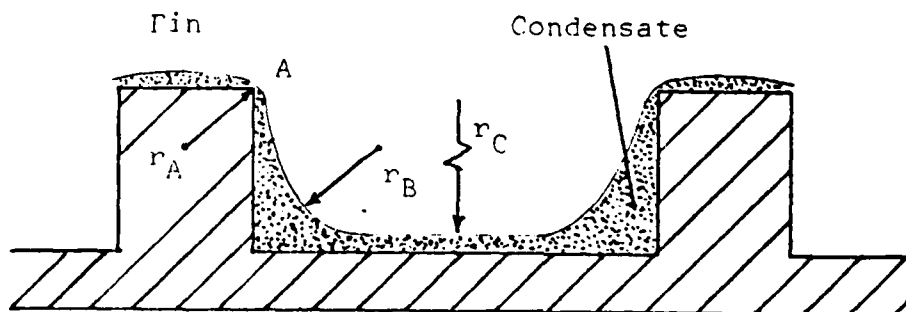
Figure 2.1   Schematic of Condensate Profile at Upper Tube Surface.

For the case of a finned tube, the radius of curvature around the outer fin perimeter is very large compared to the radius of curvature around the fin cross-section profile (Figure 2.1). Referring back to equation (2.1), it can be seen that the smaller radius of curvature term will dominate, so surface-tension effects around the fin perimeter may be neglected.

Because of the convex shape of the condensate film at point A, the pressure within the film at this point is greater than the surrounding vapor pressure. In a similar manner, the pressure at point B is less than the surrounding vapor pressure owing to the concave shape of the condensate

21

film. The relatively flat shape of the condensate film at point C leads to a pressure essentially equal to the surrounding vapor pressure. These pressures are given by:

$$P_A = P_v + \frac{\sigma}{r_A} \qquad (2.2)$$

$$P_B = P_v - \frac{\sigma}{r_B} \qquad (2.3)$$

$$P_C = P_v \qquad (2.4)$$

where

P_v = surrounding vapor pressure,

P_A, P_B, P_C = liquid pressure at points A, B, and C, and

r_A, r_B, r_C = radius of curvature of the condensate film at points A, B, and C.

At point B, the radius of curvature is small, so the pressure at point B is less than the pressure at point C. Further, from equations (2.2) and (2.3), the pressure at point A is greater than at point B. In reality, the pressure gradient within the condensate film varies along the height of the fin due to the continuously varying radius of curvature from the fin tip down to the base [3]; however, to simplify the treatment of condensate flow toward the fin base, the pressure differences between points A and B and points C and B may be simply written as:

22

$$\Delta P_{AB} = \sigma \left[\frac{1}{r_B} + \frac{1}{r_A} \right] \qquad\qquad (2.5)$$

$$\Delta P_{CB} = \frac{\sigma}{r_B} \qquad\qquad (2.6)$$

where

ΔP_{AB}, ΔP_{CB} = pressure difference between points A and B, and points C and B.

As can be seen, these pressure differences are positive, resulting in condensate flow toward point B. Due to the relatively large mass of condensate at point B, gravitational forces dominate over surface-tension forces causing a flow of condensate around the tube perimeter at the fin base. In this manner, a condensate run-off channel is formed at point B, and the improved drainage of condensate thins the film between fins and on the fin surface. This thinning, in turn, reduces the thermal resistance through the condensate film, thus producing an enhancement in addition to the gain in surface area.

It should be stressed at this point that the shape of the condensate film is highly dependent on the fin geometry. Clearly, then, the fin shape must be taken into consideration in order to maximize the beneficial effects of surface tension.

The above gains may be partially or totally offset, however, by the tendency of condensate to flood the area between fins, especially on the lower part of the tubes.

23

The extent to which the film floods the tube is defined by the condensate retention angle (ψ), as shown in Figure 2.2. In the flooded portion of the tube, the relatively thick condensate film increases the thermal resistance, thereby leading to a degradation in the heat-transfer performance. The condensate retention angle is highly dependent on fin spacing, so very closely-spaced fins may lead to completely flooded tubes.

A number of studies have been conducted to investigate the performance of finned tubes, and these are presented in the next section.

B. CONDENSATE RETENTION

In 1946, the first measurements of condensate retention were made by Katz et al. [8]. These measurements were made under static conditions (i.e., no condensation taking place), using water, aniline, acetone, and carbon tetrachloride on a number of tubes with different fin densities (276 to 984 fins/m), and fin heights (1.2 to 5.7 mm). It was shown that as much as 100% of the tube surface could be flooded by retained condensate, depending mainly on the ratio of surface tension to liquid density and on the fin spacing.

Eight years later, Gregorig [9] recognized that surface-tension effects could play an important role on a vertical, fluted surface which uses a minimum radius of curvature at the flute tip, which gradually increases toward the trough. As discussed in section A above, this variable radius of curvature results in a condensate film pressure that decreases toward the trough. In this manner, the condensate layer on the convex region of the flute is thinned significantly, thus pushing the condensate into the troughs (Figure 2.3) where gravitational forces result in enhanced drainage.

24
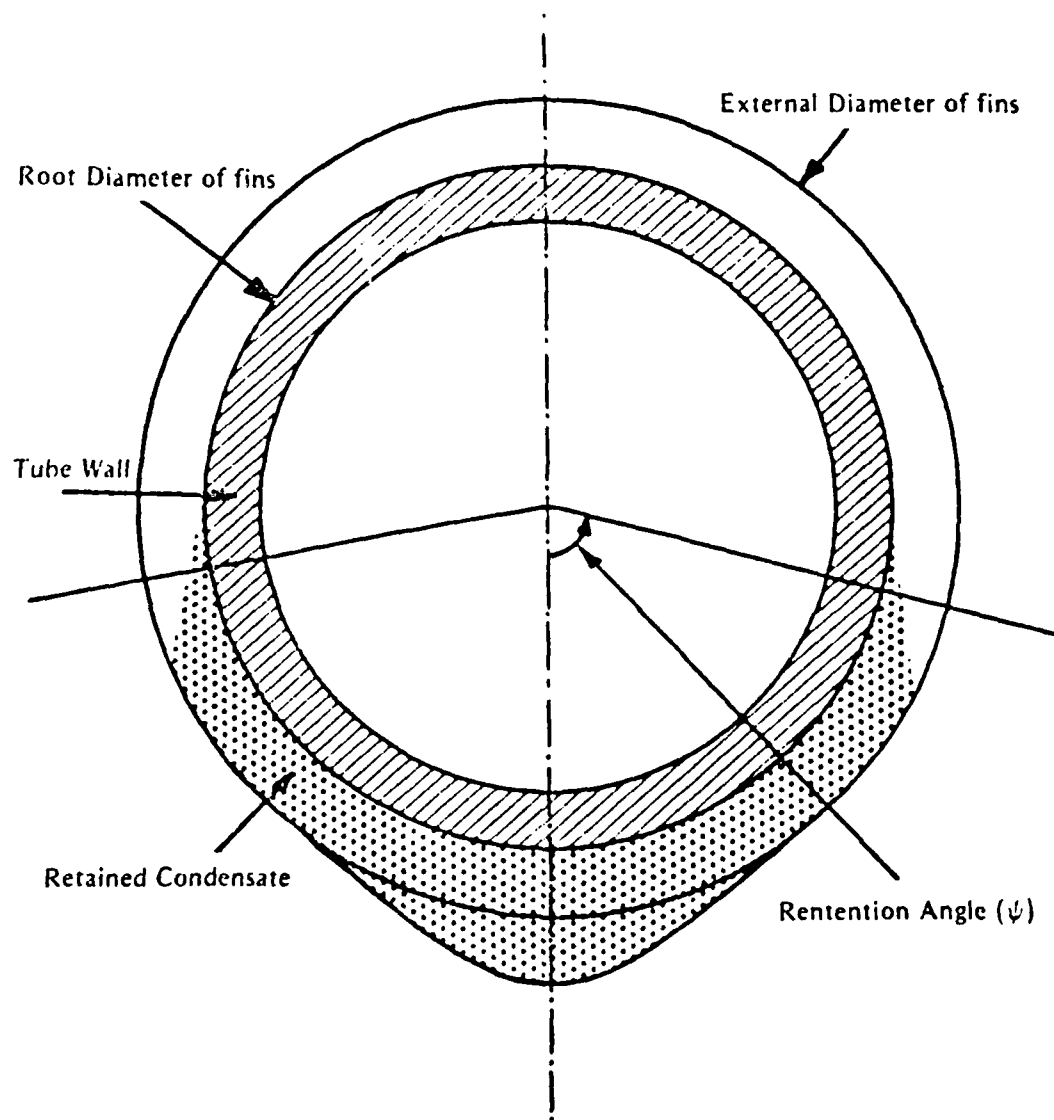
Figure 2.2   Schematic of Condensate Retention
on Finned Tubes.

25

Since the heat-transfer coefficient is inversely proportional to the thickness of the condensate layer, heat-transfer performance at the trough is degraded, but to a lesser degree than the enhancement experienced by the crest. The resulting average heat-transfer coefficient, therefore, shows a significant enhancement.
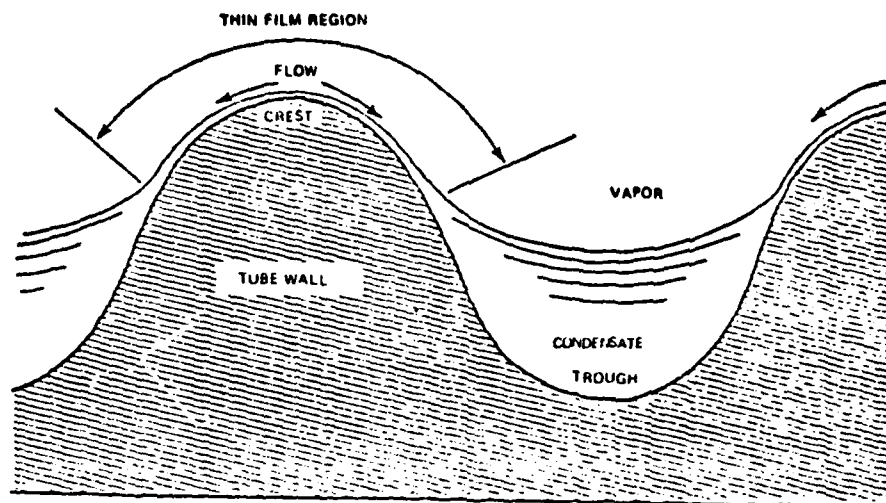
Figure 2.3   Cross Section of the Gregorig Surface

In 1981, Rudy and Webb [10] made measurements of condensate retention angles on finned tubes with three different fin densities (748, 1024, 1378 fins/meter) using water, R-11, and n-pentane as the working fluid.   Later, in 1983, Rudy and Webb [11] developed an analytical model to predict the fraction of tube surface that is flooded during condensation on a horizontal, integral-fin tube.   They found that the vertical-rise height of condensate on a finned tube was the same as that obtained on a vertically oriented, flat finned plate that was obtained by splitting and unrolling an identical finned tube.   Based on this observation, they used capillary equations that predict the liquid rise on a vertical U-shaped channel, and assuming negligible vapor shear, they predicted the condensate retention angle to be:

26

$$\psi = \cos^{-1}\left[1 - \frac{2\,\sigma\,(2\,e - t)}{\rho_f\,g\,s\,D_o}\right] \qquad (2.7)$$

where

  e = fin height,

  t = fin thickness,

  ρ_f = density of condensate,

  g = acceleration of gravity,

  s = fin spacing, and

  D_o = root diameter of tube.

This result shows that the condensate retention angle increases both with increasing fin density, and with increasing surface tension-to-density ratio. It should be kept in mind, however, that the model was based on a vertical surface, so it should only be used for angles less than about 30 degrees. For angles below this, experimental results involving the use of water, R-11, R-12, ammonia, and n-pentane were predicted to within 10 percent. It is worth mentioning that equation (2.7) had been derived in 1982, according to Russian literature, by Rifert [12].

Like Rudy and Webb [10], Owen et al. [13] also recognized the need to consider condensate retention while analyzing finned tubes. In order to correct for this, an assumption was made that the condensate retention angle was independent of condensation rate, so a static analysis was performed. A simple force balance between surface tension

27

and gravitational forces resulted in an equation for the condensate retention angle as shown below:

$$\psi = \cos^{-1}\left[1 - \frac{4\sigma}{\rho \ell\, g\, s\, D_f}\right] \qquad (2.8)$$

where

D_f = overall diameter of fins.

This equation is the same as equation (2.7), except that equation (2.8) is independent of fin thickness (t).

In 1983, Honda et al. [3] performed a theoretical analysis to determine the condensate retention angle. Using an iterative numerical scheme, they found the solution to agree with equation (2.8) obtained earlier by Owen et al.. Using data of their own, Honda et al. verified a close agreement between the predicted and experimental values of the condensate retention angle.

Yau et al. [1] conducted experiments to determine the effects of removing retained condensate from finned tubes by installing thin metal drainage strips attached edgewise to the bottom tube surface. Experiments were conducted where the vapor velocity and fin pitch were varied on finned tubes with and without drainage strips. They showed a significant reduction in the in the condensate retention angle when the finned tubes were fitted with drainage strips. Condensate retention angles for condensation of steam, ethylene glycol, and R-113 on finned tubes with drainage strips were found to fit the empirical relation listed below to within ± 10 percent:

28

$$\psi = \cos^{-1}\left[1 - \frac{1.66\ \sigma}{\rho_f\ g\ s\ D_f}\right] \qquad (2.9)$$

In 1985, Rudy and Webb [14] expanded their 1983 model in order to predict the condensate retention angle for horizontal finned tubes with fins of arbitrary shape. As before, their model was based on capillary equations that predict the amount of liquid rise, and negligible vapor shear. The resulting equation for the condensate retention angle is given by:

$$\psi = \cos^{-1}\left[1 - \frac{2\ \sigma\ (P_\ell - t_b)}{D_o\ \rho_f\ g\ [(t_b + s)\ e - A_p]}\right] \qquad (2.10)$$

where

P_ℓ = wetted perimeter of fin cross section,

t_b = fin base thickness, and

A_p = profile area of fin over fin cross section.

In order to test the validity of equation (2.10), it was compared to experimental data for horizontal finned tubes with fins of primarily trapezoidal cross section, and fin densities ranging from 630 to 1614 fins/m. Steam, R-11, and n-pentane were used as the condensing fluids. Equation (2.10) was shown to predict the experimental data to within ± 10 percent. Note that equation (2.10) reduces to equation (2.8) for fins of rectangular cross section.

C. THEORETICAL MODELS

In 1947, Beatty and Katz [15] performed a number of experiments where various refrigerants were condensed on single finned tubes. To predict the film coefficients, they started with the Nusselt equations for condensation on a horizontal tube and on a vertical plate, and with the respective proportions of horizontal tube area (between fins) and vertical fin area, they calculated the total heat transfer rate. From this, an average heat-transfer coefficient was obtained based on an equivalent tube diameter. Their final expression is simply the Nusselt equation for a smooth horizontal tube, but with the tube diameter replaced with the equivalent tube diameter. The leading coefficient was modified to fit their experimental data as shown below:

$$\overline{h} = 0.689 \left[\frac{k_f^3 \, \rho_f \, (\rho_f - \rho_v) \, g \, h_{fg}}{\mu_f \, \Delta T} \right]^{1/4} \left[\frac{1}{D_e} \right]^{1/4} \qquad (2.11)$$

$$\left[\frac{1}{D_e} \right]^{1/4} = \frac{A_o}{A_{eff}} \left[\frac{1}{D_o} \right]^{1/4} + 1.3 \, \frac{n \, A_f}{A_{eff}} \left[\frac{1}{x} \right]^{1/4} \qquad (2.12)$$

$$A_{eff} = A_s + n \, A_f \qquad (2.13)$$

$$x = \frac{\pi \, (D_f^2 - D_o^2)}{4 \, D_f} \qquad (2.14)$$

where

A_o = surface area of smooth tube,

$\overline{h}$ = average vapor-side heat-transfer coefficient,

30

k_f = thermal conductivity of condensate,

ρ_v = density of vapor,

h_{fg} = specific enthalpy of vaporization,

μ_f = viscosity of condensate,

ΔT = vapor-side temperature drop,

D_e = equivalent tube diameter,

η = fin efficiency,

A_s = surface area of smooth tube,

A_f = total surface area of finned tube, and

A_{eff} = effective area of finned tube.

Accuracy of this equation was claimed to be better than 11 percent for a wide variety of nonaqueous fluids.   It should be noted, however,   that this model ignores the effect of surface-tension forces;   so,   it is valid only for low-surface-tension fluids such as refrigerants.

Analytical and experimental studies of condensation on horizontal tubes with trapezoidally-shaped fins were performed by Zozulya, Karkhu,   and Borovkov [16,17] some years later in the 1970s.   Their experiments confirmed the need to consider surface-tension forces in addition to gravitational forces when developing mathematical models. The analytical solutions were based on the following assumptions: 1) the thin condensate film on the fins was treated as a laminar boundary layer with a pressure gradient along the fin profile caused by surface-tension forces;   2) the effect of gravitational and inertial forces on the motion of the film along the side surfaces of the fins into the

condensate-filled trough was neglected; 3) the motion of condensate in the trough area is laminar and produced by gravity; and 4) no condensation takes place on the flooded portion of the tube. Differential equations were obtained for the height of condensate between fin bases, and temperature distribution along the fin height. With the aid of a computer, solutions for these equations were obtained using numerical methods, leading to the expressions below:

$$\overline{h} = \frac{G \; h_{fg}}{F_S \; \Delta T} \tag{2.15}$$

$$F_S = \left[\frac{s}{2} + h + \frac{e}{\cos(\alpha)} \right] \frac{\pi \, D_o}{2} \tag{2.16}$$

$$G = \frac{\rho_f^2 \; g \; e^4 \; \sin^3(\pi - \psi)}{12 \; \mu_f} \left[Z + \frac{s}{2 \, e \, \tan(\alpha)} \right]^4 \tag{2.17}$$

where

G = condensate flow rate,

t_t = fin tip width,

α = fin semivertex angle, and

Z = dimensionless depth of condensate between fins.

Although the above equations appear to be fairly simple, it must be kept in mind that rather complex computer solutions

32

are required to obtain values for Z. To check the validity
of equation (2.15), (2.16) and (2.17), experiments were
performed with four different finned tubes to condense both
steam and R-113 vapor. Agreement to within 5 percent was
reported.

In 1977, Nader [18] presented an analytical model to
predict condensation on a vertical, single fin attached to a
horizontal tube. This model differed from those discussed
above in that the fin temperature was allowed to vary along
the height of the fin. For the special case where the fin
temperature is constant, the Nusselt equation was obtained.
A "condensation efficiency" was then proposed to account for
a variable fin temperature, and was defined as:

$$\phi = C_1 \frac{F_1}{F_2} \tag{2.18}$$

$$F_1 = \frac{\rho_f \ (\rho_f - \rho_v) \ g \ h_{fg} \ e^3}{k_f \ \mu_f \ \Delta T} \tag{2.19}$$

$$F_2 = \frac{t \ k_m}{2 \ e \ k_f} \tag{2.20}$$

where

C_1 = constant of proportionality, and

k_m = thermal conductivity of fin.

With this definition, the rate of condensate formation and
the rate of heat transfer (with variable fin temperature)
were found to be:

33

$$G_f = 1.8856 \left[\frac{k_f}{h_{fg}} F_1 \right]^{1/4} \phi^3 \Delta T \qquad\qquad (2.21)$$

$$Q = 1.8856 \, k_f \, F_2^{1/4} \, \phi^3 \, \Delta T \qquad\qquad (2.22)$$

where

G_f = rate of condensate formation, and

Q = total heat-transfer rate.

Thus, with a table of values for F_1 and F_2 obtained numerically, the rate of heat transfer and condensate formation could be calculated by a fairly simple expression provided the condensation efficiency is greater than 0.8. However, for values below 0.8, the accuracy of equations (2.21) and (2.22) diminishes quite rapidly.

In 1979, Patankar and Sparrow [19] treated the case of a fin attached to a cooled vertical plate or a cylinder as a three-dimensional problem. A thin fin was assumed, and temperature variations across the thickness were ignored as was lengthwise conduction. Additionally, all heat transfer was assumed due to condensation only. Compared to the ideal fin solution, results obtained by Patankar and Sparrow indicated that a significant error existed when using the ideal fin solution on all but very long fins. Based on their results, the following relations were proposed:

$$q = 1.08 \; k_m \; \frac{\Delta T}{e} \left[\frac{4 \; k_f \; \mu_f \; \Delta T}{h_{fg} \; g \; \rho_f} \right]^{1/8} \left[\frac{k_m \; t}{2 \; k_f \; e^2} \right]^{1/2} z \qquad (2.23)$$

$$0 = 0.6171 \; \frac{h_{fg} \; g \; \rho_f \; e}{\mu_f} \left[\frac{2 \; k_f \; e^2}{k_m \; t} \right]^3 \left[\frac{4 \; k_f \; \mu_f \; \Delta T}{h_{fg} \; g \; \rho_f^2} \right]^{7/8} \left[\frac{k_m \; t}{2 \; k_f \; e^2} \right]^{7/2} z \quad (2.24)$$

where

q = heat flux, and

z = axial coordinate.

According to Patankar and Sparrow, these equations should be valid for most practical applications; however, no experimental data were available at the time to confirm this.

In 1980, Rifert [20] analyzed condensation of vapor on horizontal finned tubes enhanced by the effect of surface-tension forces. In his analysis, he divided the tube into flooded and unflooded zones, and solved a two-dimensional form of the energy equation for each zone. The mean heat flux was then determined by integrating over each zone and the tube length. In cases where condensate is retained in more than half of the tube perimeter, Rifert points out that a three-dimensional form of the energy equation must be used. Solutions to these equations revealed that, in most cases, the fin temperature is very nonuniform, so the mean integral heat-transfer coefficient and its correlations should not be used. The above-mentioned zone-by-zone analysis was, therefore, recommended.

Based on their study of condensate retention mentioned earlier in section B, Rudy and Webb [10] proposed that the

Beatty and Katz [15] model be modified to account for condensate retention, as shown below:

$$\overline{h} = h_{BK} \left[\frac{\pi - \psi}{\pi} \right] \tag{2.25}$$

where h_{BK} is computed using equation (2.11). This equation neglects any heat transfer through the flooded portion of the tube. As a result, it was shown to underpredict the average heat-transfer coefficient of condensing R-11 by as much as 30 percent when a significant amount of retained condensate was present.

Using the condensate retention angle they had developed earlier (see section B), Owen et al. [13] divided a horizontal finned tube into an upper unflooded section, and a lower flooded section. Unlike Rudy and Webb [10], however, they accounted for heat-transfer through the flooded portion of the tube by noting that condensation occurs on both the surface of the retained condensate and the fin tips. An effective thermal resistance was obtained over this portion of the tube by assuming parallel paths for heat-transfer through the fins and retained condensate. The respective thermal resistances, which were added in parallel, were then added in series with the tube wall thermal resistance. The resulting heat-transfer coefficient was then found to be:

$$\overline{h} = \frac{(\pi - \psi)}{\pi} h_u + \frac{\psi}{\pi} h_\ell \tag{2.26}$$

36

where h_u is computed using equation (2.11), and

$$h_\ell = \left[\frac{e}{k_{eff}} + 1.379 \left(\frac{\mu_f \, \Delta T \, D_o}{k_f^3 \, \rho_f \, (\rho_f - \rho_v) \, g \, h_{fg}} \right)^{1/4} \right]^{-1} \quad (2.27)$$

k_{eff} = effective thermal conductivity

This equation was found to predict all the available data with an accuracy of better than 30 percent.

Rudy and Webb [21] used equation (2.7) a short time later while developing an equation for the heat-transfer coefficient. The model for this undertaking was based on surface-tension-driven radial flow of condensate on the fin surface, with a linear pressure gradient along the fin height, and gravity-drained flow of condensate in the channel between fins. The Nusselt equation for horizontal tubes was used for the tube area between fins, while the fin surface was treated by an equivalent gravity model developed by Webb et al. [22] and Rudy [23] earlier. As before, vapor shear and heat transfer through the flooded portion were neglected, yielding a heat-transfer coefficient of:

$$\bar{h} = \left[0.725 \, \frac{\pi \, D_o \, L}{A_{ht}} \left(\frac{k_f^3 \, \rho_f^2 \, h_{fg} \, g}{D_o \, \mu_f \, \Delta T} \right)^{1/4} \right.$$

$$\left. + \, 0.943 \, n \, \frac{A_{ft}}{A_{ht}} \left(\frac{k_f^3 \, \rho_f \, h_{fg} \, \sigma \, (r_A + r_B)}{\mu_f \, e^2 \, r_A \, r_B \, \Delta T} \right)^{1/4} \right] \frac{(\pi - \psi)}{\pi} \quad (2.28)$$

37

where

I = length of tube,

A_{bt} = surface area of tube between fins, and

A_{ft} = fin surface area.

This expression provided an accuracy of better than 10% for condensation of R-11 on short, finely-spaced fins, but the accuracy dropped sharply for larger fins spaced further apart. This was apparently due to the assumed linear pressure gradient on the fin surface, and breakdown of the model as gravity forces became dominant. The use of equation (2.28) should be restricted to fin densities from 1200 to 1400 fins/m, and fin heights of less than 1 mm.

In 1984, Honda et al. [24] developed a model to predict the heat-transfer coefficient that took surface-tension effects and the non-isothermal behavior of fins into account. In order to obtain a solution, however, iterative finite difference techniques that required a considerable amount of computer time were used. Nonetheless, they showed that this model was able to predict the average heat-transfer coefficient for most available experimental data (which included 11 fluids, and 22 tubes) within 20 percent. Predictions involving the condensation of steam provided the largest errors (as much as 40%), due in part to the high surface tension of water. This reflects the fact that surface-tension effects are still not completely accounted for. Compared to the other models discussed thus far, however, the model of Honda et al. shows considerable promise in spite of its complexity.

In 1983, Adamek [27] defined a family of condensate surface profiles whose curvatures are given by:

$$\frac{1}{r} = \frac{\theta_m}{S_m} \frac{(\xi + 1)}{\xi} \left[1 - \left(\frac{s}{S_m}\right)^{\xi} \right] \qquad (2.29)$$

where

θ_m = rotation angle of normal to condensate film surface,

S_m = length of convex surface of fin condensate film,

s = coordinate along condensate film surface from fin tip.

The parameter ξ in equation (2.29) characterizes the aspect ratio of the fin cross section. A number of ξ values and their corresponding condensate surface profiles are shown in Figure 2.3. With the above information, Adamek obtained an expression for the heat-transfer coefficient of the fin surface as shown below:

$$h_f = 2.149 \frac{k_f}{S_m} \left[\frac{\sigma \, h_{fg} \, \theta_m \, S_m \, \rho_f}{\mu_f \, k_f \, \Delta T} \frac{(\xi + 1)}{(\xi + 2)^3} \right]^{1/4} \qquad (2.30)$$

These fin profiles were used by Webb et al. [25] and Rudy et al. [26] in 1985 to develop a model for condensation on horizontal finned tubes. This model divided the tube into flooded, and unflooded regions, and further divided the unflooded region into tube (area between fins) and fin areas. To predict heat transfer from the unflooded fin surfaces, they used the heat-transfer coefficient proposed by Adamek. The Adamek fin profile used to approximate their trapezoidal fins is shown in Figure 2.4. The Nusselt

39
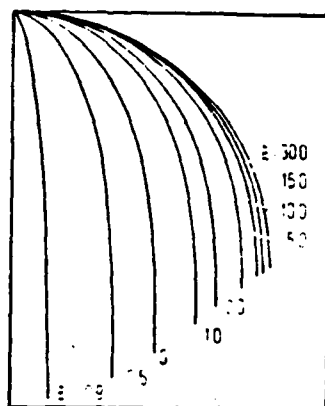
Figure 2.3   Adamek [27] Condensate Surface Profiles
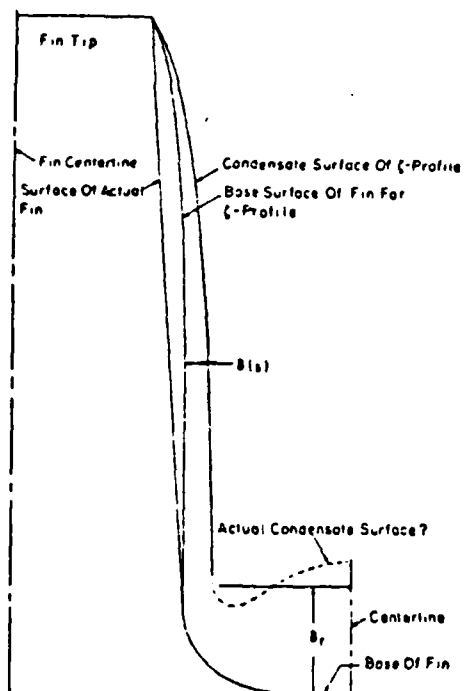
Figure 2.4   Fin Geometry for the Webb et al. Model [22]

40

equation, written in terms of the film Reynolds number, was used to predict heat transfer from the unflooded tube surface between fins. Writing the Nusselt equation this way takes into account the additional condensate thickness that results from the drainage of condensate formed on the fin surface. For the flooded region, a two-dimensional computer code was used to solve for the heat flux into the tube-side coolant (q_{b2}), which was compared to the limiting case of heat flux (q_{b1}) assuming zero fin thickness. This ratio $(\phi = q_{b2}/q_{b1})$ was used along with a linear temperature profile across the condensate film to establish a heat-transfer coefficient for this region. The resulting average heat-transfer coefficient is given below:

$$h_{ow} = h \eta_o = \left[h_r \frac{A_{ht}}{A_{sf}} + \eta h_f \frac{A_{ft}}{A_{sf}} \right] \frac{\pi - \psi}{\pi} + h_b \frac{\psi}{\pi} \qquad (2.31)$$

$$h_r = 1.514 \left[\frac{\mu_f^2}{k_f^3 \rho_f^2 g} Re_f \right]^{-1/3} \qquad (2.32)$$

$$h_b = \phi \frac{k_f}{e} \qquad (2.33)$$

$$\eta_o = 1 - (1 - \eta) \frac{A_{ft}}{A_{ht} + A_{ft}} \qquad (2.34)$$

where h_f is calculated using equation (2.30), and

A_{sf} = smooth tube area based on the fin diameter,

Re_f = film Reynolds number,

41

ϕ = ratio of tube side heat flux with fins to tube
side heat flux with fins of zero thickness.

A detailed step-by-step procedure, recommended for obtaining a solution of equation (2.31), is provided in Appendix A.

To allow for heat transfer from the fin tip, and to account for decreased heat transfer due to the thick condensate film in the trough area, Webb et al. replaced S_m with $S_m + t/2 - \delta_r$, where δ_r is the average condensate film thickness in the trough area in the unflooded region:

$$\delta_r = \frac{k_f}{h_r} \qquad (2.35)$$

Since the effects due to $t/2$ and δ_r in the modified S_m tend to cancel each other, Webb et al. reported only a negligible change in S_m. This model was shown to predict the heat-transfer coefficient for R-11 condensing on horizontal finned tubes with fin densities of 748, 1024, and 1378 fins/m within 20 percent.

III. DESCRIPTION OF TEST APPARATUS

A. TEST APPARATUS

The same test apparatus used by Georgiadis [7] was used for this investigation. A schematic of this apparatus is shown in Figure 3.1. Steam was generated in the boiler, which consisted of a 304.8 mm (12 in.) Pyrex glass section containing ten 4000-Watt, 480-Volt Watlow immersion heaters. After passing through a 304.8 mm (12 in.) to 152.4 mm (6 in.) reducing section, the steam flowed upward through a 2.44 m (8 ft.) long section of Pyrex glass piping. At this point, a 180-degree bend in the piping re-directed the steam downward, where after 1.52 m (5 ft.) of Pyrex glass piping, it entered the stainless steel test section illustrated by Figure 3.2. The test tube was mounted horizontally in the test section behind a view port, which allowed visual observation of the condensation process. Steam not condensed by the test tube continued downward to the auxiliary condenser, where it was condensed by two 9.5 mm (3/8 in.) diameter water-cooled copper tubes helically coiled to a height of 457 mm (18 in.). The condensate was then returned to the boiler by gravity.

Filtered tap water was used to cool the test tube on a once-through basis. This water was first collected in a large sump with a capacity of about 0.4 cubic meters (Figure 3.3), then pumped through a flow meter, and the test tube by two centrifugal pumps connected in series. A valve on the discharge side of the second pump allowed the velocity of water flowing through the test tube to be varied from 0 to 4.4 m/s (14.4 ft/sec). The auxiliary condenser was cooled by a continuous supply of tap water, which was throttled to control the internal pressure of the test apparatus.

43
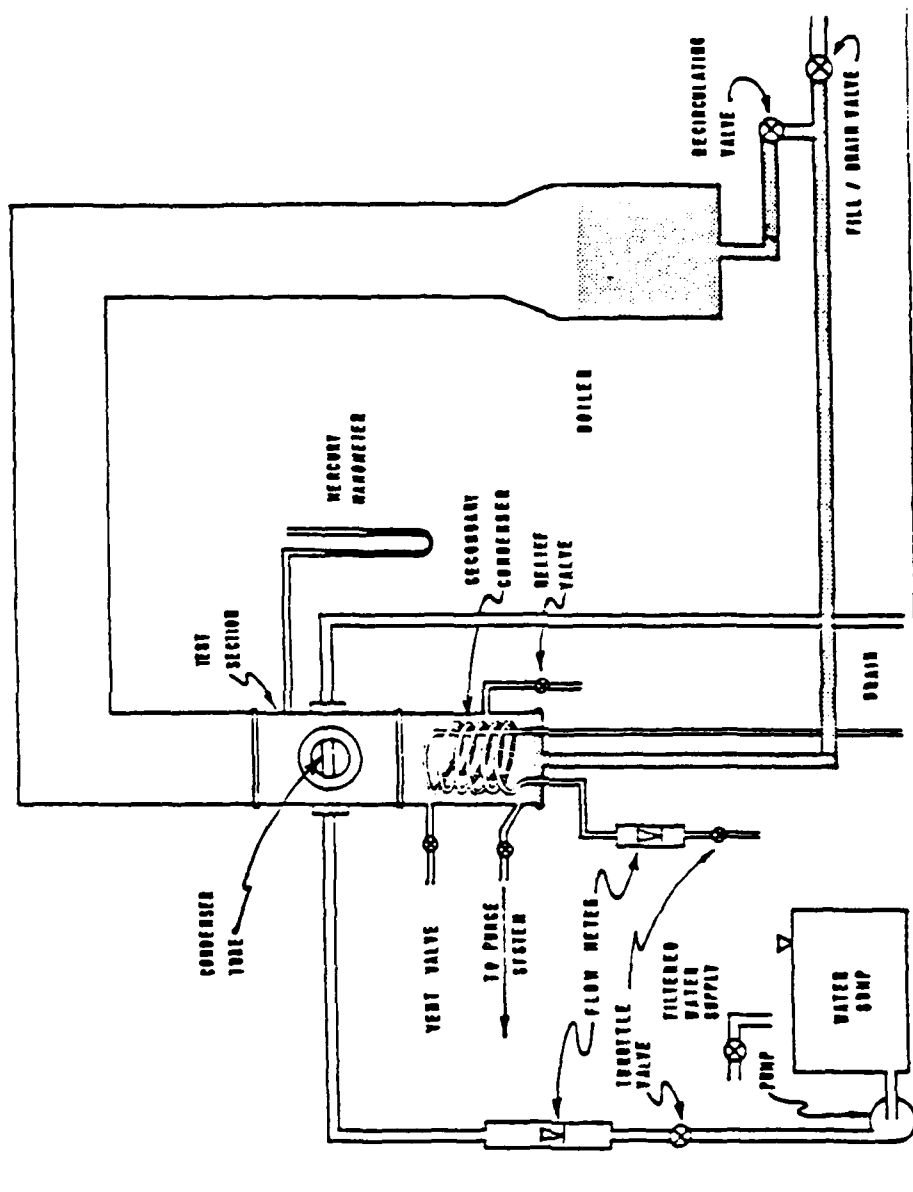
Figure 3.1   Schematic of Test Apparatus

44
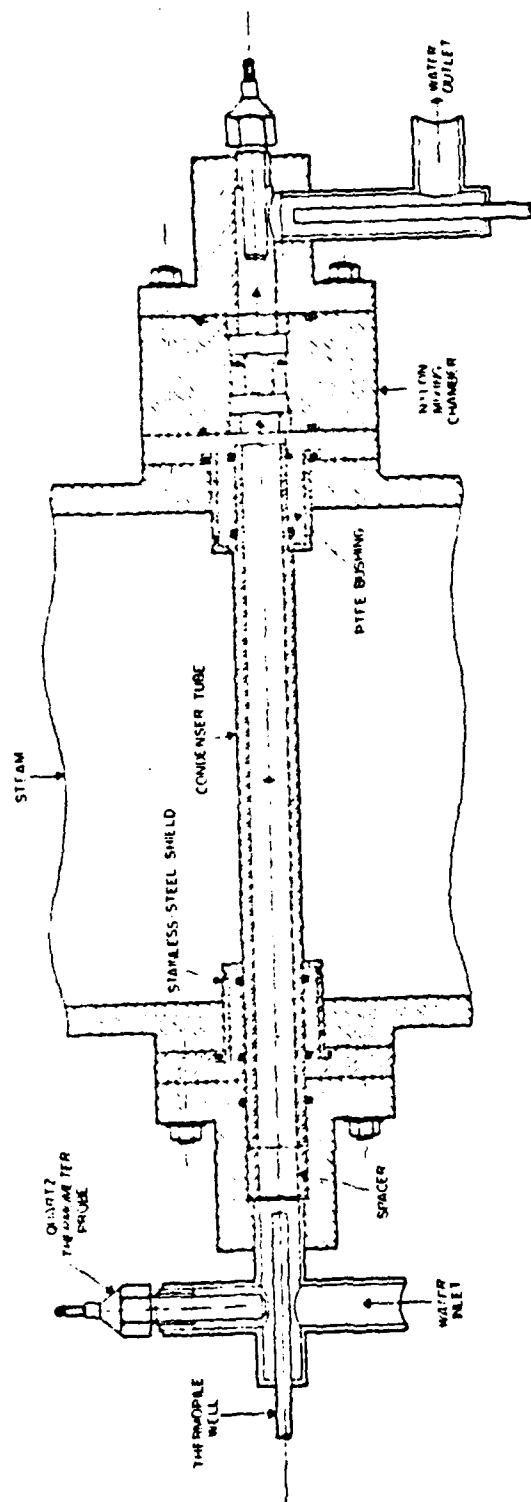
Figure 3.2   Schematic of Test Section (Insert Removed)

45

The system used to remove non-condensing gases is shown in Figure 3.3. The vacuum pump continually drew a sample mixture of any possible non-condensing gases and moisture from the auxiliary condenser. This mixture was then passed through a heat exchanger, where the moisture was condensed before it entered the sump, using the same filtered tap water described earlier.

B. INSTRUMENTATION

The electrical power input to the boiler immersion heaters was controlled by a panel-mounted potentiometer. A converter with an input voltage of 440 VAC generated a signal which was fed to the data acquisition system to calculate the boiler input power. A more detailed description of the boiler power supply is provided by Poole [6].

The internal system pressure was measured manually using a U-tube, mercury-in-glass manometer graduated in millimeters. Steam, condensate return, and ambient temperatures were measured using calibrated copper-constantan thermocouples. These thermocouples had an accuracy within ± 0.1 K. The cooling water temperature rise was measured by two Hewlett-Packard (HP) 2804A quartz thermometers, along with a 10-junction, series-connected copper-constantan thermopile as a backup. Throughout this investigation, the quartz thermometers and the thermopile agreed to within ± 0.03 K.

C. DATA ACQUISITION SYSTEM

To monitor the system temperatures and boiler input power (using the converter signal), an HP 9826A computer was used to control an HP 3497A Data Acquisition System. Raw data were processed immediately and, at the same time, stored on diskett for reprocessing at a later time.

46
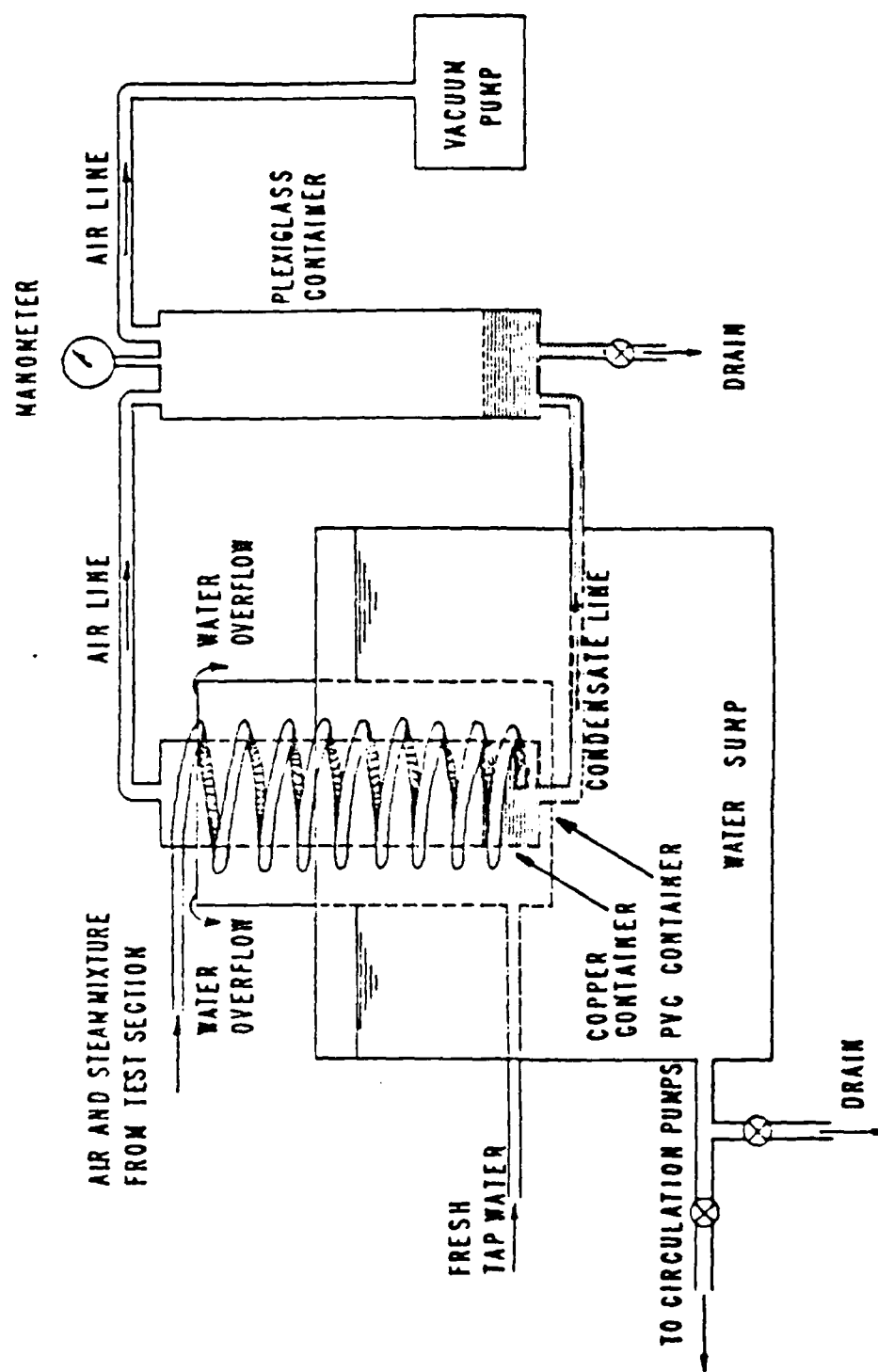
Figure 3.3 Schematic of Vacuum System and Cooling Water Sump

47

D. TUBES TESTED

For this thesis effort, eighteen copper tubes, and a stainless steel tube were manufactured. They are presented in Table I. The first eight tubes with rectangularly-shaped fins were tested in order to complete the sequence of data initiated by Georgiadis [7]. This completed the systematic variation of fin spacing, thickness, and height so that the optimum dimensions could be determined. Figure 3.4 shows a photograph of the four tubes with fin thickness of 1.0 mm, fin height of 0.5 mm, and spacings of 1.0, 1.5, 2.0, and 4.0 mm (tube numbers 26 to 29). Also shown is the insert used to enhance the inside heat-transfer coefficient, which will be discussed in more detail in the next chapter. Figure 3.5(a) shows a cross section of a rectangular fin with a fin height of 1.5 mm, a fin spacing of 1.5 mm, and a fin thickness of 1.0 mm. In addition to the tubes with rectangularly-shaped fins, six tubes were tested to study the effect of fin shape on the heat-transfer performance. Tubes number 40 and 42 were made of stainless steel to test the effect of fin-metal thermal conductivity on the heat-transfer performance. Due to limited machine-shop facilities available, the "parabolic" fins on two of the tubes were not truly parabolic, as shown in Figure 3.5(b). A cross section of a commercially-available finned tube produced by the Wolverine Division of United Oil Products is also shown in Figure 3.5(c) for comparison. The smooth tubes were tested in order to determine the water-side heat-transfer coefficients, and to serve as a comparison for the finned tubes.

E. VACUUM INTEGRITY

For any condensation experiment, especially when operating under vacuum conditions, a leak-free apparatus is of

48

TABLE 1

Geometry of Tubes Tested

Tube Number	Fin Type	Fin Base Thickness t_b (mm)	Fin Tip Thickness t_t (mm)	Inter-Fin Spacing s (mm)	Fin Height e (mm)	Fin Root Diameter D_o (mm)	Tube Inside Diameter D_i (mm)	Tube Material
26	Rectangular	1.00	1.00	1.00	0.50	19.05	12.7	Copper
27	Rectangular	1.00	1.00	1.50	0.50	19.05	12.7	Copper
28	Rectangular	1.00	1.00	2.00	0.50	19.05	12.7	Copper
29	Rectangular	1.00	1.00	4.00	0.50	19.05	12.7	Copper
30	Rectangular	1.00	1.00	1.00	1.50	19.05	12.7	Copper
31	Rectangular	1.00	1.00	1.50	1.50	19.05	12.7	Copper
32	Rectangular	1.00	1.00	2.00	1.50	19.05	12.7	Copper
33	Rectangular	1.00	1.00	4.00	1.50	19.05	12.7	Copper
34	Triangular	1.00	0.00	0.60	1.00	19.05	12.7	Copper
35	Trapezoidal	1.00	0.50	1.00	1.00	19.05	12.7	Copper
36	Spiral	2.10	0.00	0.00	1.00	19.05	12.7	Copper
37	Parabolic	0.50	0.00	0.70	1.00	19.05	12.7	Copper
38	Parabolic	0.50	0.00	1.50	1.00	19.05	12.7	Copper
39	Rectangular	1.00	1.00	1.50	1.00	13.70	13.5	S.S.
40	Rectangular	1.00	1.00	1.50	1.00	13.70	13.5	Copper
41	Smooth	-	-	-	-	13.70	13.5	S.S.
42	Smooth	-	-	-	-	13.70	13.5	S.S.
43	Wolverine	0.40	0.10	0.80	1.33	15.80	12.7	Copper
44	Smooth	-	-	-	-	15.80	12.7	Copper

S.S. = Stainless Steel
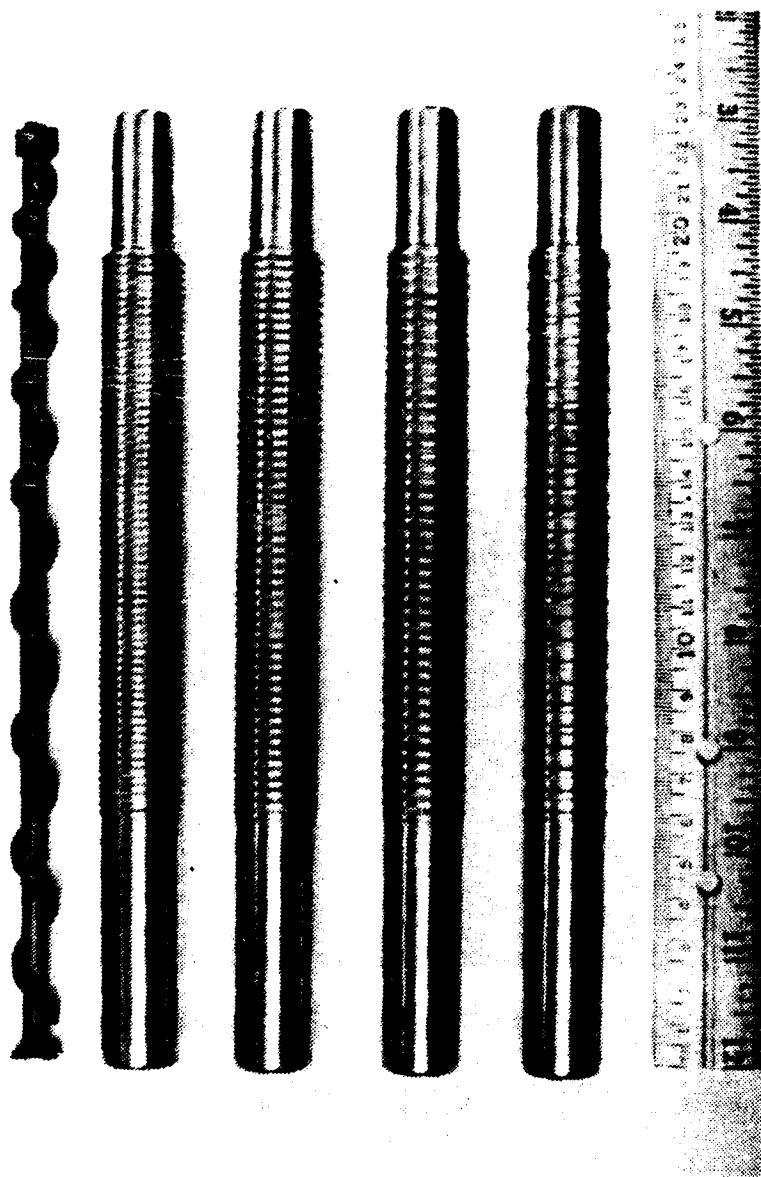
Figure 3.4   Photograph of Finned Tubes with a Fin
Height of 0.5 mm and Insert.
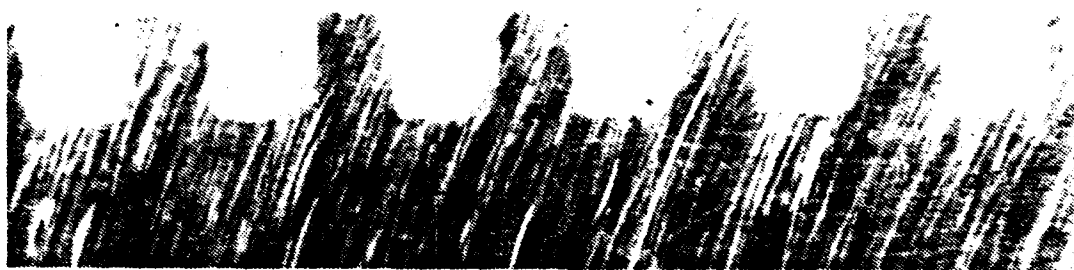
(a)
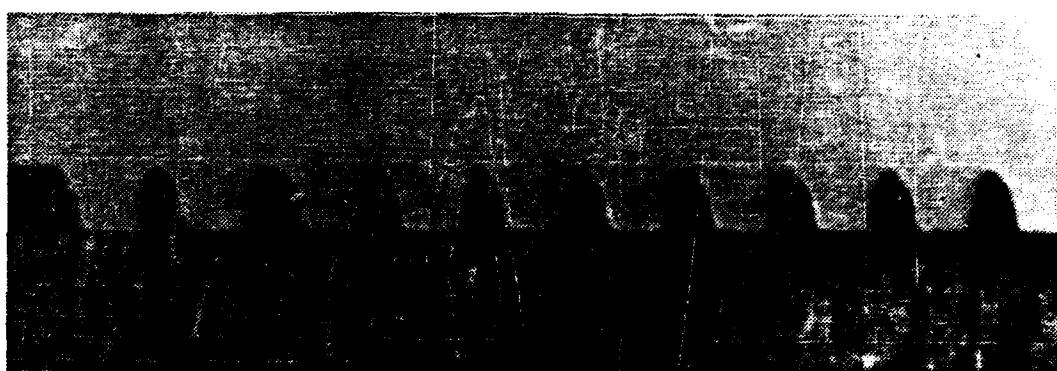
(b)
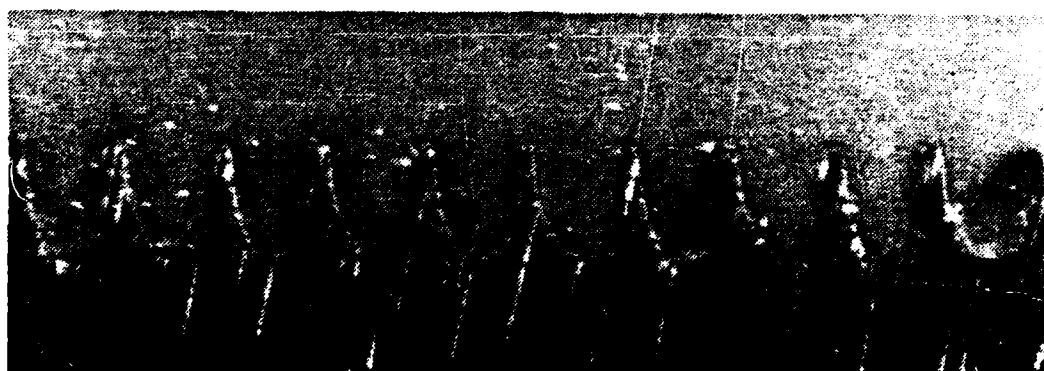
(c)

Figure 3.5 Cross-Sectional Photographs of (a) Rectangular
Fins, (b) "Parabolic" Fins, and (c) "Wolverine" Fins.

51

vital importance. The presence of any leaks would allow the admission of non-condensing gases, whose deleterious effects would invalidate any data being collected. To prevent this problem, vacuum integrity tests were performed on the test apparatus both before and after the data acquisition phase of this thesis effort (a time period of about four months). The first test revealed a leak rate represented by a pressure rise of 1.0 mmHg over a period of five days, while the pressure rise during the final test was 1.0 mmHg over a 24-hour period. These tests were performed at an absolute pressure of about 85 mmHg. This negligible leak rate, together with continuous venting of the test apparatus during data runs, eliminated the deleterious effects of non-condensing gases on the heat-transfer results reported in this thesis.

IV. DATA COLLECTION AND REDUCTION

A. SYSTEM OPERATION

In order to ensure filmwise condensation, all tubes were treated with a solution containing equal parts of sodium hydroxide and ethyl alcohol. The tubes were placed in a steam bath and several layers of the solution were applied with a tooth brush every 10 minutes. After about one hour, the tube surfaces were completely blackened. The same procedure was repeated prior to each data run, but the tube was only steamed for ten to fifteen minutes. Following the steam bath, the tubes were rinsed with tap water before installing them in the test apparatus. Georgiadis [7] discusses this procedure in more detail.

The test apparatus was brought to operating pressure and temperature using the procedures provided by Georgiadis [7]. Steady-state conditions were assumed to occur once the test section steam temperatures, as well as the cooling water inlet and outlet temperatures stabilized. Two sets of data were then taken for each of the heat fluxes, which were determined by the flow rate of cooling water through the test tube. Starting at a flow rate of 80 percent (4.44 m/s for 19 mm O.D. tubes, and 3.92 m/s for 13.7 and 15.8 mm O.D. tubes), flow rates were reduced to 70, 60, 45, 35, 26, and 20 percent, then brought back up to 55 and 80 percent. These settings were selected since they provided nearly equally-spaced heat flux values. It should be noted that continuous adjustments of cooling water flow through the auxiliary condenser were required to maintain system pressure as flow rates through the test tube were changed.

53

Visual observations of condensation taking place on the test tube were made on a regular basis to ensure uniform filmwise condensation. A more reliable indication of this, however, was the trend of data taken as the cooling water flow rates were increased back up to 80 percent. If the final value of the steam-side heat-transfer coefficient at 80 percent was significantly higher than those at the beginning of the data run, dropwise condensation was assumed to have occurred, and the data were disregarded. All data presented in this thesis displayed less than 5% disagreement in the steam-side heat-transfer coefficient between initial and final data sets.

B. THE DROPWISE CONDENSATION PROBLEM

The purpose of this thesis was to take strictly filmwise condensation data, using primarily copper tubes. Due to the poor wettability of copper with water, especially when even minute amounts of contamination are present, there is a tendency to condense steam in the partial dropwise mode. Dropwise condensation is far more effective than filmwise condensation; so, its presence can lead to large errors in the data.

By following procedures set forth by Georgiadis [7], the dropwise problem was minimized. During the initial testing phase of this thesis, however, a small amount of dropwise condensation was encountered. This problem was soon traced to the boiler water, which had not been changed for some time. By changing the water after every three or four runs, the problem was eliminated.

C. STEAM VELOCITY LIMITATIONS

A major assumption in the Nusselt theory is that vapor velocity does not induce shear forces on the vapor-liquid

54

interface. Since system pressure in the test apparatus was
controlled by condensing steam in the auxiliary condenser, a
reasonable steam velocity was always present. Since steam
velocity (i.e., steam flow rate) depends on boiler power
input, decreasing the power results in lower vapor veloci-
ties. Under vacuum conditions, (about 85 mmHg) a maximum
velocity of about 8 m/s was possible at full boiler power
(36 kW). However, at these high velocities, the entire
apparatus experienced considerable vibration. As discussed
by Georgiadis [7], a steam velocity of 2 m/s under vacuum
provided the most stable operating conditions. This corre-
sponding boiler power (about 9 kW) was low enough to mini-
mize system vibrations, yet high enough to avoid rapid
fluctuations in condenser pressure due to the intermittent
break-up of vapor bubbles in the boiler. To allow a suffi-
cient amount of steam to reach the auxiliary condenser when
operating at atmospheric pressure, the maximum boiler power
was required. This resulted in a steam velocity of approxi-
mately 1 m/s.

D. DATA REDUCTION

All the programs, property functions, and calibration
data used for this thesis effort were essentialy the same as
those used by Georgiadis [7] and Poole [6]. Because six of
the tubes (tube numbers 39 thru 44) tested during this
effort had inside diameters different than any tube tested
previously, and two (tubes number 40, and 42) were manufac-
tured from stainless steel, some minor modifications were
necessary for the data reduction program (program DRP6).
These modifications included options for different tube
diameters, tube inserts, thermal conductivity, mixing-
chamber calibrations, and leading constants for the inside
heat-transfer coefficients.

55

The mixing-chamber (see Figure 3.2) calibration was required to account for the temperature rise that occurred across the mixing chamber, due primarily to turbulent viscous dissipation. The purpose of the mixing chamber is to ensure a uniform temperature at the cooling water discharge, so that accurate temperature measurements can be made. Since tubes with different inside diameters, requiring different inserts, result in different pressure drops, calibrations had to be performed for each inside diameter.

A modified Wilson Plot program [7] was used to compute the leading constants for the Sieder-Tate equation used to determine the water-side heat-transfer coefficient. Data taken on smooth tubes were used to determine the leading constants, which were then used to reduce data taken on similar tubes with identical internal dimensions.

V. RESULTS AND DISCUSSION

A. INTRODUCTION

During this thesis effort, a number of data runs were made using the procedures described in Chapter IV. For both vacuum and atmospheric conditions, every tube was tested at least three times, on different days, to ensure the data were repeatable. Complete filmwise condensation was maintained, and the computed non-condensing gas concentration was held below 1.0 percent for all accepted data runs. It was estimated that an error of ± 0.2 K in the steam temperature, or an error of ± 1.0 mmHg in the system pressure would lead to an error of ± 1.2 percent in the non-condensing gas concentration. This shows that the computed non-condensing gas concentration was zero to within the accuracy of temperature and pressure measurements. As discussed earlier in Chapter III, the test apparatus would allow only a negligible amount of non-condensing gas to be present in the apparatus. The non-condensing gas concentration was computed for the system temperature and pressure during every data run to ensure no major leaks developed. A summary of tubes tested between Georgiadis [7] and this thesis effort and the resulting enhancements are provided in Table II.

B. WATER-SIDE HEAT-TRANSFER COEFFICIENTS

The water-side heat-transfer coefficients, enhanced by the use of an insert, were obtained by Georgiadis [7] for the tubes with an inside diameter of 12.7 mm. Both a "direct method," and a "modified Wilson method" were used, and are discussed below.

57

TABLE II

Summary of Tubes Tested and Their
Heat-Transfer Performance

Tube Nr.	Fin Type	s (gm)	t(l) (mm)	e (mm)	Do (mm)	Area (mm²)	Ar	Eo(+) Vac	Eo(θ) Atm	Eo/Ar Vac	Eo/Ar Atm	e/s	s/Do
S01*	Smo	–	–	–	19.05	7980.64	1.00	1.00	1.00	1.00	1.00	–	–
I02*	Ins	–	–	–	19.05	7980.64	1.00	1.00	1.00	1.00	1.00	–	–
I03*	Ins	–	–	–	19.05	7980.64	1.00	1.00	1.00	1.00	1.00	–	–
F04*	Rec	0.50	1.00	1.00	19.05	19738.65	2.47	2.55	4.38	1.03	1.77	2.00	0.03
F05*	Rec	1.00	1.00	1.00	19.05	16799.15	2.10	3.75	5.20	1.78	2.47	1.00	0.05
F06*	Rec	1.50	1.00	1.00	19.05	15035.45	1.88	4.01	5.66	2.13	3.01	0.67	0.08
F07*	Rec	2.00	1.00	1.00	19.05	13859.65	1.74	3.24	4.91	1.86	2.83	0.50	0.10
F08*	Rec	4.00	1.00	1.00	19.05	11508.05	1.44	3.09	4.10	2.14	2.84	0.25	0.21
F09*	Rec	9.00	1.00	1.00	19.05	9744.34	1.22	2.23	2.50	1.82	2.05	0.11	0.47
F10*	Rec	0.50	0.75	1.00	19.05	21922.68	2.75	2.91	4.66	1.06	1.70	2.00	0.03
F11*	Rec	1.00	0.75	1.00	19.05	17939.24	2.25	3.35	5.24	1.49	2.33	1.00	0.05
F12*	Rec	1.50	0.75	1.00	19.05	15726.22	1.97	3.71	5.64	1.88	2.86	0.67	0.08
F13*	Rec	2.00	0.75	1.00	19.05	14317.93	1.79	3.52	5.45	1.96	3.04	0.50	0.10
F14*	Rec	4.00	0.75	1.00	19.05	11649.60	1.46	3.25	4.08	2.23	2.79	0.25	0.21
F15*	Rec	0.50	0.50	1.00	19.05	25198.72	3.16	2.72	4.53	0.86	1.43	2.00	0.03
F16*	Rec	1.00	0.50	1.00	19.05	19459.36	2.44	3.17	4.89	1.30	2.00	1.00	0.05
F17*	Rec	1.50	0.50	1.00	19.05	16589.68	2.08	3.49	5.46	1.68	2.63	0.67	0.08
F18*	Rec	2.00	0.50	1.00	19.05	14867.87	1.86	3.36	5.07	1.80	2.72	0.50	0.10
F19*	Rec	4.00	0.50	1.00	19.05	11806.88	1.48	2.47	3.78	1.67	2.55	0.25	0.21
F20*	Rec	1.00	0.50	1.00	19.05	15203.02	1.90	3.38	4.73	1.77	2.48	1.00	0.05
F21*	Rec	1.25	1.50	1.00	19.05	15119.23	1.89	3.72	5.13	1.96	2.71	0.80	0.07
F22*	Rec	1.00	1.25	2.00	19.05	26455.52	3.31	4.22	5.82	1.27	1.76	2.00	0.05
F23*	Rec	1.50	1.00	2.00	19.05	22760.54	2.85	4.82	6.43	1.69	2.25	1.33	0.08
F24*	Rec	2.00	1.00	2.00	19.05	20297.23	2.54	4.66	6.23	1.83	2.45	1.00	0.10
F25*	Rec	4.00	1.00	2.00	19.05	15370.59	1.93	3.71	4.87	1.93	2.53	0.50	0.21
F26	Rec	1.00	1.00	0.50	19.05	12285.16	1.54	2.56	4.02	1.66	2.61	0.50	0.05
F27	Rec	1.50	1.00	0.50	19.05	11424.26	1.43	2.63	3.94	1.84	2.75	0.33	0.08
F28	Rec	2.00	1.00	0.50	19.05	10850.32	1.36	2.93	4.35	2.16	3.20	0.25	0.10
F29	Rec	4.00	1.00	0.50	19.05	9702.45	1.22	2.41	3.37	1.98	2.77	0.13	0.21
F30	Rec	1.00	1.00	1.50	19.05	21522.60	2.70	3.30	5.02	1.22	1.86	1.50	0.05
F31	Rec	1.50	1.00	1.50	19.05	18814.21	2.36	3.92	6.16	1.66	2.61	1.00	0.08
F32	Rec	2.00	1.00	1.50	19.05	17008.61	2.13	3.99	6.10	1.87	2.86	0.75	0.10
F33	Rec	4.00	1.00	1.50	19.05	13397.43	1.68	3.18	4.66	1.89	2.77	0.38	0.21

TABLE II (continued)

Tube Nr.	Fin Type	s (mm)	t(#) (mm)	e (mm)	Do. (mm)	Area (mm²)	Ar	Eo(+) Vac	Eo(@) Atm	Eo/Ar Vac	Eo/Ar Atm	e/s	s/Do
F34	Tri	0.60	1.00	1.00	19.05	14742.68	1.85	3.66	5.95	1.98	3.22	1.67	0.03
F35	Tra	1.00	1.00	1.00	19.05	14851.86	1.86	3.60	5.28	1.93	2.84	1.00	0.05
F36	Spi	0.00	2.10	1.00	19.05	10940.84	1.37	4.04	5.66	2.95	4.13	-	0.00
F37	Par	0.70	0.50	1.00	19.05	19832.83	2.49	3.61	6.87	1.45	2.76	1.43	0.04
F38	Par	1.50	0.50	1.00	19.05	15091.89	1.89	4.00	5.96	2.12	3.15	0.67	0.08
F39	Rec	1.50	1.00	1.00	13.70	11001.14	1.92	2.74	4.50	1.43	2.35	0.67	0.11
F40	Rec	1.50	1.00	1.00	13.70	11001.14	1.92	1.01	1.46	0.53	0.76	0.67	0.11
S41	Smo	-	-	-	13.70	5739.36	1.00	1.00	1.00	1.00	1.00	-	-
S42	Smo	-	-	-	13.70	5739.36	1.00	1.00	1.00	1.00	1.00	-	-
F43	Wol	0.80	1.33	0.40	15.80	21314.45	3.22	3.03	4.89	0.94	1.52	1.66	0.05
S44	Smo	-	-	-	15.80	6619.12	1.00	1.00	1.00	1.00	1.00	-	-

(+): Heat Flux = 3.5E5 W/m**2
(@): Heat Flux = 1.0E6 W/m**2
(#): t Measured at Fin Base
(*): Tubes Tested by Georgiadis [7]

59

1. The Direct Method

For the "direct method," a smooth tube was manufactured with six wall thermocouples inserted around its perimeter. During data runs under vacuum and atmospheric conditions, readings from these six thermocouples were obtained and averaged, in order to determine an average tube wall temperature for each heat flux. It should be noted that the wall temperature was quite non-uniform around the tube perimeter. Georgiadis [7] reported up to an 18-K drop in the wall temperature from the top to the bottom of the tube. Evaluation of the uncertainty resulting from this temperature variation was considered beyond the scope of the investigation. The average wall temperature was then used along with the cooling water inlet and outlet temperatures to determine the log-mean-temperature difference (LMTD). With values for heat flux and LMTD known, the value of the water-side heat-transfer coefficient was obtained. This, in turn, was used to determine the leading coefficient for the Sieder-Tate-type equation shown below:

$$Nu = C \, Re^{0.8} \, Pr^{1/3} \left[\frac{\mu_c}{\mu_w} \right]^{0.14} + B \tag{5.1}$$

A more detailed step-wise solution procedure is given by Georgiadis [7]. For the previously-mentioned tubes of 15.8 mm and 19.05 mm O.D., Georgiadis determined the coefficient C to be 0.0635. The constant B = 26.4 is an additional parameter found to improve the fit of equation (5.1). Note that C = 0.0635 is about 2.5 times greater than the well-known Sieder-Tate coefficient of 0.027 [28] for long tubes with smooth inner walls. This is due primarily to the insert used to enhance the water-side heat-transfer coefficient.

2. The Modified Wilson Method

A complete description of this method is provided in Appendix B. Briefly, this method uses a Sieder-Tate-type equation for the water-side heat-transfer coefficient, and an equation (discussed below) for the steam-side heat-transfer coefficient. Both equations contain leading coefficients that must be determined iteratively while being used in a linear equation to generate the Wilson plot. The iterations were performed on the HP 9826A computer mentioned previously in Chapter III, using program "WILSON6."

The "modified Wilson method" used during this investigation consisted of one minor modification from that of Georgiadis. For this thesis, a Fujii-type [29] equation was used instead of the Nusselt-type equation for the steam-side coefficient. This modification was made to account for the small steam velocity (about 1 m/s) that was present during the runs. For this reason, use of the Fujii-type equation appears to be more accurate than the use of the Nusselt-type equation. This modification resulted in a slightly higher value (up to 3 percent) for the leading coefficient C. The program "WILSON6" described earlier, allows an option for selecting either the Fujii-type or Nusselt-type equation for the steam-side coefficient.

Using a Nusselt-type equation for the steam-side coefficient, Georgiadis [7] found the leading coefficient (for equation (5.1)) C to be 0.071, with the B value set equal to zero. This C value is about 10 percent higher than the value (C = 0.0635) obtained by the "direct method," but since the "direct method" is generally felt to be more reliable, the values of 0.0635 and 26.4 were used for the constants C and B respectively for this thesis effort with tubes of 12.7 mm inside diameter (see Table I).

61

3. Water-Side Coefficients For Thin-Wall Tubes

Due to the thin (i.e., 0.5 mm thickness) tube walls for tubes 39 thru 42, it was not possible to manufacture an instrumented tube. For this reason, the "modified Wilson method," together with the Fujii-type equation for the steam-side coefficient, was used to determine the leading coefficient for equation (5.1) for both the copper tube (tube number 41), and the stainless steel tube (tube number 42). For the copper tube, a value of C = 0.0756 was obtained, while for the stainless steel tube, a value of C = 0.0688 was obtained. Although the inner tube diameters for both tubes are the same (i.e., 13.5 mm), the much higher thermal conductivity of copper, which results in circumferential heat conduction through the tube wall, leads to its higher value for C. A summary of the leading coefficients used in equation (5.1) for all the tubes is presented in Table III.

C. REPEATABILITY OF DATA

Since the reliability of data taken was of vital importance, all data runs were repeated, as Georgiadis [7] did, at least three times on different days. The computed steam-side coefficients for similar conditions (i.e., same tube and the same operating conditions) from different days agreed to within ± 5 percent. Additionally, data runs were performed on two finned tubes (tubes number 6 and 17), under similar conditions to verify the repeatability with data taken by Georgiadis. Figure 5.1 shows that the experimental steam-side heat-transfer coefficients of Georgiadis and those obtained during this investigation agree to within ± 5 percent. The curves shown in this figure (and all other figures of a similar nature that follow) are the least-squares-fit curves according to the following equation:

TABLE III

Measured Coefficients Used in Equation (5.1)

Tube Number	Tube Type	Tube Material	C	B	Comments
1-38	Thick-Wall	Copper	0.0635	26.5	Georgiadis [7]
39,41	Thin-Wall	Copper	0.0756	–	Modified Wilson Method
40,42	Thin-Wall	Stainless Steel	0.0688	–	Modified Wilson Method
43,44	Wolverine	Copper	0.0635	26.5	Georgiadis [7]

63
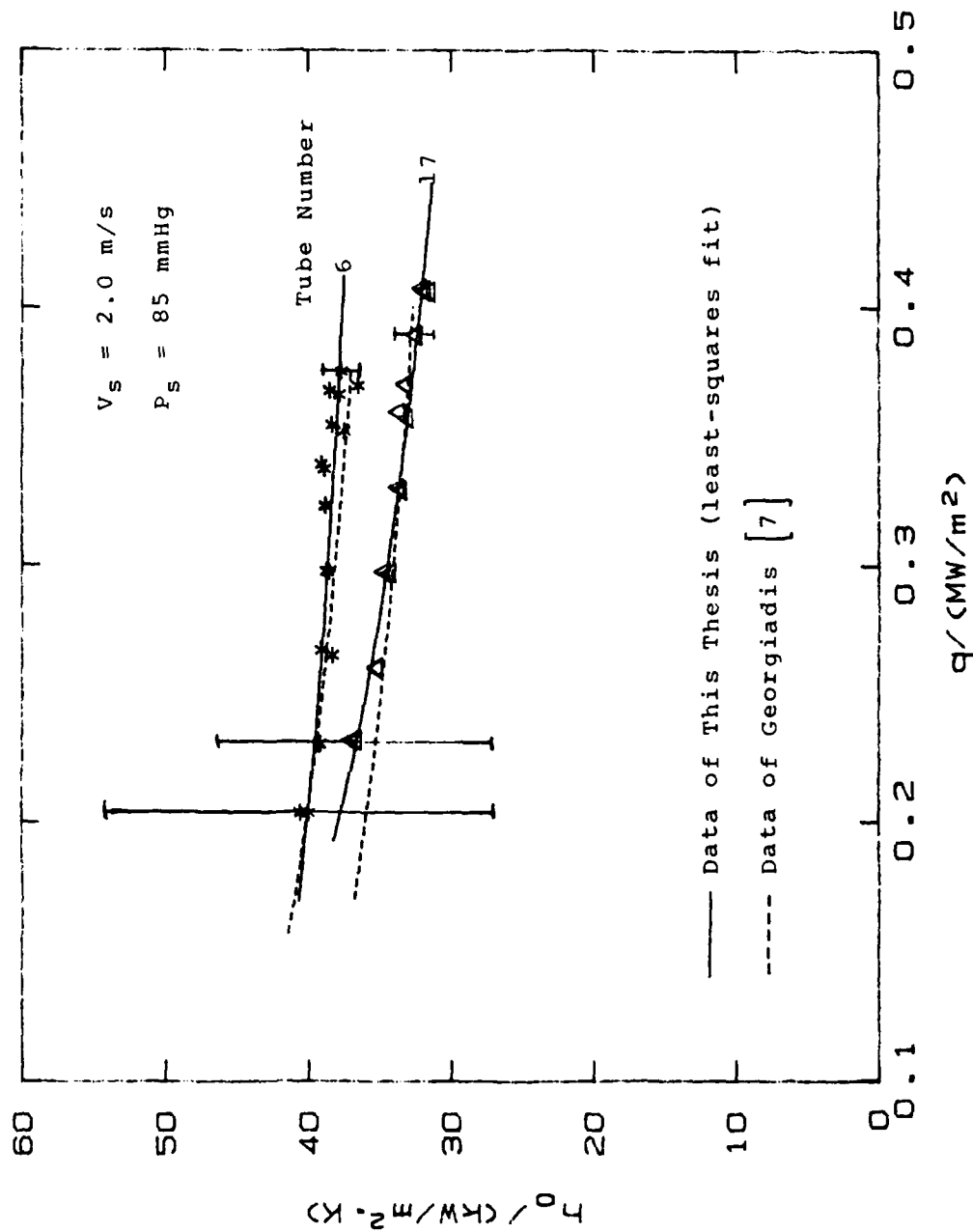
Figure 5.1 Comparison of Finned Tube Data with
Data of Georgiadis [7] (s = 1.5 mm, t = 1.0 mm, and e = 1.0 mm).

$$q = a \, \Delta T^h \tag{5.2}$$

where a and b are experimentally determined constants. These curves were selected instead of those based on the steam-side coefficient versus heat flux since the uncertainty band on ΔT is more uniform than the uncertainty band based on the steam-side coefficient. A brief discussion of the uncertainty bands is presented in Appendix D, along with a listing of the uncertainty analysis program "UNA6" and a few sample runs.

D. EFFECTS OF FIN SPACING AND FIN HEIGHT ON PERFORMANCE

Data were taken on eight tubes (see Table II) with fins of rectangular shape (tubes number 26 thru 33) under vacuum (approximately 85 mmHg) and atmospheric conditions. Four tubes had a fin height of 0.5 mm, and fin spacings of 1.0, 1.5, 2.0, and 4.0 mm, while the remaining four tubes had a fin height of 1.5 mm, and the same sequence of fin spacings. Georgiadis [7] reported data on rectangularly-shaped fins with the same fin spacings, but with fin heights of 1.0 mm, and 2.0 mm. A complete listing of tubes tested by Georgiadis is also presented in Table II (tubes 1 thru 25).

Data reductions were performed on the HP 9826A computer, using a program named "DRP6." This program was essentially the same one used by Georgiadis ("DRP4"), with modifications to allow for variations in tube diameters, and tube material. Data obtained for all tubes tested during this thesis effort (tubes number 26 thru 44) are presented in Appendix C.

65

1. Effects of Fin Spacing

This section presents results showing the variations of the steam-side heat-transfer coefficient with heat flux having fin spacing as a parameter. Figures 5.2 and 5.3 present data for tubes with a fin height of 0.5 mm under vacuum and at atmospheric pressure respectively. The smooth tube data and the theoretical prediction of Nusselt are are included for comparison. In a similar way, Figures 5.4 and 5.5 present data for tubes with a fin height of 1.5 mm. These figures show that the best heat-transfer performance occurs for the tubes with a fin spacing of 2.0 mm, while the worst performance occurs for the tubes with a fin spacing of 4.0 mm. Note that these trends are the same both under vacuum and at atmospheric conditions.

The comparison of finned tubes is made through the enhancement ratio. This ratio is defined as the steam-side heat-transfer coefficient of a finned tube to that of the smooth tube (same diameter as the finned tube root diameter) at the same heat flux. As was shown by Georgiadis [7], the uncertainty in calculating the steam-side heat-transfer coefficient increases with decreasing heat flux; so, heat flux values of 0.35 and 1.0 MW/m² were chosen for vacuum and atmospheric conditions respectively. Cross plots of the enhancement ratio versus fin spacing are shown in Figures 5.6 and 5.7 for fin heights of 0.5, 1.0, 1.5. and 2.0 mm (curves representing e = 1.0 and 2.0 mm are from Georgiadis [7]). Enhancements as high as 4.8 and 6.4 can be seen for vacuum and atmospheric conditions respectively. Once again, fin spacings of approximately 2.0 mm for the tubes with fin heights of 0.5 and 1.5 mm are shown to provide the optimum performance. Data provided by Georgiadis [7] for fin heights of 1.0 and 2.0 mm, however, demonstrate an optimum heat-transfer performance for fin spacings of 1.5 mm. As a

66
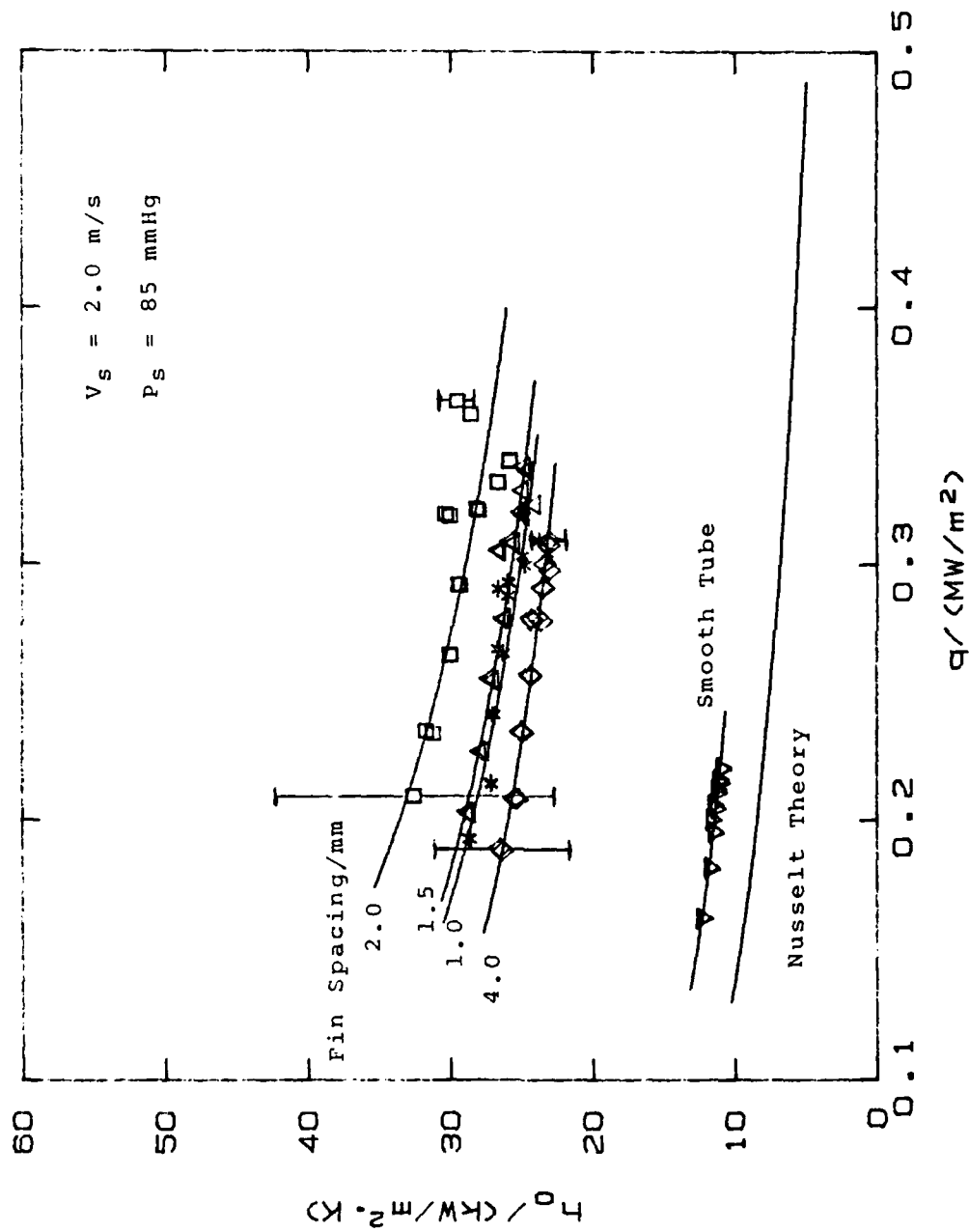
Figure 5.2 Variation of Heat-Transfer Coefficient with Heat Flux for the Set of Tubes with e = 0.5 mm (Vac. Run).

67
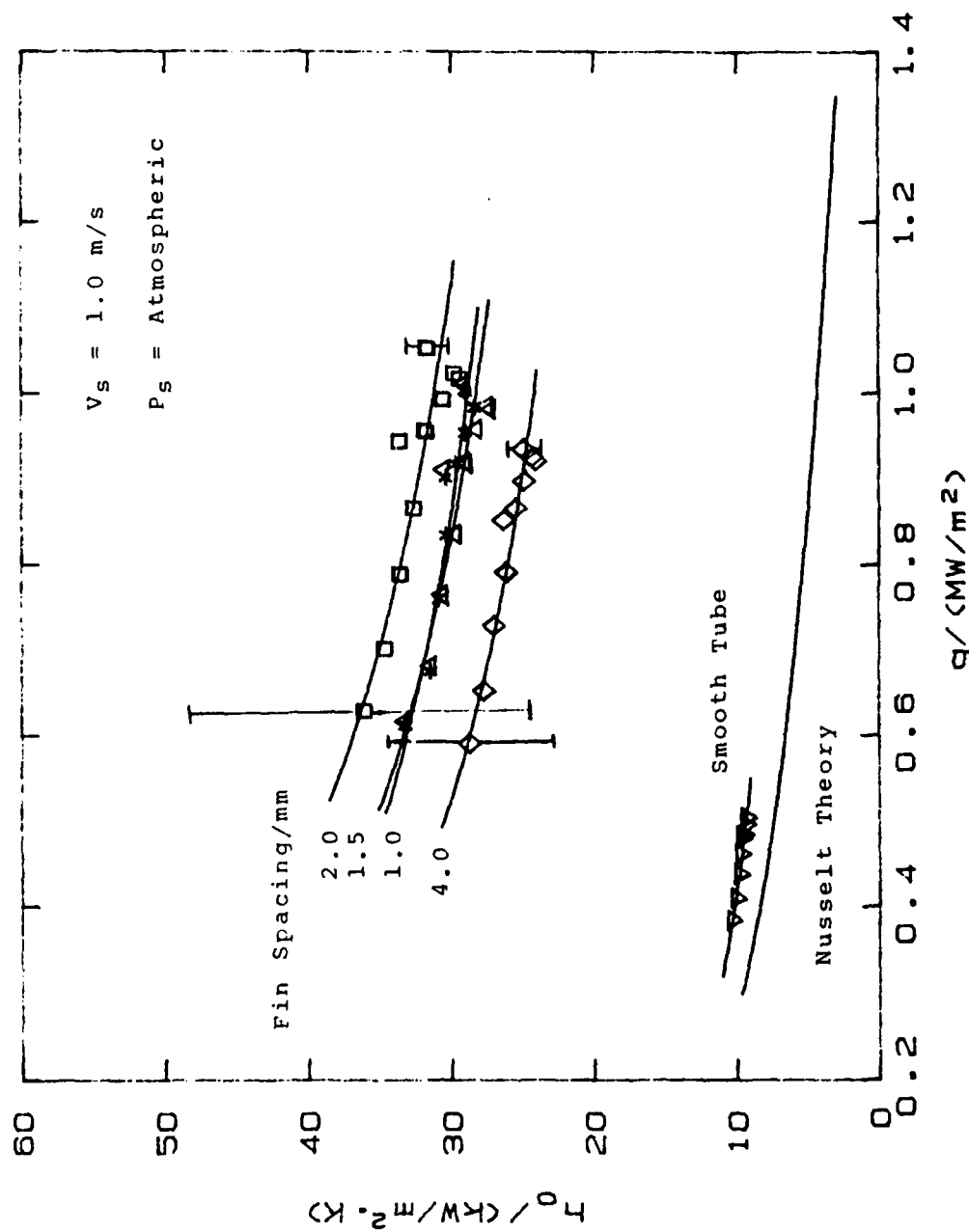
Figure 5.3 Variation of Heat-Transfer Coefficient with Heat Flux for the Set of Tubes with e = 0.5 mm (Atm. Runs).

68
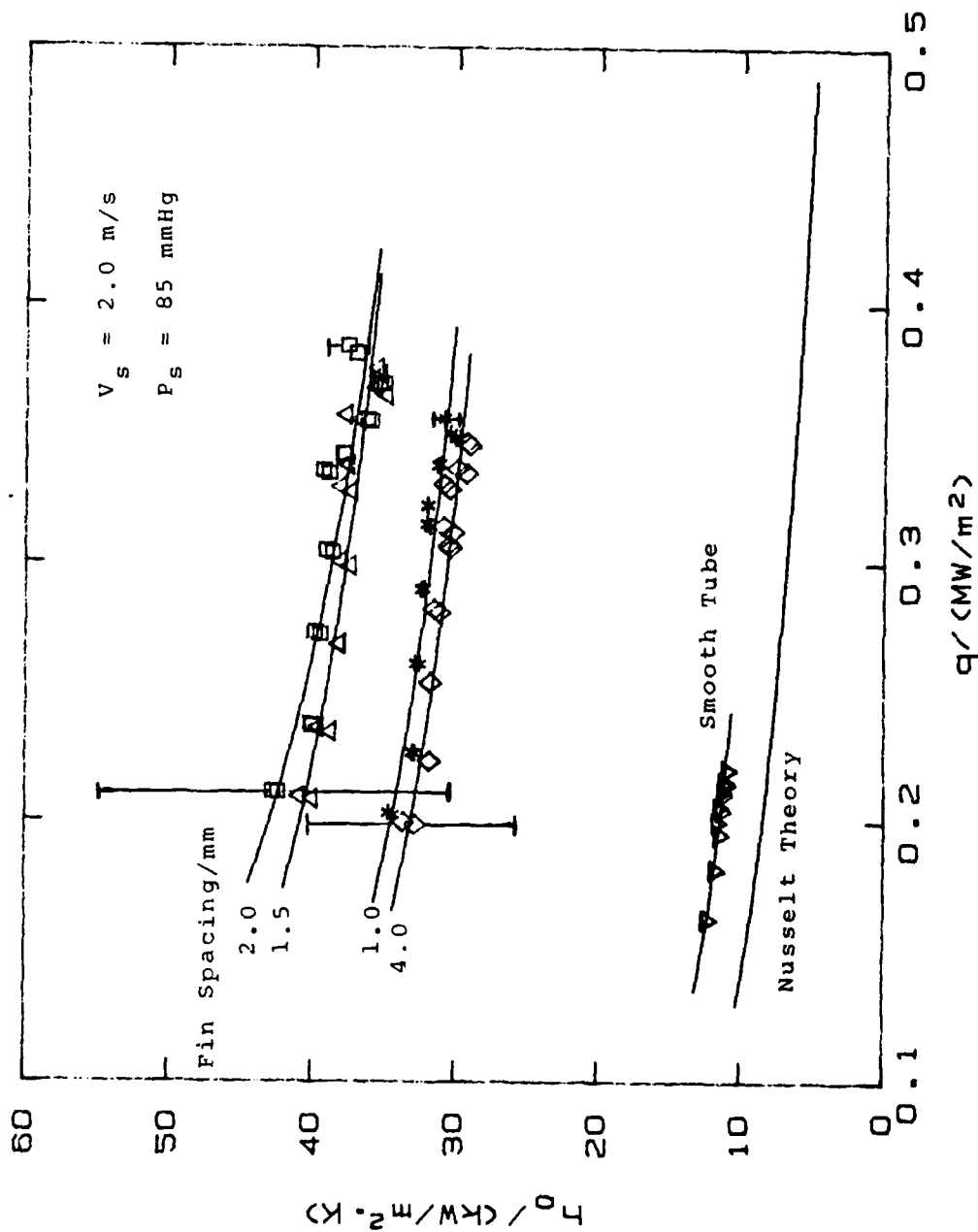
Figure 5.4 Variation of Heat-Transfer Coefficient with Heat Flux for the Set of Tubes with e = 1.5 mm (Vac. Runs).

69
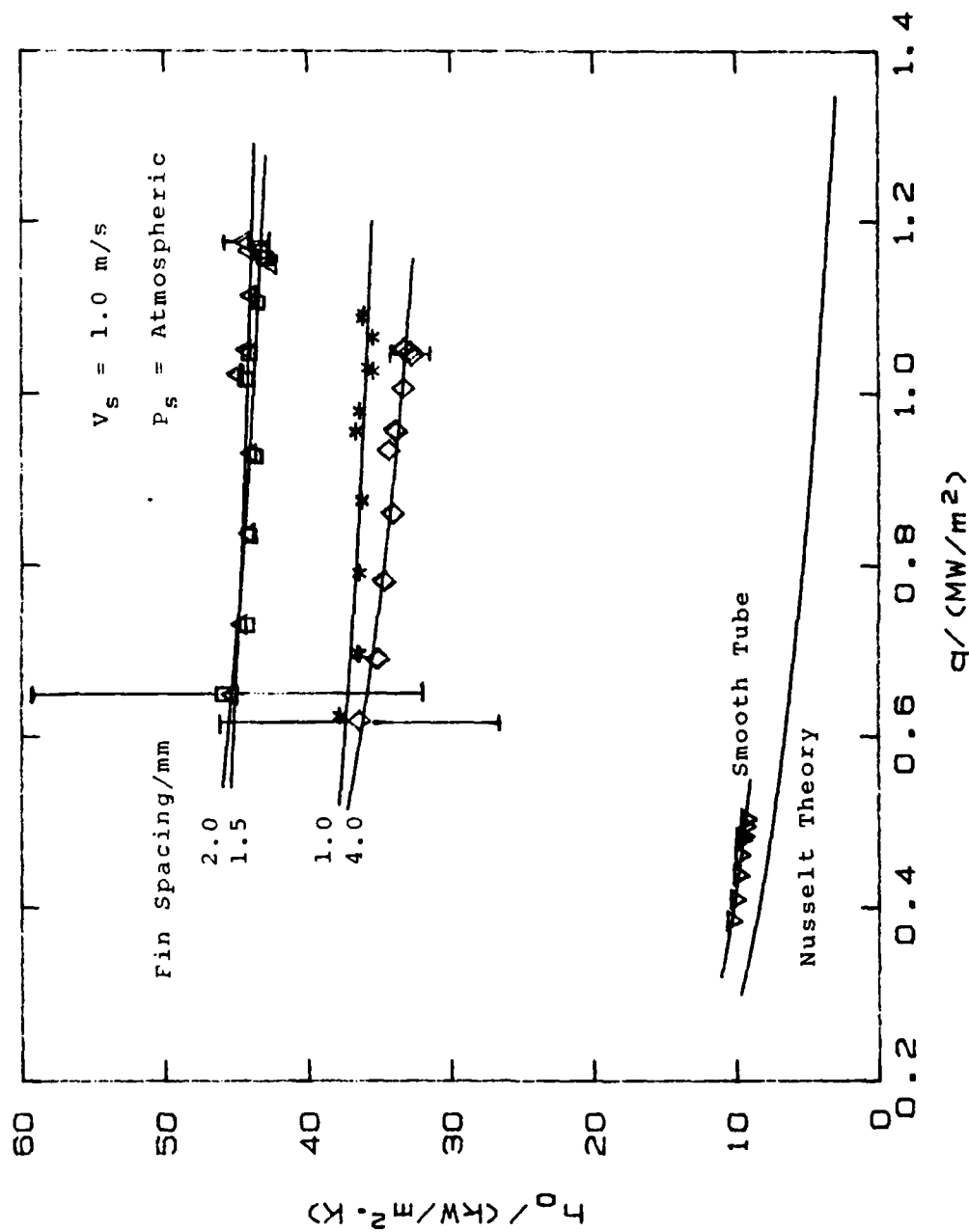
Figure 5.5 Variation of Heat-Transfer Coefficient with Heat Flux for the Set of Tubes with e = 1.5 mm (Atm. Runs).

70
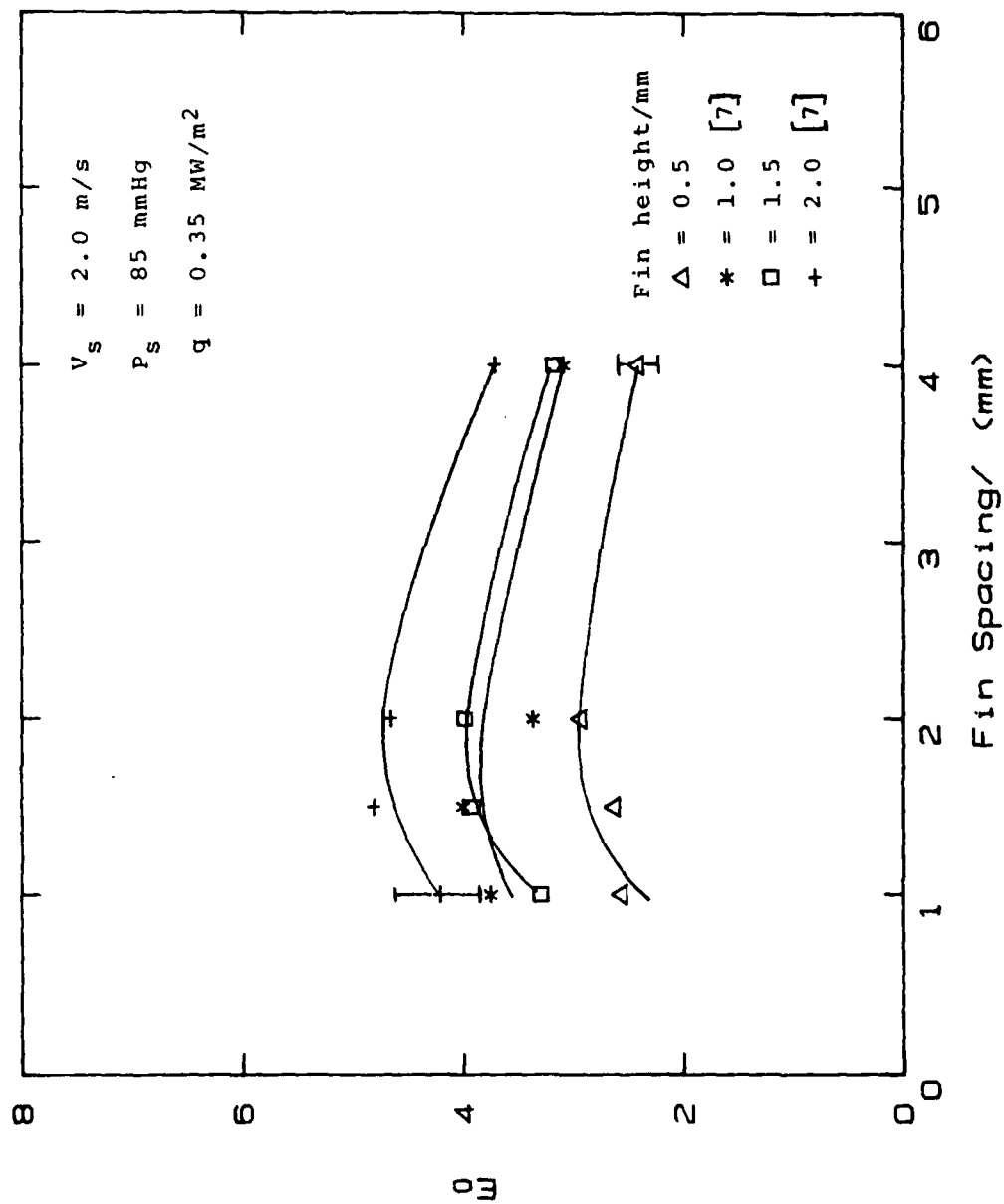
Figure 5.6 Cross Plot Showing Best Fin Spacing Among Tubes with e = 0.5, 1.0, 1.5, and 2.0 mm (Vac. Runs).

71
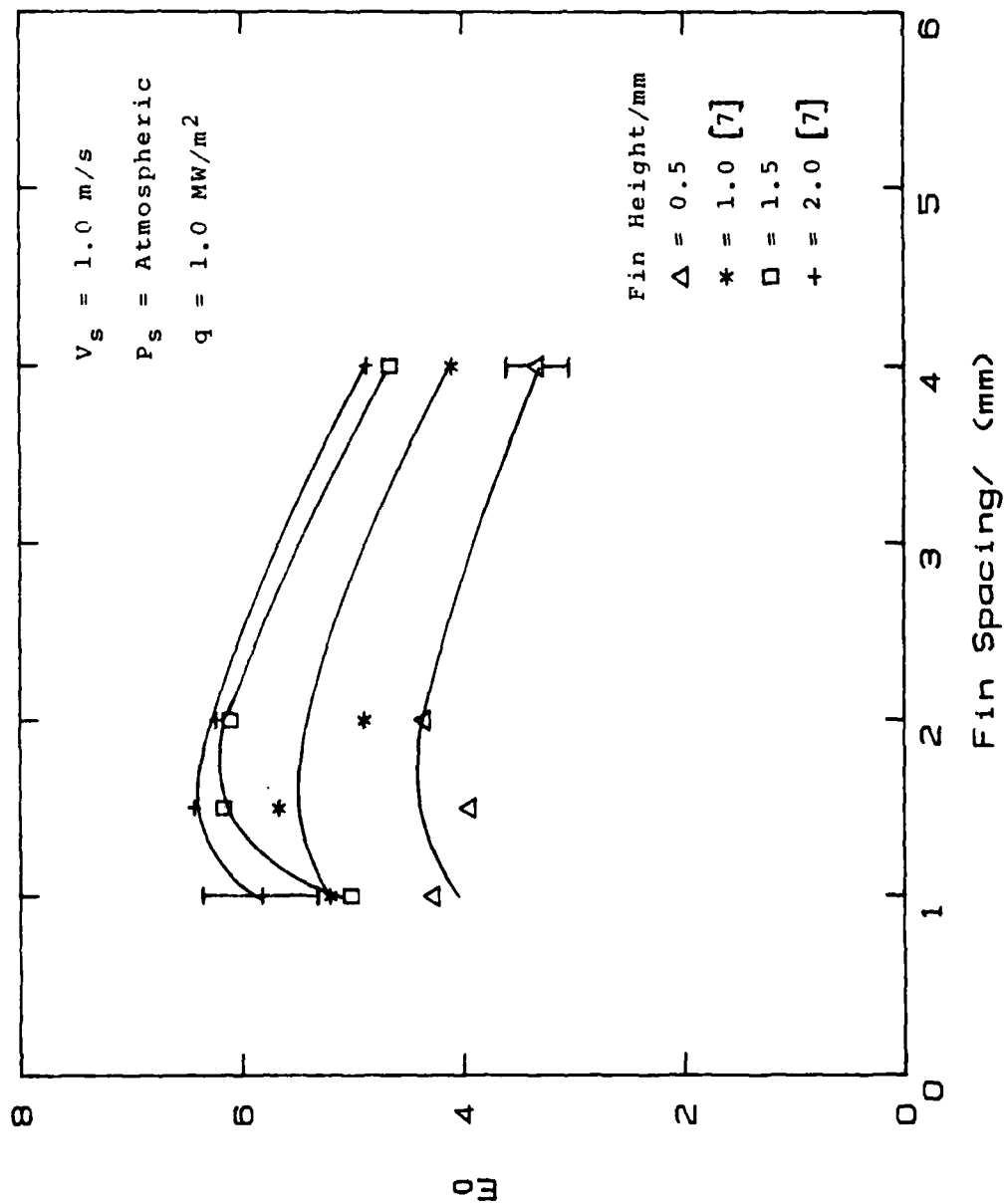
Figure 5.7   Cross Plot Showing Best Fin Spacing Among Tubes
with e = 0.5, 1.0, 1.5, and 2.0 mm (Atm. Runs).

72

result, there does not appear to be a clear trend for the optimum fin spacing as a function of fin height.

On one hand, the difference in performance between the s = 1.5 and 2.0 mm finned tubes, as well as the s = 0.5 and 1.0 mm finned tubes is less than the experimental uncertainty (± 15 percent), so that the optimum spacing may be somewhere between 1.5 and 2.0 mm. On the other hand, each data point in these figures has been repeated within 5 percent (i.e., computed steam-side heat-transfer coefficient) on different days. Also, as discussed earlier, the data taken on tubes 6 and 17 by Georgiadis were repeated within 3 percent during this investigation. Therefore, the slightly disagreeing trends shown by Georgiadis and by this investigator (see Figures 5.6 and 5.7) may be justified by the very complex nature of the condensation phenomenon on finned tubes.

The presence of an optimum fin spacing, however, is easy to understand. The 1.0-mm fin spacing, which provides the largest increase in surface area, performed worse than the 2.0-mm fin spacing due to the relatively large condensate retention angle with the 1.0 mm fin spacing. Visual observations showed that the condensate retention angle was around 110 degrees for the tube with s = 1.0 mm, while it was about 40 degrees for the tube with s = 2.0 mm. The additional thermal resistance induced by this layer of condensate overpowers the benefit gained from increased surface area, so the heat-transfer performance is reduced. As fin spacing increases, the condensate retention angle decreases, as does the thickness of the condensate film between fins on the upper portion of the tube. Beyond fin spacings of 2.0 mm, the decrease in surface area tends to overshadow the other effects, resulting in decreased heat-transfer performance compared to the tube with the "optimum" spacing.

2. Effects of Fin Height

As mentioned earlier, fin heights of 0.5 and 1.5 mm were examined during this thesis effort, and data for the tubes with fin heights of 1.0 and 2.0 mm were available from Georgiadis [7]. Table II shows that the general trend is an increase of enhancement ratio as fin height increases, which results from the increase of surface area provided by the higher fins.

To study the enhancement obtained beyond the increase in surface area due to finning, two additional columns are provided in Table II. These columns represent enhancement ratio/area ratio (Eo/Ar) at both vacuum and atmospheric conditions. As can be seen, Eo/Ar values range from 0.86 to 2.23 under vacuum conditions, and from 1.43 to 3.20 at atmospheric pressure. Figures 5.8 and 5.9 present plots of of Eo/Ar as a function of fin spacing under vacuum conditions, and at atmospheric pressure respectively. The relatively small values of Eo/Ar = 0.86 (vacuum) and Eo/Ar = 1.43 (atmospheric) for tube number 15 are due to the small fin spacing which results in a completely flooded tube. On the other hand, the values of Eo/Ar = 2.23 (vacuum) for tube number 14, and Eo/Ar = 3.20 (atmospheric) for tube number 28, show that significant enhancements beyond the area ratio are obtainable when the amount of condensate flooding is kept small. It appears that surface-tension forces are mostly responsible for this enhancement beyond the area ratio.

As discussed in Chapter II, the condensate thinning provided by surface-tension effects is related to the pressure gradient from the fin tip to the fin root. For short fins, this pressure gradient is relatively larger than for high fins, resulting in improved thinning of the condensate film. On the other hand, as fin height increases, surface

74
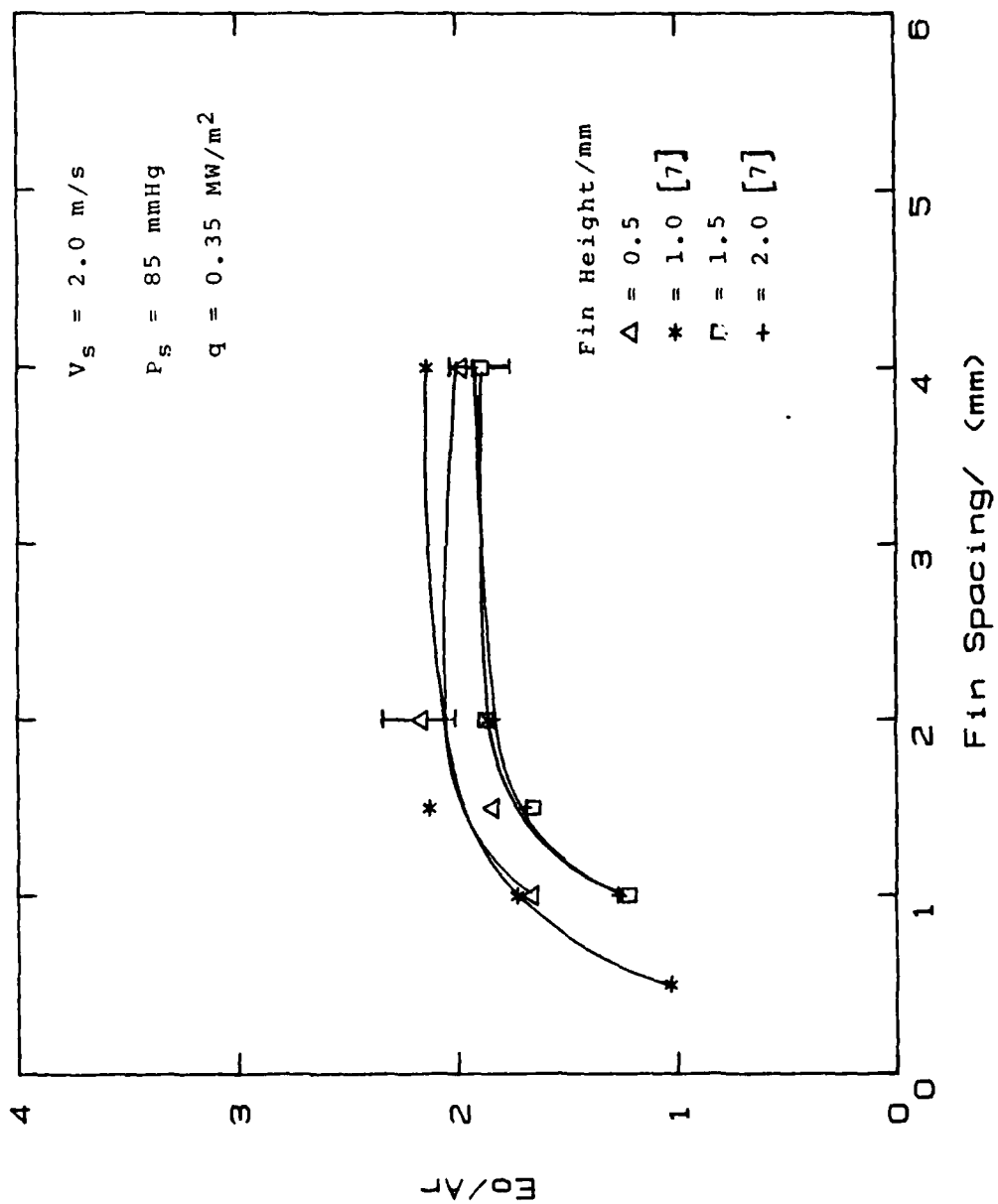
Figure 5.8 Cross Plot Showing Best Eo/Ar Among Tubes with e = 0.5, 1.0, 1.5, and 2.0 mm (Vac. Runs).

75
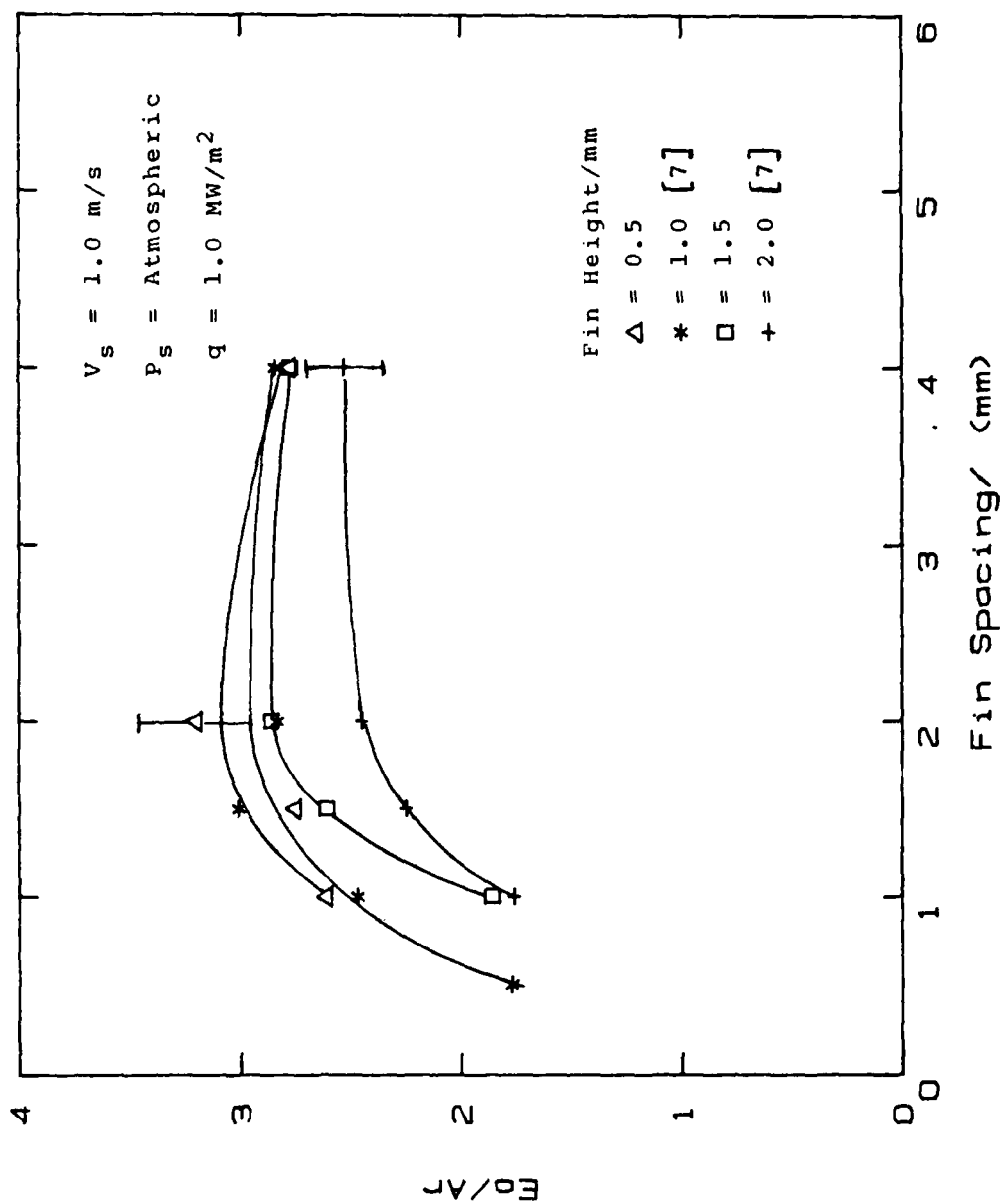
Figure 5.9 Cross Plot Showing Best Eo/Ar Among Tubes with e = 0.5, 1.0, 1.5, and 2.0 mm (Atm. Runs).

area increases and the condensate retention angle decreases. Both of these effects lead to increased heat-transfer performance, but when combined with the poorer thinning effect, the Eo/Ar ratio decreases somewhat for the larger fin heights.

E. EFFECT OF FIN GEOMETRY ON PERFORMANCE

In order to study the effect of fin geometry, data were taken on tubes with fins of triangular, trapezoidal, and parabolic shapes (tubes number 34, 35, 37, 38), as well as on a spirally-finned tube with threads of triangular shape (tube number 36). Fin dimensions (i.e., fin spacing, height, and thickness) for these tubes were chosen so that the resulting total surface areas would be approximately equal to that of the "optimum" tube with rectangularly-shaped fins and a fin height of 1.0 mm (tube number 6). In this manner, the effects of increased surface area were eliminated, allowing a comparison between tubes where fin geometry was the only variable. A commercially-available "Wolverine" tube (tube number 43), whose fin geometry is shown in Figure 3.5(c), was also tested. Dimensions for the above fins are given in Table II.

1. Effect of Fin Shape

This section examines the effect that fin shape has on the heat-transfer performance of finned tubes. The performance of tubes number 34, 35, 36, 37, and 43 under vacuum conditions is shown in Figure 5.10, while Figure 5.11 depicts their performance at atmospheric pressure. The dashed curve in these figures represents a least-squares fit for data taken on the "optimum" tube with rectangularly-shaped fins and a fin height of 1.0 mm (tube number 6). In both cases, the "Wolverine" tube (tube number 43) gave the

77
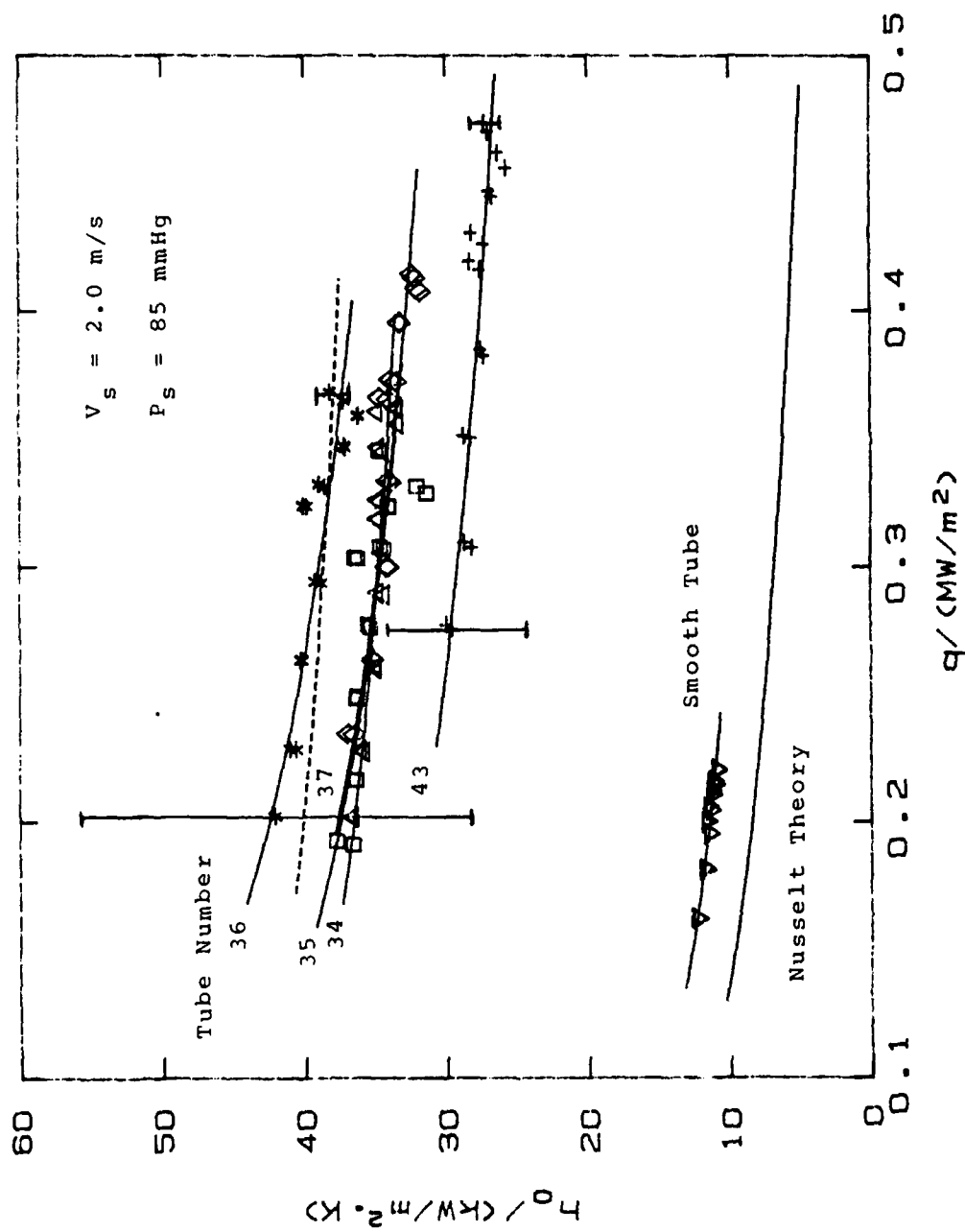
Figure 5.10 Variation of Heat-Transfer Coefficient for Tubes with Pins of Different Shapes (Vac. Runs).

78
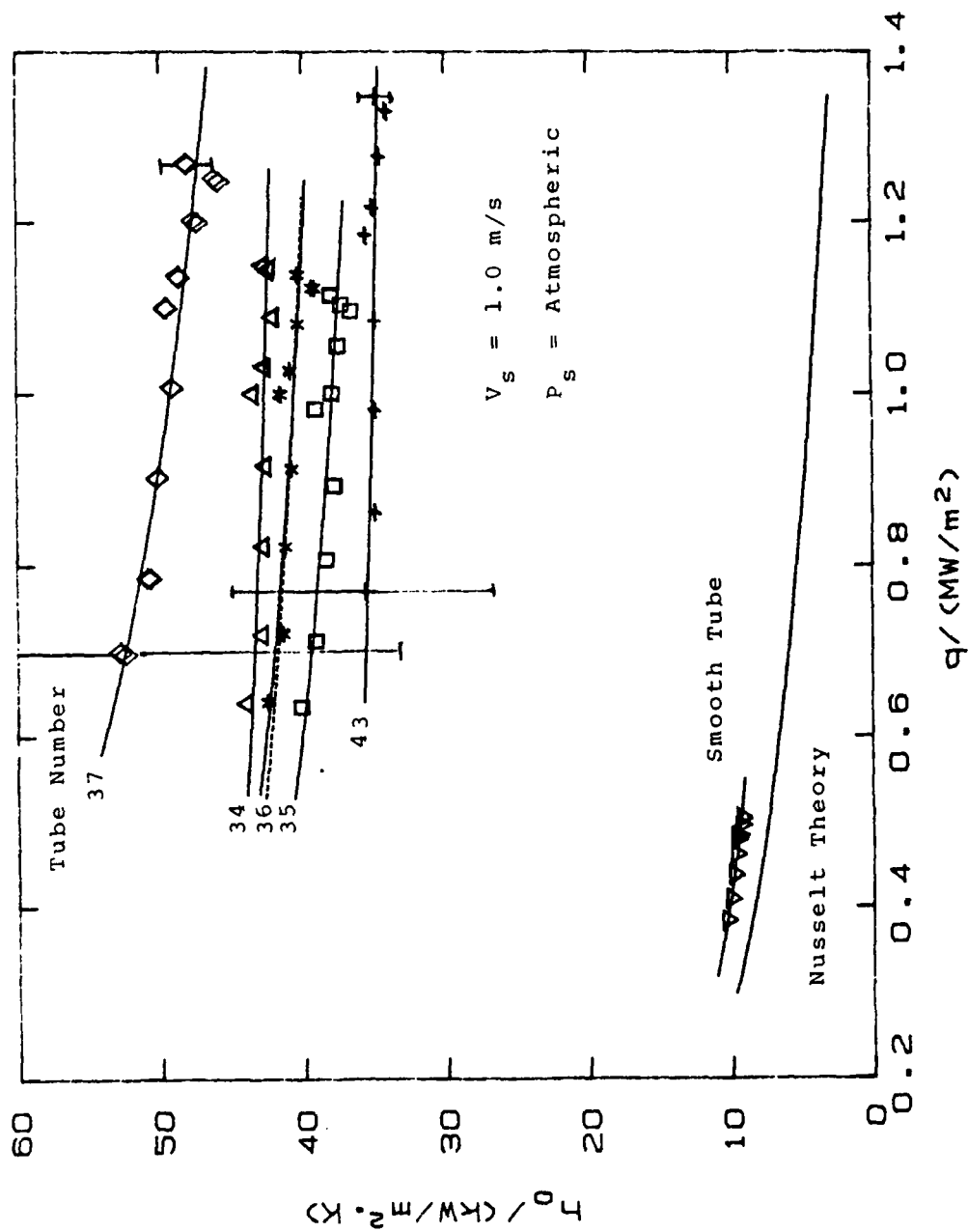
Figure 5.11 Variation of Heat-Transfer Coefficient for Tubes
With Fins of Different Shapes (Atm. Runs).

worst performance. This was due primarily to the small fin spacing (0.7 mm) that resulted in a completely flooded tube. Based on the results of Georgiadis [7], the small fin thickness (0.3 mm) of the Wolverine tube may also be responsible for its poor performance. Georgiadis showed that for a fin spacing of 1.0 mm the tubes with a fin thickness of 0.5 mm (tube number 16) performed 16 percent and 6 percent poorer, under vacuum and at atmospheric pressure respectively, than the tube with a fin thickness of 1.0 mm (tube number 5). Based on this observation, the small fin thickness is also responsible for the poorer performance of the "Wolverine" tube in comparison, for example, to the tube with fins of parabolic shape (tube number 37), which was also completely flooded by condensate. Therefore, the poor performance of this tube is probably due more to increased condensate flooding and smaller fin thickness than to fin shape. On the other hand, the best performance was observed for the spirally-finned tube (tube number 36) under vacuum conditions, and the tube with parabolic fins, where fin spacing was 0.7 mm (tube number 37), at atmospheric pressure. The fact that tube number 37 performed well at atmospheric pressure, but poorer than the spirally-finned tube under vacuum conditions was somewhat unexpected. It must be kept in mind that these data runs were repeated at least three times on different days, thus confirming this trend. One possible explanation centers on variable fluid properties, as discussed below.

Under vacuum conditions, the condensate retention angle is significantly smaller for tube number 36 (about 30 degrees) than for tube number 37 (completely flooded), and the saturation temperature is about 50 K lower. Therefore, the relatively high heat-transfer coefficient of the spirally-finned tube is due mainly to its small condensate retention angle. When the condensing temperature is raised,

80

both surface tension and viscosity decrease. For example, the surface tension decreases by about 10 percent, and the viscosity decreases by about 45 percent when the temperature is raised from 40 °C to 90 °C (assumed approximate film temperatures). Decreased viscosity should result in higher heat-transfer coefficients at atmospheric pressure than under vacuum conditions for a given tube. Further, it may be possible that the effect of viscosity is dependent on the fin shape. Unfortunately, no equations exist to support this hypothesis. The effect of surface tension, on the other hand, is fairly well understood; the condensate reten- tion angle decreases with decreasing surface tension. Therefore, the reduction in retention angle (from vacuum to atmospheric pressure) for the tube with "parabolic" fins is greater than the reduction for the spirally-finned tube, since the latter was already small under vacuum conditions. Thus, the reduced retention angle on the tube with "para- bolic" fins provides an increased heat-transfer performance, surpassing the performance of the spirally-finned tube.

The performance of the remaining two tubes (tubes number 34 and 35) is the same under vacuum conditions, but at atmospheric pressure, the tube with triangularly-shaped fins (tube number 34) outperformed the tube with trapezoidal fins (tube number 35) by about 10 percent. An argument similar to the one above may explain this behavior.

2. Effects on Enhancement Ratio

Referring to Table II, it can be seen that all of the above tubes provided significant heat-transfer enhance- ments over smooth-tube values. Note that the enhancement obtained under vacuum conditions for tube number 36 was the same as obtained for the "optimum," rectangularly-shaped finned tube with the same fin height (tube number 6). Under atmospheric conditions, however, the tube with fins of

81

parabolic shape (tube number 37) performed significantly better than any of the tubes with rectangular fins of the same height (1.0 mm).

Like the tubes with rectangular fins, most of these tubes displayed enhancements above the area ratio, as shown by the two Eo/Ar columns in Table II. These ratios range from 0.94 to 2.95 under vacuum conditions, and from 1.52 to 4.13 at atmospheric pressure. Like tube number 15, the small values of 0.94 and 1.52 for the "Wolverine" tube resulted from the large amount of retained condensate, and by the very thin fins (about 0.3 mm) as discussed earlier. As was the case for rectangular fins, the highest Eo/Ar of 2.95 and 4.13 were shown for the tube (tube number 36) with a relatively small area ratio of 1.37, indicating once again the importance of surface-tension effects.

3. The Performance of "Parabolic" Fins

In order to study the parabolic fin more closely, a tube with parabolic fins was manufactured (tube number 38) with the same fin height, spacing, and thickness as tube number 17 (tested by Georgiadis [7] and this investigator). The performance of these two tubes is compared in Figure 5.12 under vacuum conditions, and in Figure 5.13 at atmospheric pressure. Clearly, the parabolic fins provide a greater enhancement than the rectangular fins. The reason for this, as mentioned earlier, is probably the continuous change of radius of curvature (increasing from the trough area to fin tip) for the parabolic shape. The resulting pressure gradient along the fin height is more favorable (than on rectangular fins), which, in turn, leads to improved drainage from the fin surface. This effect was seen most clearly on tube number 37. Another observation (that contributes to improved heat transfer) made on the tube with "parabolic" fins is that, although completely

82
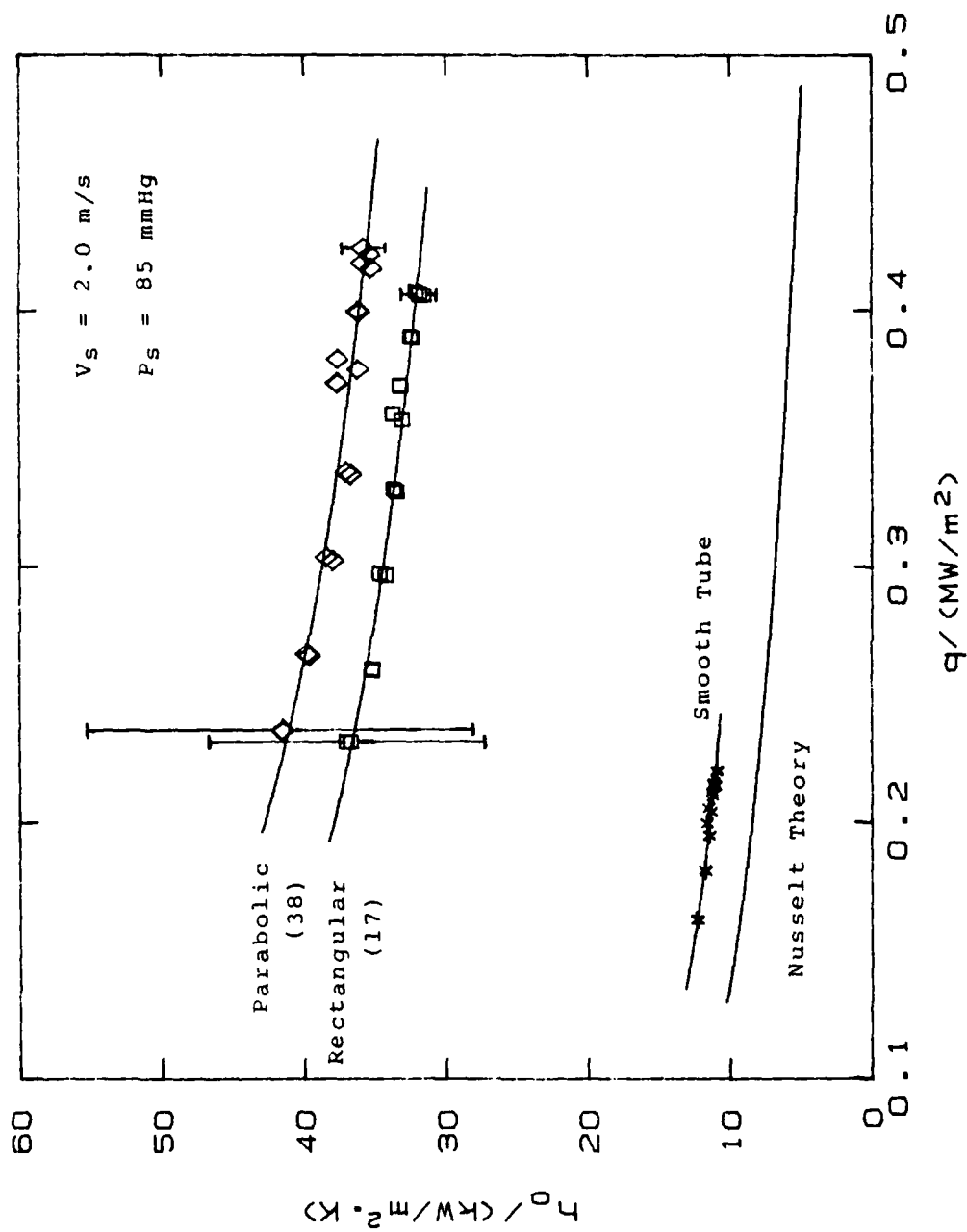
Figure 5.12   A Comparison Between Fins of Rectangular Shape and Parabolic Shape (Vac. Runs).

83
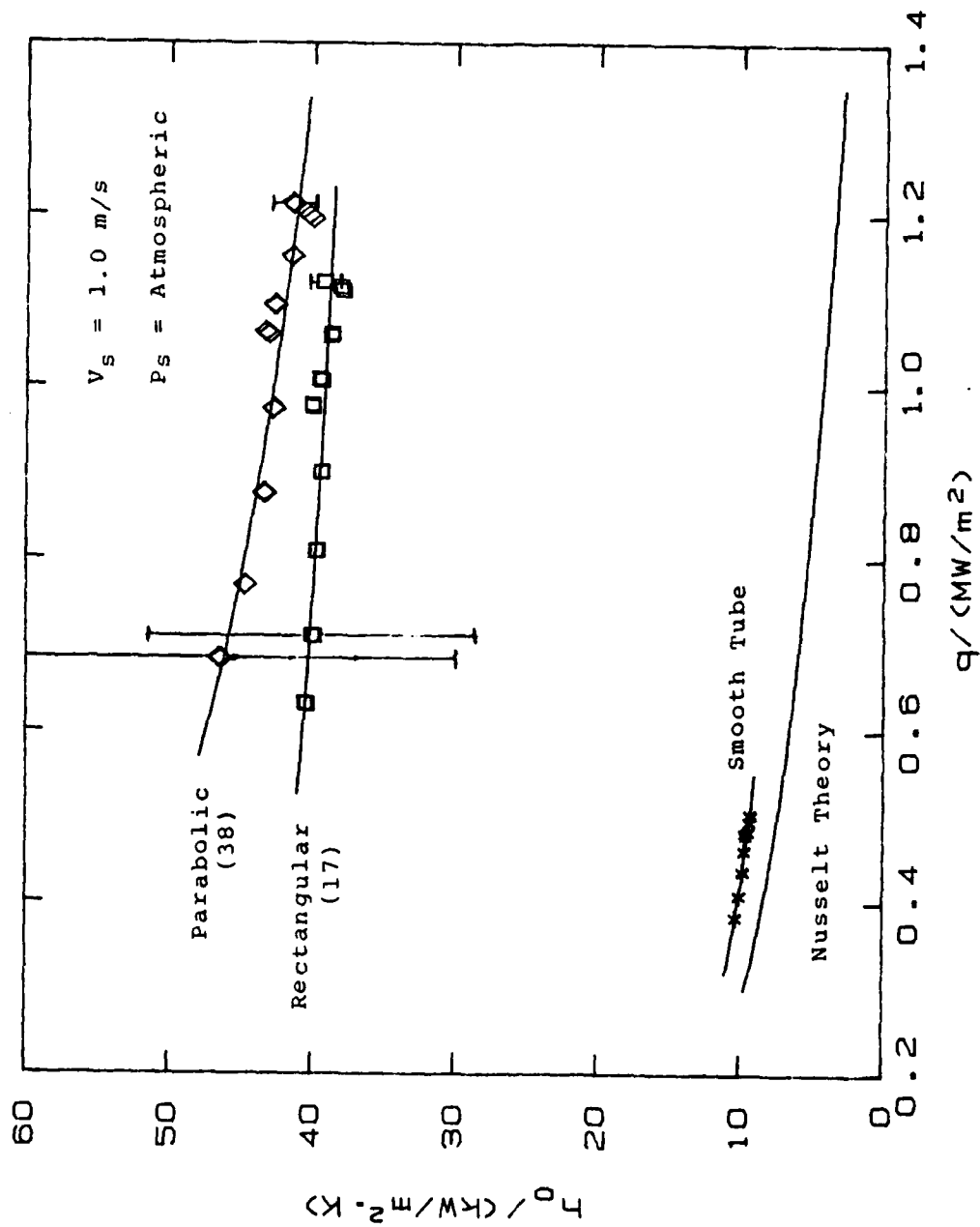
Figure 5.13   A Comparison Between Fins of Rectangular Shape and Parabolic Shape (Atm. Runs).

flooded, the fin tips (about half the fin height) were visible along the majority of the fin circumference (except for about the bottom 30 degrees).

As discussed in section E.1, tube number 37 performed poorer than the spirally finned tube (tube number 36) under vacuum conditions. The reasons for this are not fully understood; so, further tests of these fin geometries (i.e., spiral and parabolic) should be performed.

F. EFFECT OF FIN-METAL THERMAL CONDUCTIVITY ON STEAM-SIDE COEFFICIENT

To investigate the effect of fin-metal thermal conductivity on the heat-transfer performance, a stainless steel tube (tube number 40) was manufactured with the same fin dimensions as the "optimum" copper tube (tube number 6) with rectangular fins, and a fin height of 1.0 mm. Due to the low thermal conductivity of stainless steel, it was necessary to reduce the tube wall thickness to 0.5 mm to prevent an excessive wall thermal resistance. A copper tube (tube number 39) with the same dimensions as the stainless steel tube was manufactured for comparison. Also, two smooth tubes having an outside diameter equal to the root diameter of the finned tubes (tubes number 41 and 42) were manufactured; the first tube was made of copper, and the other was made of stainless steel. The results for data runs taken under vacuum conditions, and at atmospheric pressure are shown by Figures 5.14 and 5.15 respectively.

As expected, the copper finned tube provided a significant enhancement, while the stainless steel finned tube actually reduced the heat-transfer performance slightly in comparison to the smooth tube (tube number 42). The thermal conductivity of stainless steel is much lower than that of copper (i.e., 15 W/m.K compared to 385 W/m.K), so the

85
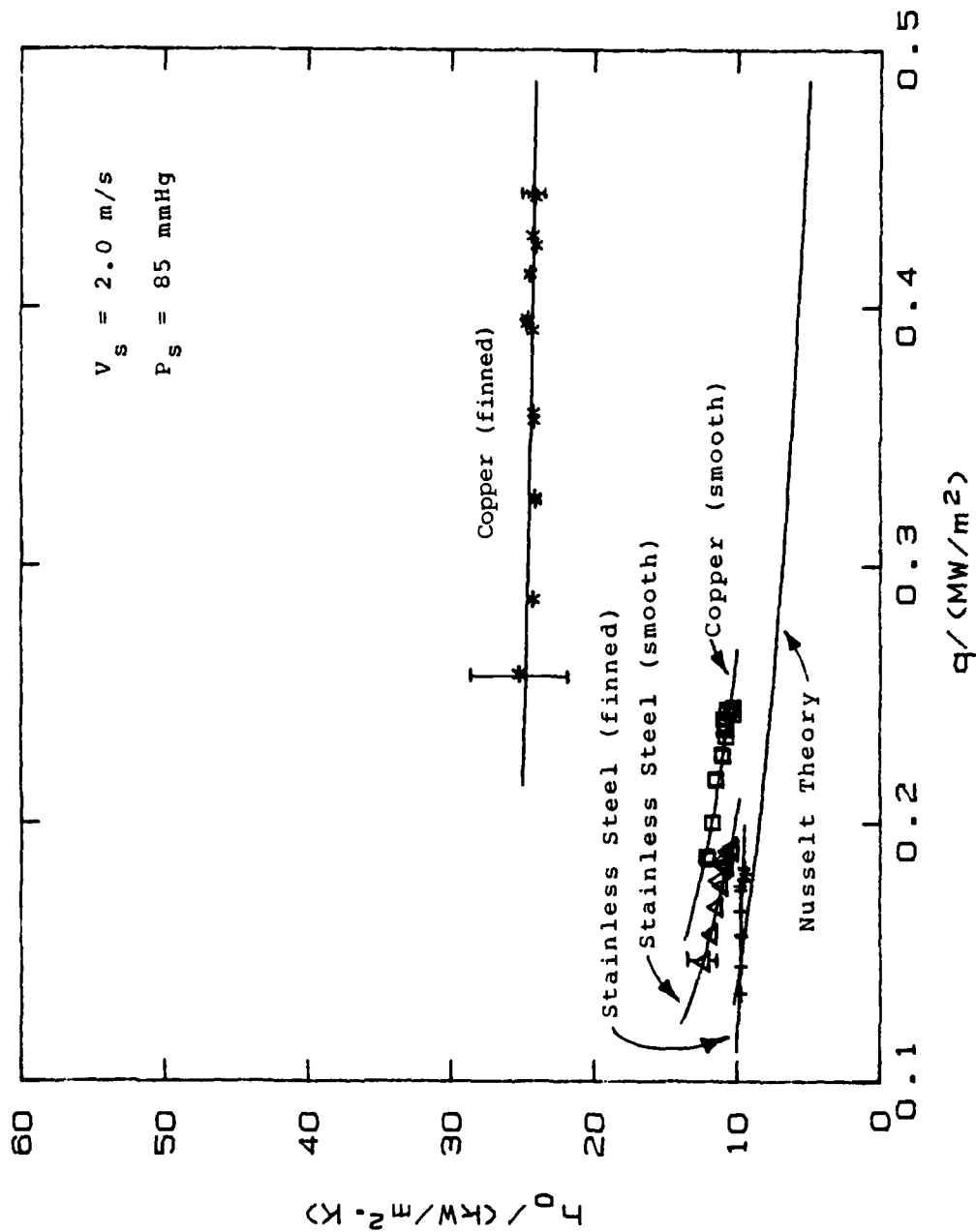
Figure 5.14 Comparison of Heat-Transfer Performance Between Stainless Steel and Copper Tubes (Vac. Runs).

86
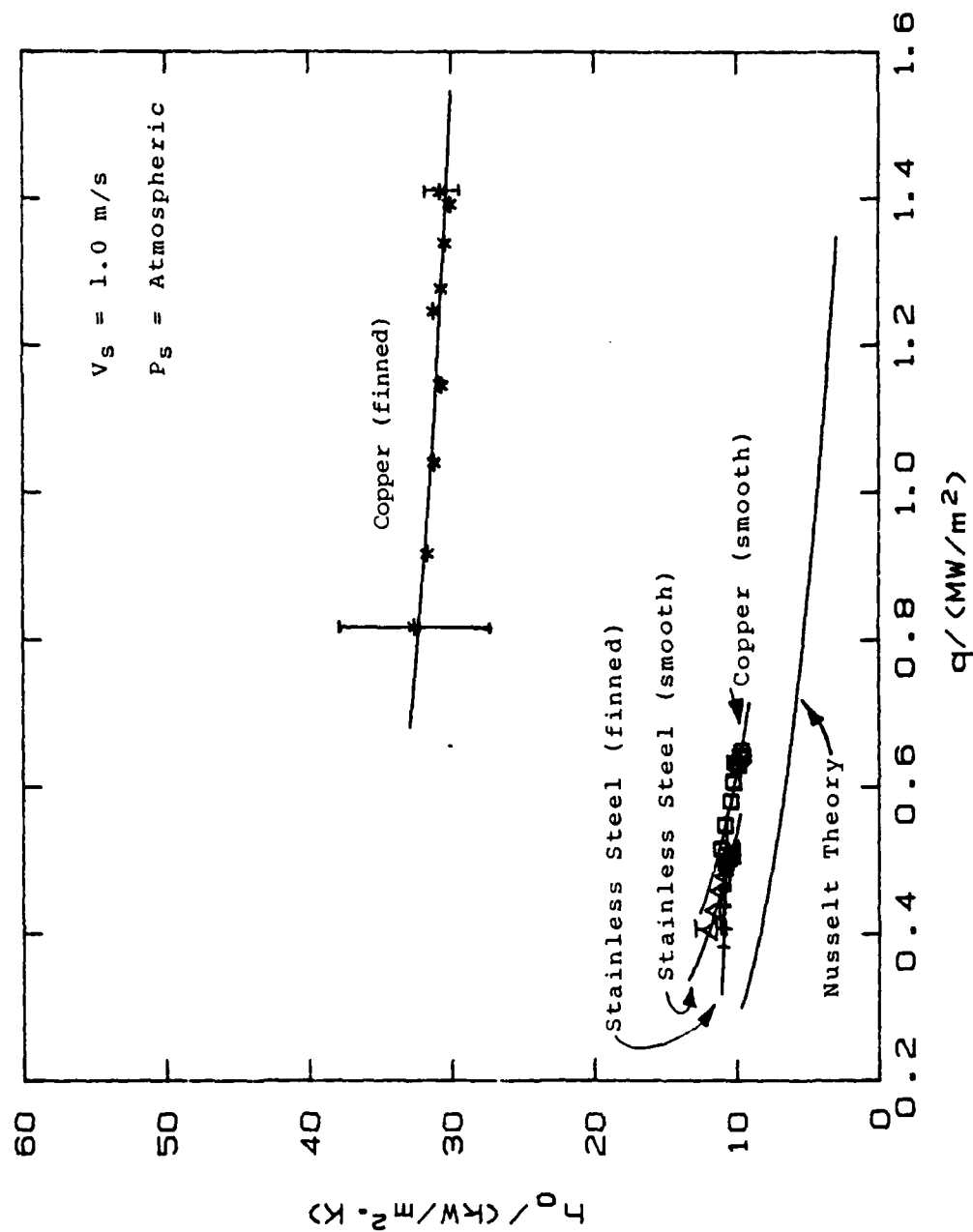
Figure 5.15 Comparison of Heat-Transfer Performance Between Stainless Steel and Copper Tubes (Atm. Runs).

87

thermal resistance of the stainless steel fins is significantly higher, resulting in a poorer fin efficiency. This is combined with the deleterious effects of retained condensate (introduced by the use of fins) so that the above factors dominate over the beneficial thinning of the condensate film between fins. The net effect, then, is a slight degradation of the heat-transfer performance compared to a smooth tube.

G. EFFECT OF STEAM VELOCITY

As discussed in Chapter II, most models of film condensation on finned tubes have neglected the effect of vapor shear. For this reason, a decision was made to perform runs for the "optimum" tube (tube number 6) with rectangular fins, and fin height of 1.0 mm, at nominal steam velocities of 2, 4, 6, and 8 m/s. Steam velocity through the test section was controlled by the boiler input power, and since a steam velocity of 1 m/s was the maximum obtainable at atmospheric pressure, the data runs were performed under vacuum conditions only. The results of data taken for the above-mentioned steam velocities are shown in Figure 5.16.

The trend shown in Figure 5.16 indicates that increased steam velocity (i.e., increased vapor shear) leads to enhancements of up to 10 percent as steam velocity increases from 2 to 8 m/s. This is to be expected since the shear stress at the liquid-vapor interface tends to pull the condensate toward the bottom of the tube, thereby thinning the condensate film at the top part of the tube.

The above-mentioned data were compared to data taken by Yau et al. [1] for steam velocities of 0.5, 0.7, and 1.1 m/s at atmospheric pressure. They reported enhancements of up to 40 percent for the steam velocity of 1.1 m/s compared to the 0.5 m/s velocity. The rather large

88
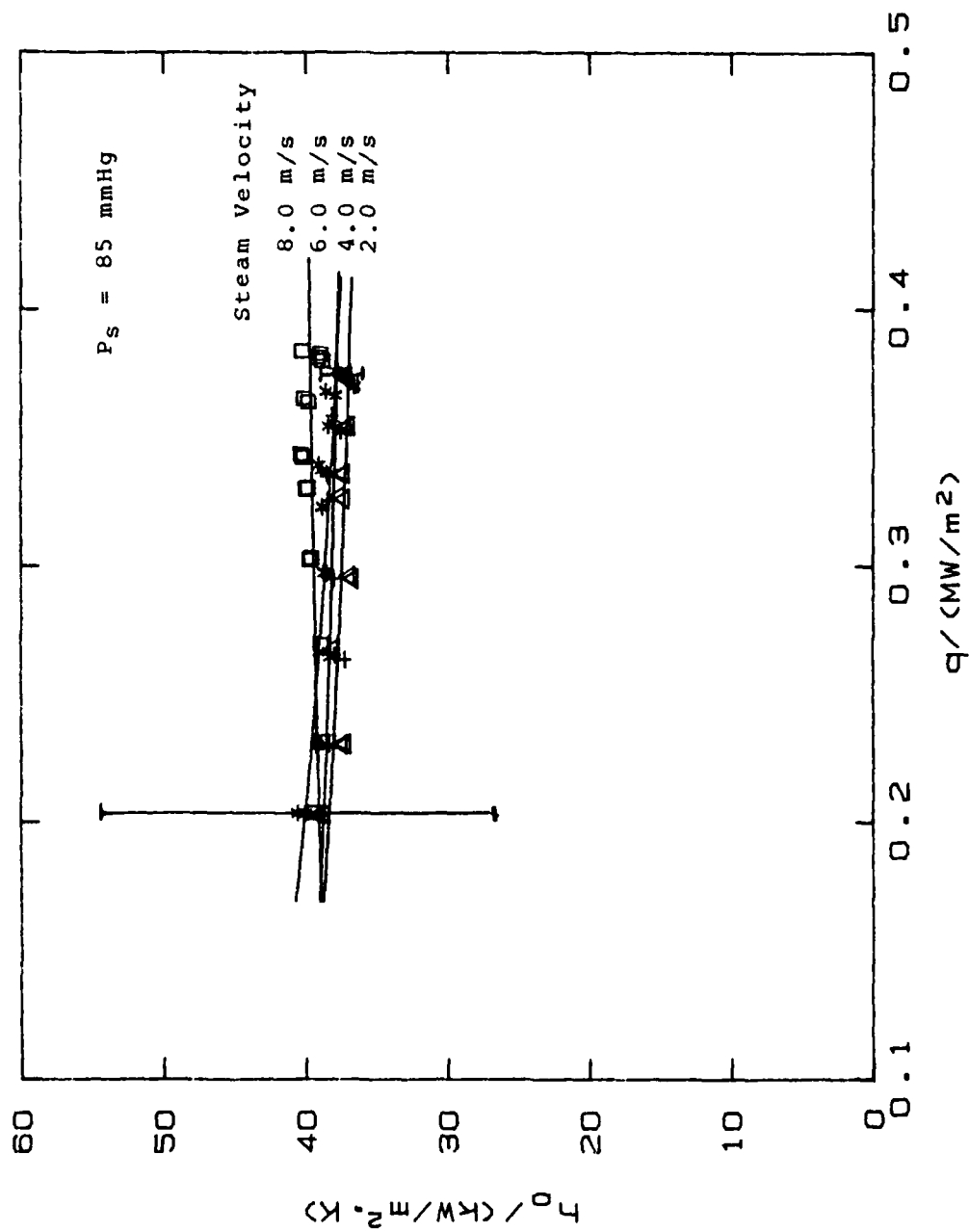
Figure 5.16 Effect of Steam Velocity on Heat-Transfer Performance on Finned Tube Number 6.

difference in enhancements reported by Yau et al. compared
to those of this investigation was not expected. It should
he kept in mind, however, that the data of Yau et al. were
collected at atmospheric pressure (compared to vacuum condi-
tions for this investigation), where the increased satura-
tion pressure leads to a lower condensate viscosity (about
45 percent as discussed in section E.1). This, in turn,
allows condensate to flow more freely so that the effect of
shear stresses acting on the liquid-vapor interface would be
more pronounced. Another factor to be considered is the
slightly larger fin spacing used by Yau et al. (2.0 mm
compared to 1.5 mm for this investigation). If the fin
spacing is very small, the vapor shear may not be "felt" on
the sides of the fins or on the fin bases. This is due to
the fact that the steam flows around the tube, thus leaving
nearly stagnant steam between fins. As the fin spacing
increases though, the fin sides and bases will be more
"accessible" to steam, therefore, giving rise to the benefi-
cial effects of vapor shear. Thus, the larger enhancements
of Yau et al. [1] compared to this investigation may be
explained by the two phenomenon just described.

An attempt was made to correlate the data using a
Fujii-type [29] equation given by:

$$\frac{Nu}{Re_{rp}^{0.5}} = c\ F^d \tag{5.3}$$

where

$$Nu = \frac{h_{af}\ D_o}{k_f} \tag{5.4}$$

90

$$Re_{tp} = \frac{\rho_f\ V_s\ D_o}{\mu_f} \tag{5.5}$$

$$F = \frac{g\ D_o\ \mu_f\ h_{fg}}{V_s^2\ k_f\ \Delta T} \tag{5.6}$$

V_s = steam velocity

h_{af} = steam-side heat-transfer coefficient based
on actual surface area (including fins)

Re_{tp} = two-phase Reynolds number

c, d = constants to be determined experimentally

The constants c and d used in the Fujii equation [29], which was developed to account for vapor shear on smooth tubes, were 0.96 and 0.2 respectively. Values of c = 1.302 and d = 0.236, however, were found to more closely fit the data of this investigation after a least-squares fit was performed. A comparison of the experimental data to this curve is shown in Figure 5.17. Although a fairly close agreement has been obtained, the orientation of data clusters does not match the slope of the least-squares line generated by globally fitting all the data. It is possible that the errors in the experimental constants used in the Sieder-Tate-type equation are partly responsible for this questionable trend. Georgiadis [7] showed that using larger values (from the "modified Wilson method") of the Sieder-Tate coefficient (C) tends to rotate the data clusters to more closely match the experimental correlation. Further, a Fujii-type correlation may be inappropriate for finned tubes due mainly to condensate retention that occurs.

91
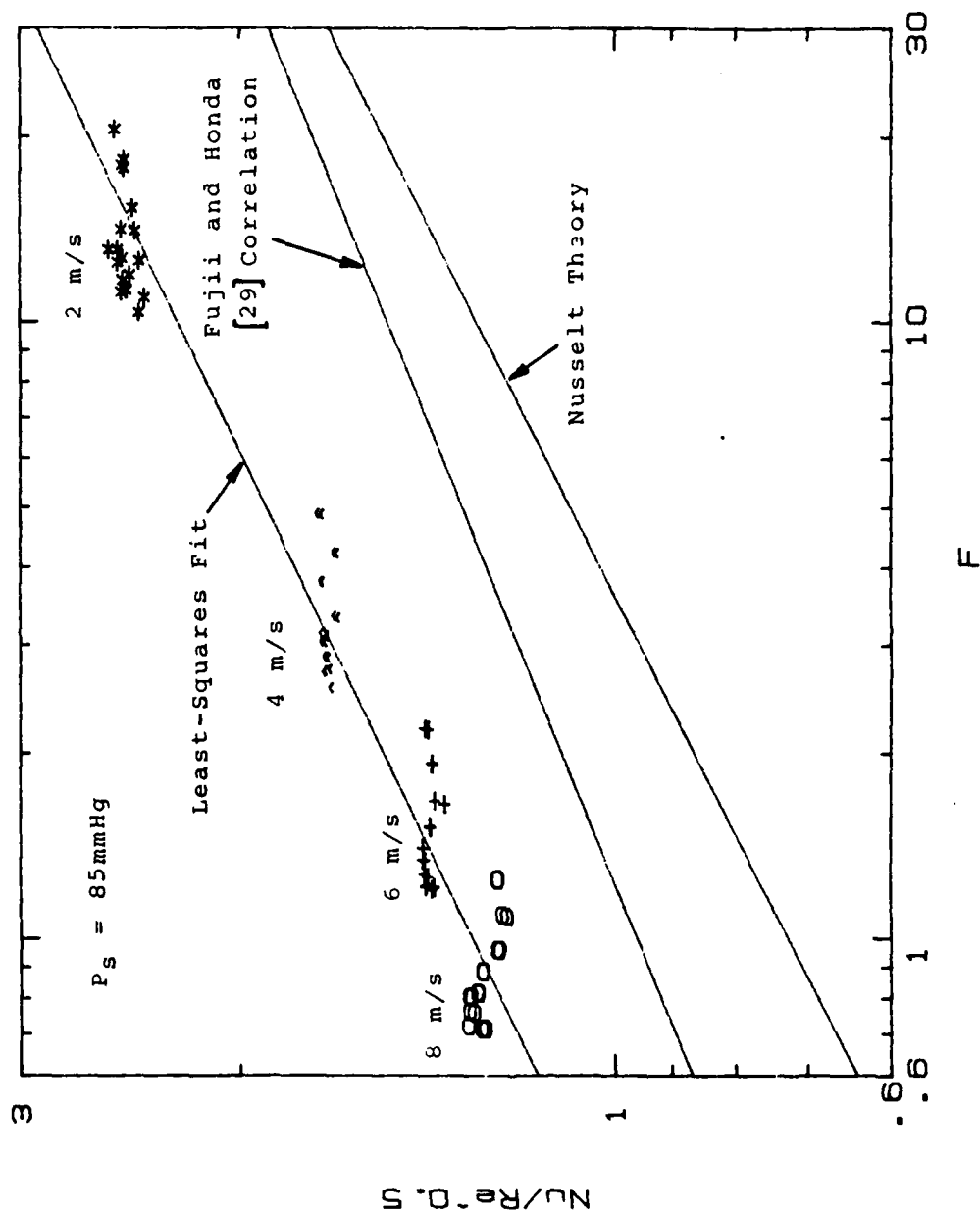
Figure 5.17 Comparison of Experimental Data to a Fujii-Type Equation (Equation 5.3).

Note that the slope of the line predicted by equation (5.3) for the experimental data does not match the slope of the Fujii equation mentioned earlier, but instead, nearly matches the slope of the Nusselt equation for smooth tubes given by:

$$h = 0.728 \left[\frac{k_f^3 \, \rho_f^2 \, g \, h_{fg}}{\mu_f \, D_o \, \Delta T} \right]^{1/4} \tag{5.7}$$

which can be rewritten as:

$$\frac{Nu}{Re_{tp}^{0.5}} = 0.728 \, F^{1/4} \tag{5.8}$$

In this manner, the effect of vapor shear, at least on the tube tested (tube number 6), is very small compared to smooth tubes [7]. In fact, using the experimentally-found d-value in equation (5.3), the steam-side coefficient and steam velocity are related as follows:

$$h \sim V_s^{0.028} \tag{5.9}$$

Once again, this observation shows that the effect of steam velocity on the steam-side heat-transfer coefficient is very small.

A vertical shift of the least-squares-fit compared to the Nusselt theory results from the insreased c-value (1.302 compared to 0.728) of equation (5.8). In fact, the ratio of the experimental c-value to the coefficient in the Nusselt equation (i.e., 1.302/0.728 = 1.788) represents the heat-transfer enhancement in excess of the area increase due to

93

finning. Therefore, the c-value depends fin geometry, and surface tension of the condensate etc..

In view of the above discussion, further attempts to modify the Nusselt equation to include vapor shear, surface-tension effects, and fin geometry etc. may lead to an accurate correlation for the steam-side heat-transfer coefficient for finned tubes.

H. EFFECT OF INTERNAL AND EXTERNAL ENHANCEMENTS ON THE OVERALL COEFFICIENT

Up to this point, all discussions have delt with enhancements to the steam-side heat-transfer coefficient. Even with large steam-side enhancements, however, a large thermal resistance through the tube wall, or on the water side may dominate, and completely negate the steam-side enhancement. For this reason, a decision was made to test the "optimum" tube with rectangular fins (fin height of 1.0 mm - tube number 6), and the corresponding smooth tube (tube number 1), with and without the insert. The results of these data runs, taken under vacuum conditions, are shown in Figure 5.18. At a water velocity of about 3 m/s, use of the insert in the smooth tube resulted in a 40 percent increase of the overall coefficient, as did the use of external fins without the insert. By combining the use of fins and the insert, an enhancement of nearly 155 percent was attained. It must be noted, however, that the insert used during these experiments is not suited for use in condensers due to the very high pressure drop it creates. Instead, Webb et al. [30] showed that the use of internal flutes, fins, or circumferential ribs may be considered to increase the water-side coefficient by a factor of up to 2.0 (compared to 2.5 obtained by the insert used during this investigation). As a result, it appears that the use of

94

END

FILMED

DTIC

1.0   2.8   2.5

1.1

1.25   1.4   1.6
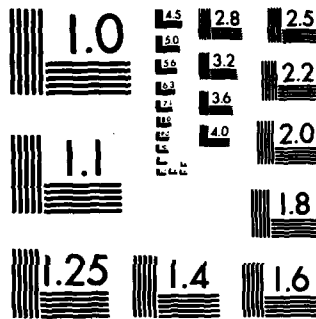
MICROCOPY RESOLUTION TEST CHART
NATIONAL BUREAU OF STANDARDS-1963-A

external fins together with internal enhancements, could increase the overall heat-transfer coefficient by approximately 100 percent.

I. DEVELOPMENT OF AN EXPERIMENTAL CORRELATION

Using the 1985 model of Webb et al. [25] (discussed in Chapter II) as a starting point, attempts were made to correlate the experimental data obtained for tubes with rectangularly-shaped fins. Time limitations prevented an in-depth effort, but a few simple modifications were made. Before discussing these modifications, the general scheme of the Webb et al. model will be discussed. A more detailed step-by-step discussion is provided in Appendix A.

First, a value for the parameter ξ must be determined for the fin geometry in question. With this value known, the heat-transfer coefficient for the unflooded fin surfaces can be obtained using equation (2.30). Values for the heat-transfer coefficients of the unflooded tube area between fins, and for the flooded region are determined next using equations (2.32) and (2.33) respectively. The above-mentioned heat-transfer coefficients are then substituted into equation (2.31) to obtain the average heat-transfer coefficient for the finned tube in question.

A careful review of the Webb et al. model revealed two deficiencies worth noting. First, in their two-dimensional analysis of the flooded tube region, the heat-transfer coefficient for the flooded root area between fins was applied to the fin tips. Figure 2.4 shows that a constant, relatively thick condensate film is assumed which, when applied to the fin tips, results in an underprediction of the heat transfer. Use of the Nusselt equation for smooth tubes would be more appropriate for fin tips in this region. Additionally, the effects of convection in this region are

95
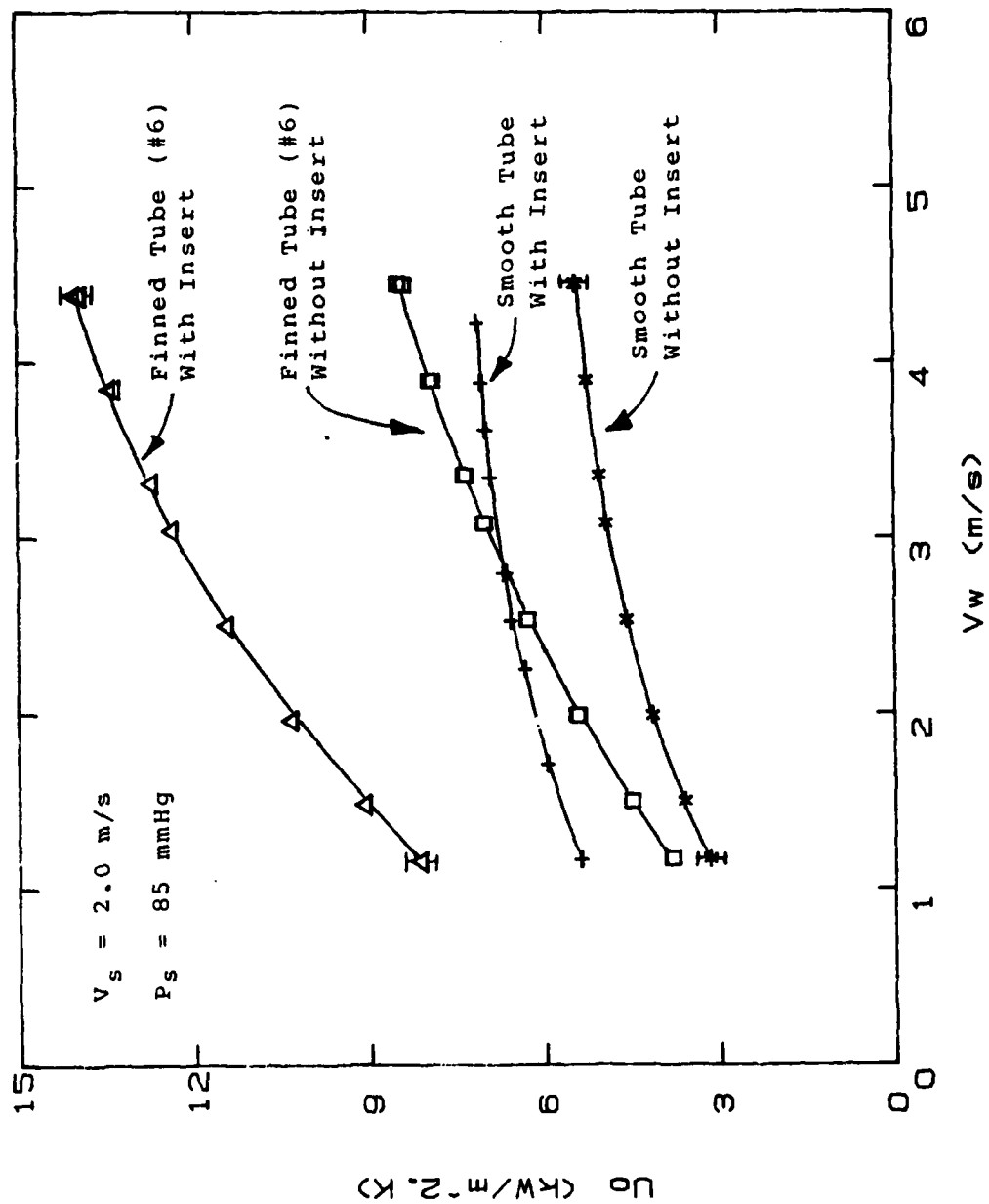
Figure 5.18 Overall Heat-Transfer Coefficient for a Smooth Tube and Finned Tube with and without Insert (Vac. Runs).

96

ignored; however, to include these effects would make a solution extremely complex.

The second deficiency, probably valid only for rectangularly-shaped fins, involves the assumed condensate film shape between fins on the unflooded tube surface. Figure 2.4 shows a depression in the film next to the fin base, with an increasing condensate thickness away from it. Condensate film shapes observed during this investigation continued to decrease away from the fin base as shown by Figure 2.1, probably due to the thinning effect of surface-tension forces. Based on the assumption of a relatively thick condensate film, predictions using the Webb et al. model will underpredict heat transfer from this part of the tube.

To use the Webb et al. model for rectangular fins, a value of -0.9 was chosen for ξ. A value of -1.0, which corresponds to a straight line (i.e., straight side of the rectangular fin) would seem more appropriate; however, this value would lead to zero heat transfer from the fin sides using equation (A.1). Webb et al. used values around -0.7 to -0.8 for their slightly trapezoidal fins; so the value of -0.9 was assumed to be reasonable. Using this value along with a ϕ value of 5.0 (used by Webb et al.) resulted in significant underprediction of the experimental data obtained by this investigator and by Georgiadis [7], as shown in Figure 5.19.

In an attempt to improve the predictions, values for the ϕ ratios were calculated using the paralled heat flow paths proposed by Owen et al. [13] discussed earlier in Chapter II. These ϕ values are dependent on fin spacing, and should decrease with increasing fin spacing. This trend was observed, and for the set of tubes with both fin height and fin thickness of 1.0 mm (s = 0.5, 1.0, 1.5, 2.0, and 4.0 mm - tubes number 4 to 8), resulted in ϕ values that

97
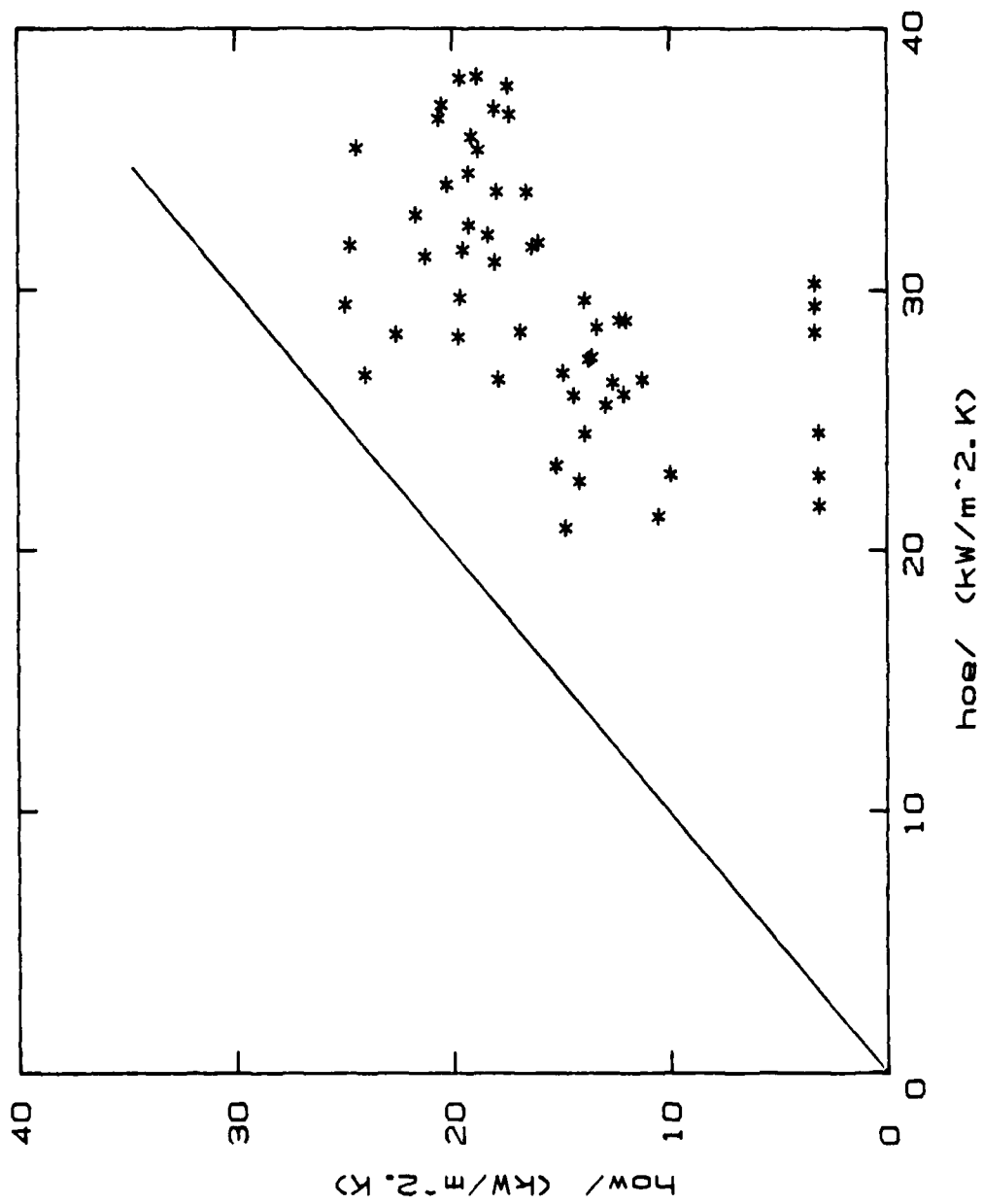
Figure 5.19 Comparison of Webb et al. Model to
Experimental Data for Rectangularly-Shaped Finned Tubes.

98

ranged from 1.7 (s = 0.5 mm) to 1.2 (s = 4.0 mm). Using the
Webb et al. model once again, but with a constant average
value of 1.5, gave the results shown in Figure 5.20 for the
above-mentioned tubes (tubes number 4 to 8). This Figure
also shows a plot of the Webb et al. model using the vari-
able (i.e., 1.7 to 1.2) which made almost no difference.
Once again, the experimental data, also shown in Figure 5.20
were significantly underpredicted.

In order to correct for the assumed thick condensate
layer between fins, the work of Fujii et al. [31] was used.
Their paper delt with smooth tube enhancements from coiling
a wire around the tube circumference, and provided an equa-
tion to account for the thinning effect between wire wraps
as shown below:

$$\frac{Nu_f}{Nu_s} = \frac{s}{(s + t)} \left[\frac{4 (1 + A)}{3} \right]^{1/4} \tag{5.10}$$

where

$$A = \frac{4 \sigma D_o}{\rho_f g s^2 r_s} \tag{5.11}$$

$$r_s = 0.03 \left[\frac{2 \sigma}{\rho_f g} \right]^{3/2} D_w^{-2} \tag{5.12}$$

D_w = wire diameter (taken as the fin height
      for use in the Webb et al. model)

Adding this correction factor to the heat-transfer coeffi-
cient for the unflooded root area between fins made a
significant improvement for the group of tubes mentioned

99
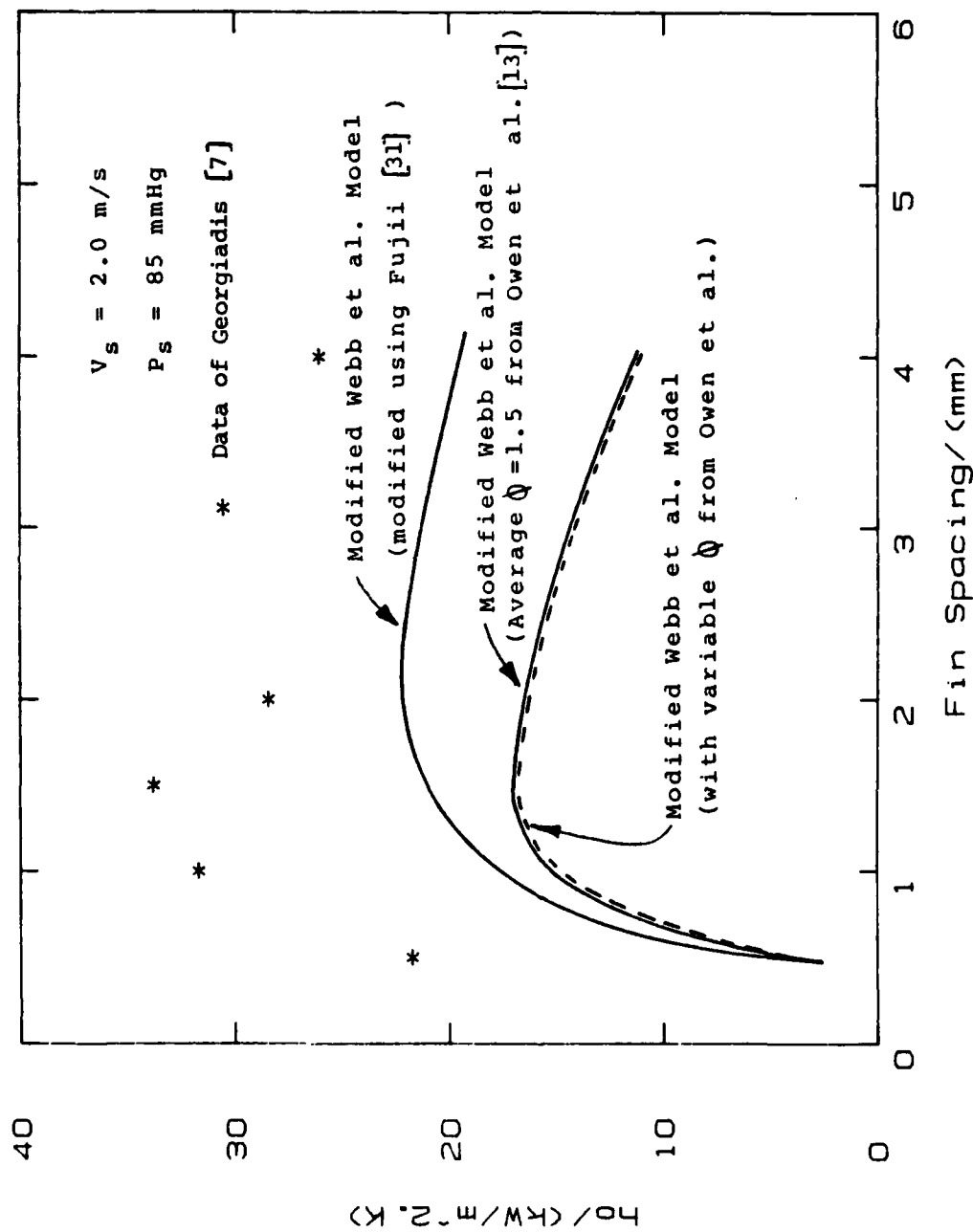
Figure 5.20 Prediction of Experimental Data for Rectangularly-Shaped Finned Tubes with e = 1.0, and t = 1.0.

earlier (tubes number 4 to 8) as shown by Figure 5.20. Nonetheless, experimental data were still underpredicted.

In summary, it should be kept in mind that this model was not developed for rectangular fins. The most significant discrepancy, however, appears to be on the prediction of heat transfer through the flooded area. This model predicts only minimal heat transfer through the flooded portion of the tube, whereas Wanniarachchi et al. [2] reported enhancements at least equal to the area ratio for completely flooded tubes. Additionally, there may be other phenomena which have not been taken into account (such as intense convection in the condensate) which, if included, may improve the predictions. Nonetheless, this model shows promise and should be pursued further.

VI. CONCLUSIONS AND RECOMMENDATIONS

A. CONCLUSIONS

1. The use of fins may lead to significant enhancements of the steam-side heat-transfer coefficient. Under vacuum conditions, enhancements as high as 4.0 (tube number 36) were realized, while enhancements of up to 6.9 (tube number 37) were realized at atmospheric pressure. These enhancements, which were up to three times greater than the area ratio (finned tube area / smooth tube area) are due to the thinning effect of surface-tension forces.

2. For rectangularly-shaped fins with fin heights of 0.5 and 1.5 mm, the 2.0 mm fin spacing appears to be the optimum among the fin spacings tested (1.0, 1.5, 2.0, and 4.0 mm). This was the case for both vacuum and atmospheric conditions. For similar tubes with fin heights of 1.0 and 2.0 mm, Georgiadis [7] found the optimum spacing to be 1.5 mm.

3. The use of fins on a stainless steel (low-thermal-conductivity-metal) tube degraded the heat-transfer performance in comparison to its corresponding smooth tube. In this case, the poor fin effeciency combined with the deleterious effects of retained condensate dominated over the beneficial thinning of the condensate film between fins, resulting in a net reduction of the heat-transfer performance.

4. Fin geometry affects the extent to which the surface-tension forces thin the condensate film on the fin surfaces. Parabolically-shaped fins were shown to

102

maximize the thinning effect of surface-tension forces.

5. Increasing steam velocity (i.e., vapor shear) from 2 to 8 m/s increased the steam-side coefficient by about 10 percent (under vacuum conditions), in contrast to Yau et al. [1], who showed a 40 percent increase when steam velocity was increased from 0.5 to 1.1 m/s (at atmospheric pressure).

6. For the "optimum" tube with rectangular fins and fin height of 1.0 mm (tube number 6), the overall heat-transfer coefficient without the insert showed an enhancement of 40 percent over the corresponding smooth tube. With the insert in place, the finned tube showed overall enhancements of about 155 percent.

7. Most theoretical models developed thus far to predict the heat-transfer performance of steam condensation on horizontal finned tubes neglect one or more phenomena of major importance. Thus, there are no models currently available to accurately predict the performance of finned tubes used to condense steam.

B. RECOMMENDATIONS

1. Make further refinements to the Webb et al. [25] model in an effort to predict the experimental data within a reasonable accuracy.

2. Manufacture and test additional finned tubes with parabolic and spiral fin shapes with different dimensions (i.e., fin spacing, height, and thickness). In this manner, determine the optimum dimensions for each fin shape.

103

3. Manufacture and test a series of tubes with varying tube diameter to study the effect of diameter on the heat-transfer performance. For this purpose, select the optimum, rectangular-shaped fins (s = 1.5 mm, e = 1.0 mm, and t = 1.0 mm).

4. Collect data on finned tubes fitted with drainage strips made out of both solid and porous metal to determine the enhancements they provide.

5. Continue tests on finned tubes with tube-metal thermal conductivities between those of copper and stainless steel, such as copper-nickel alloys and aluminum.

6. Conduct data runs at atmospheric pressure with steam velocities of 0.5, 0.7, and 1.1 m/s, using tube number 6 to compare with the data of Yau et al. [1].

7. Perform data runs using different fluids with widely varying fluid properties (i.e., surface tension, viscosity, etc.) to further study these effects, and to compare with existing theoretical models and experimental correlations.

APPENDIX A
PROCEDURE FOR USE OF THE WEBB ET AL. [25] MODEL

As proposed by Webb et al., solving for the steam-side heat-transfer coefficient proceedes as follows:

1. First, a value for ξ must be determined. This parameter, as shown by figure 2.4, is a measure of the fin aspect ratio (e/t), and it must be determined using an iterative method. It is a function of fin geometry only, and should match the fin side profile as closely as possible. Webb et al. [25] provide details of this method, and no further discussion is provided on this since a true ξ-value does not exist, as defined by Adamek [27], for a rectangular-shaped fin.

2. With the value of known, determine the heat-transfer coefficient for the fin sides in the unflooded portion of the tube. This value is obtained using the following equation [25, 27]:

$$h_f = 2.149 \frac{k_f}{S_m} \left[\frac{\sigma \, h_{fg} \, O_m \, S_m \, \rho_f}{\mu_f \, k_f \, \Delta T} \frac{(\xi + 1)}{(\xi + 2)^3} \right]^{1/4} \qquad (A.1)$$

3. Determine the heat-transfer coefficient for the unflooded root area between fins using the Nusselt equation written in terms of the film Reynolds number. For this purpose, use the following iterative method:

105

a)   Calculate the condensation rate ($\dot{m}$) using:

$$\dot{m} = \frac{n \; h_f \; A_{ft} \; \Delta T}{h_{fg}} \tag{A.2}$$

b)   Assume:

$$\dot{m}_r = \dot{m} \tag{A.3}$$

c)   Calculate the film Reynolds number by:

$$Re_f = \frac{4 \; \dot{m}_r}{\mu_f \; [(s + t_h) - t_h]} \tag{A.4}$$

d)   Calculate h_r using:

$$h_r = 1.514 \left[\frac{\mu_f^{\,2}}{k_f^{\,3} \; \rho_f^{\,2} \; g} \; Re_f \right]^{-1/3} \tag{A.5}$$

e)   Calculate the base heat flow by:

$$Q_r = h_r \; A_{ht} \; \Delta T \tag{A.6}$$

f)   Solve for $\dot{m}$ using:

$$\dot{m}_r = m + \frac{Q_r}{h_{fg}} \tag{A.7}$$

g)   Repeat steps c thru f until convergence is obtained.

4. Determination of the heat-transfer coefficient in the flooded part of the tube requires that a computer solution be used to solve the two-dimensional conduction problem of heat flow through the fins and retained condensate. This solution provides a ratio (ϕ) of actual heat flow into the coolant divided by the heat flow that would result from fins of zero thickness. The heat-transfer coefficient is then determined by:

$$h_h = \phi \frac{k_f}{e} \qquad (A.8)$$

5. The fin efficiency is determined next using the following equation:

$$\eta = \frac{\tanh [m (e + t/2)]}{m (e + t/2)} \qquad (A.9)$$

where

$$m = \left[\frac{2 \, h_f}{k_m \, t} \right]^{1/2} \qquad (A.10)$$

It should be kept in mind that this fin efficiency is only valid for "thin" fins. Nonetheless, its use is justified since there are no equations available specifically for "thick" fins.

6. The heat-transfer coefficient for the entire tube, then, is obtained by substituting the above quantities into the following equation:

$$h_{ow} = h \, \eta_o = \left[h_r \frac{A_{ht}}{A_{sf}} + n \, h_f \frac{A_{ft}}{A_{sf}} \right] \frac{\pi - \psi}{\pi} + h_h \frac{\psi}{\pi} \qquad (A.11)$$

108

APPENDIX B
MODIFIED WILSON METHOD

The "modified Wilson method" calculates the leading coefficient for the Sieder-Tate equation. This method assumes a form of correlation for both the water-side and steam-side heat-transfer coefficients, each of which contains a coefficient to be determined by iteration. In the past, a Nusselt-type equation was used for the steam-side heat-transfer coefficient as shown below [7]:

$$h_o = \beta \left[\frac{k_f^3 \, \rho_f \, (\rho_f - \rho_v) \, h_{fg}}{\mu_f \, D_o \, q} \right]^{1/3} \quad (B.1)$$

Equation (B.1) results in a β value of 0.655 for conditions where no vapor shear is present. The presence of vapor shear generally results in a higher value, which must be determined iteratively. The use of this equation should, therefore, be restricted to relatively low vapor shear conditions (i.e., vapor velocity less than 1.0 m/s). Note that a Nusselt-type equation does not represent the "correct form," as it contains no terms involving vapor shear. To avoid this deficiency, a correlation developed by Fujii and Honda [29] which takes the effect of vapor shear into account was used, and is shown below:

$$\frac{Nu}{Re_{tp}^{0.5}} = 0.96 \, F^{1/5} \quad (B.2)$$

Rewriting equation (B.2) to express h as a function of heat flux and vapor velocity results in:

$$h_o = \beta \left[\frac{\beta \; h_{fg}}{q} \right]^{1/4} \left[\mu_f^3 \; D_o^3 \; \rho_f^3 \; V_s \right]^{1/8} k_f = \beta \; \Gamma \tag{B.3}$$

The constant β in equation (B.3) is to be determined by iteration. A Sieder-Tate-type equation is used for the water-side heat-transfer coefficient, as shown below:

$$\frac{h_i \; D_i}{k_f} = C \; Re^{0.8} \; Pr^{1/3} \left[\frac{\mu_c}{\mu_w} \right]^{0.14} = C \; \Omega \tag{B.4}$$

Equations (B.3) and (B.4) are then substituted into the equation for the overall heat-transfer resistance given below:

$$\frac{1}{U_c \; A_o} = \frac{1}{h_i \; A_i} + \frac{1}{h_o \; A_o} + \frac{P_w}{A_o} \tag{B.5}$$

A linear equation used to generate the Wilson plot is obtained, and shown below:

$$Y = \left[\frac{X}{C} + \frac{1}{\beta} \right] \Gamma \tag{B.6}$$

$$y = \frac{D_o \; \Gamma}{\Omega \; k_f} \tag{B.7}$$

$$Y = \frac{X}{C} + \frac{1}{\beta} \tag{B.8}$$

110

The parameters X and Y are determined from fluid-property values and heat-flux measurements taken during data runs using an uninstrumented smooth tube. Iterations between the coefficient C, and the coefficient β , are continued until convergence of the coefficients (between two successive iterations) within 0.1 percent occurs. The slope of the Wilson plot generated is the reciprocal of the desired Sieder-Tate coefficient.

APPENDIX C
LISTING OF RAW DATA

The following pages contain raw data obtained for tubes
number 26 thru 44 under vacuum conditions and at atmospheric
pressure. Raw data for tubes number 1 thru 25 are presented
by Georgiadis [7].

Tube Number: 25
File Name: F26V28
Pressure Condition: Vacuum
Steam Velocity: 2.6 (m/s)

Data #	Vw (m/s)	Tin (C)	Tout (C)	Ts (C)
1	4.40	20.97	22.01	48.54
2	4.40	20.90	21.96	48.65
3	3.87	20.76	21.93	48.35
4	3.87	20.69	21.89	48.44
5	3.33	20.64	21.97	48.43
6	3.33	20.64	21.97	48.42
7	2.51	20.69	22.29	48.43
8	2.51	20.69	22.29	48.46
9	1.97	20.77	22.61	48.33
10	1.97	20.75	22.60	48.38
11	1.49	20.88	23.05	48.51
12	1.49	20.86	23.04	48.56
13	1.16	21.05	23.55	48.51
14	1.16	21.03	23.54	48.49
15	3.06	20.27	21.79	48.47
16	3.06	20.36	21.79	48.43
17	4.41	20.16	21.25	48.36
18	4.41	20.31	21.40	48.36

Tube Number: 26
File Name: F26A80
Pressure Condition: Atmospheric
Steam Velocity: 1.0 (m/s)

Data #	Vw (m/s)	Tin (C)	Tout (C)	Ts (C)
1	4.41	20.65	24.02	99.82
2	4.41	20.55	23.92	99.91
3	3.87	20.45	24.17	99.85
4	3.87	20.44	24.16	99.92
5	3.33	20.39	24.56	99.96
6	3.33	20.36	24.52	99.94
7	2.52	20.36	25.36	99.93
8	2.52	20.33	25.33	99.90
9	1.98	20.39	26.20	99.94
10	1.98	20.37	26.17	99.83
11	1.49	20.50	27.35	99.37
12	1.49	20.48	27.33	99.89
13	1.16	20.65	28.58	100.03
14	1.16	20.64	28.57	99.98
15	3.06	19.90	24.35	99.96
16	3.06	19.90	24.35	100.01
17	4.41	19.71	23.14	99.88
18	4.41	19.70	23.13	99.85

113

Tube Number: 27
File Name: F27V32
Pressure Condition: Vacuum
Steam Velocity: 2.0 (m/s)

Data #	Vw (m/s)	Tin (C)	Tout (C)	Ts (C)
1	4.41	19.45	19.57	48.38
2	4.41	19.29	20.50	48.37
3	3.87	19.17	20.42	48.54
4	3.87	19.16	20.40	48.57
5	3.33	19.05	20.45	48.53
6	3.33	18.99	20.39	48.55
7	2.52	19.07	20.74	48.39
8	2.52	19.04	20.71	48.45
9	1.98	19.10	20.95	48.42
10	1.98	19.08	21.02	48.43
11	1.49	19.22	21.52	48.50
12	1.49	19.19	21.48	48.54
13	1.17	19.35	21.98	48.48
14	1.17	19.34	21.97	48.48
15	3.06	18.67	20.17	48.40
16	3.06	18.66	20.16	48.44
17	4.42	18.48	19.63	48.41
18	4.42	18.48	19.63	48.48

Tube Number: 27
File Name: F27A77
Pressure Condition: Atmospheric
Steam Velocity: 1.0 (m/s)

Data #	Vw (m/s)	Tin (C)	Tout (C)	Ts (C)
1	4.42	18.81	22.16	99.82
2	4.42	18.81	22.17	99.84
3	3.88	18.85	21.58	99.88
4	3.88	18.85	22.58	99.88
5	3.34	18.91	23.08	99.92
6	3.34	18.91	23.07	99.87
7	2.52	19.03	24.04	99.89
8	2.52	19.03	24.04	99.84
9	1.98	19.17	25.00	99.88
10	1.98	19.17	24.99	99.78
11	1.49	19.36	26.36	99.86
12	1.49	19.36	26.26	99.86
13	1.17	19.60	27.58	99.92
14	1.17	19.60	27.59	99.86
15	3.06	18.95	23.43	99.93
16	3.06	18.94	23.43	99.93
17	4.42	18.77	22.22	99.88
18	4.42	18.77	22.23	99.87

114

Tube Number: 28
File Name: F28A78
Pressure Condition: Atmospheric
Steam Velocity: 1.0 (m/s)

Data #	Vw (m/s)	Tin (C)	Tout (C)	Ts (C)
1	4.42	18.68	22.15	99.26
2	4.42	18.68	22.18	99.90
3	3.88	18.74	22.60	99.88
4	3.83	18.75	22.61	99.90
5	3.34	18.82	23.14	99.94
6	3.34	18.83	23.16	99.96
7	2.52	18.97	24.14	99.89
8	2.52	18.97	24.15	99.98
9	1.98	19.11	25.11	99.83
10	1.98	19.11	25.13	99.89
11	1.49	19.33	26.42	99.93
12	1.49	19.33	26.43	100.00
13	1.17	19.55	27.63	99.89
14	1.17	19.55	27.69	99.85
15	2.06	18.91	23.56	99.91
16	3.06	18.91	23.56	99.84
17	4.42	18.75	22.34	99.91
18	4.42	18.75	22.34	99.89

Tube Number: 28
File Name: F28V37
Pressure Condition: Vacuum
Steam Velocity: 2.0 (m/s)

Data #	Vw (m/s)	Tin (C)	Tout (C)	Ts (C)
1	4.42	18.89	20.06	48.46
2	4.42	18.89	20.05	48.41
3	3.88	18.79	20.03	48.44
4	3.88	18.79	20.08	48.43
5	3.34	18.78	20.23	48.44
6	3.34	18.76	20.22	48.44
7	2.52	18.87	20.61	48.42
8	2.52	18.87	20.61	48.40
9	1.98	18.99	21.01	48.46
10	1.98	18.98	21.00	48.42
11	1.49	19.16	21.52	48.44
12	1.49	19.16	21.54	48.44
13	1.17	19.36	22.07	48.50
14	1.17	19.36	22.07	48.52
15	3.06	18.69	20.26	48.33
16	3.06	18.68	20.26	48.29
17	4.42	18.71	19.95	48.48
18	4.42	18.74	19.96	48.49

115

Tube Number: 29
File Name: F29V39
Pressure Condition: Vacuum
Steam Velocity: 2.0 (m/s)

Data #	Vw (m/s)	Tin (C)	Tout (C)	Ts (C)
1	4.40	21.35	21.37	48.38
2	4.40	21.30	21.35	48.37
3	3.86	21.07	21.25	48.35
4	3.86	21.01	22.15	48.35
5	3.32	20.92	22.18	49.31
6	3.32	20.92	22.19	48.33
7	2.51	20.91	22.45	48.49
8	2.51	20.87	22.41	48.50
9	1.97	20.92	22.72	48.44
10	1.97	20.92	22.72	48.42
11	1.49	21.06	23.17	48.44
12	1.49	21.04	23.15	49.47
13	1.16	21.19	23.63	49.55
14	1.16	21.18	23.63	48.62
15	3.06	20.46	21.84	48.41
16	3.06	20.45	21.82	49.37
17	4.41	20.24	21.30	49.42
18	4.41	20.38	21.44	48.37

Tube Number: 29
File Name: F29A31
Pressure Condition: Atmospheric
Steam Velocity: 1.0 (m/s)

Data #	Vw (m/s)	Tin (C)	Tout (C)	Ts (C)
1	4.42	19.45	22.50	99.92
2	4.42	19.45	22.62	99.99
3	3.87	19.51	23.00	99.87
4	3.87	19.50	23.00	99.98
5	3.33	19.57	23.49	99.90
6	3.33	19.58	23.50	99.91
7	2.52	19.72	24.45	99.68
8	2.52	19.71	24.46	99.83
9	1.98	19.86	25.42	99.83
10	1.98	19.86	25.43	99.91
11	1.49	20.06	26.57	99.86
12	1.49	20.06	26.67	92.96
13	1.17	20.28	27.93	99.98
14	1.17	20.28	27.93	100.01
15	3.06	19.65	23.85	99.90
16	3.06	19.64	23.85	99.94
17	4.42	19.49	22.68	99.84
18	4.42	19.48	22.68	93.76

116

Tube Number: 30
File Name: F30A6E
Pressure Condition: Atmospheric
Steam Velocity: 1.0 (m/s)

Data #	Vw (m/s)	Tin (C)	Tout (C)	Ts (C)
1	4.39	22.56	26.21	99.97
2	4.39	22.52	26.18	99.90
3	3.86	21.81	25.84	99.99
4	3.86	21.82	25.83	99.86
5	3.32	21.81	26.26	99.95
6	3.32	21.76	26.21	99.95
7	2.51	21.69	26.94	99.79
8	2.51	21.61	26.87	99.92
9	1.97	21.64	27.70	99.87
10	1.97	21.63	27.69	99.36
11	1.49	21.71	28.79	99.94
12	1.49	21.68	28.77	99.97
13	1.16	21.82	29.92	99.90
14	1.16	21.90	29.90	95.86
15	0.05	21.03	25.75	99.81
16	0.05	21.01	25.73	99.90
17	4.41	20.87	24.59	99.78
18	4.41	20.89	24.63	100.03

Tube Number: 30
File Name: F30V23
Pressure Condition: Vacuum
Steam Velocity: 2.0 (m/s)

Data #	Vw (m/s)	Tin (C)	Tout (C)	Ts (C)
1	4.41	20.29	21.47	48.48
2	4.41	20.29	21.49	48.50
3	3.87	20.23	21.56	48.47
4	3.87	20.21	21.53	48.35
5	3.33	20.17	21.53	48.34
6	3.33	20.13	21.54	48.29
7	2.51	20.23	21.97	48.45
8	2.52	20.23	21.96	48.52
9	1.98	20.33	22.23	48.47
10	1.98	20.32	22.32	48.51
11	1.49	20.50	22.80	48.31
12	1.49	20.50	22.86	48.31
13	1.16	20.70	23.34	48.43
14	1.16	20.70	23.32	48.38
15	0.06	20.04	21.59	48.51
16	0.06	20.03	21.59	48.52
17	4.41	19.87	21.08	48.41
18	4.41	20.07	21.27	48.40

117

Tube Number: 31
File Name: F21A67
Pressure Condition: Atmospheric
Steam Velocity: 1.0 (m/s)

Data #	Vj (m/s)	Tin (C)	Tout (C)	Ts (C)
1	4.40	21.82	25.76	99.81
2	4.40	21.79	25.79	99.80
3	3.86	21.44	25.80	99.95
4	3.86	21.52	25.87	100.00
5	3.32	21.52	26.28	99.90
6	3.32	21.49	26.27	99.94
7	2.51	21.53	27.12	99.88
8	2.51	21.51	27.10	99.85
9	1.97	21.59	27.99	100.02
10	1.97	21.56	27.97	100.06
11	1.49	21.71	29.14	99.87
12	1.49	21.70	29.13	99.82
13	1.16	21.87	30.31	99.96
14	1.16	21.85	30.29	99.86
15	3.05	21.18	26.23	99.66
16	3.05	21.18	26.24	100.04
17	4.40	21.13	25.16	99.91
18	4.40	21.16	25.18	99.90

Tube Number: 31
File Name: F31V20
Pressure Condition: Vacuum
Steam Velocity: 2.0 (m/s)

Data #	Vj (m/s)	Tin (C)	Tout (C)	Ts (C)
1	4.41	20.68	21.93	48.42
2	4.41	20.67	21.93	48.35
3	3.87	20.64	22.02	48.33
4	3.87	20.56	21.95	48.36
5	3.33	20.47	22.00	48.37
6	3.33	20.47	22.00	48.38
7	2.52	20.52	22.10	48.33
8	2.52	20.51	22.10	49.31
9	1.97	20.61	22.67	48.33
10	1.97	20.61	22.66	48.35
11	1.49	20.77	23.15	48.42
12	1.49	20.76	23.16	48.48
13	1.16	20.97	23.67	48.57
14	1.16	20.97	23.68	48.56
15	3.05	20.30	21.92	48.37
16	3.06	20.30	21.93	48.39
17	4.41	20.11	21.38	48.35
18	4.41	20.10	21.39	48.48

Tube Number: 32
File Name: F32V26
Pressure Condition: Vacuum
Steam Velocity: 2.6 (m/s)

Data #	V_w (m/s)	T_{in} (C)	T_{out} (C)	T_s (C)
1	4.41	20.42	21.68	48.40
2	4.41	20.47	21.74	48.37
3	3.87	20.36	21.74	48.39
4	3.87	20.40	21.78	49.40
5	3.33	20.31	21.86	48.52
6	3.33	20.30	21.85	48.47
7	2.52	20.39	22.22	48.44
8	2.52	20.38	22.21	48.42
9	1.98	20.49	22.57	48.38
10	1.98	20.47	22.56	48.39
11	1.49	20.64	23.06	48.46
12	1.49	20.64	23.04	48.41
13	1.16	20.83	23.57	48.45
14	1.16	20.83	23.57	48.47
15	3.06	20.14	21.80	48.53
16	3.06	20.13	21.79	48.51
17	4.41	20.02	21.33	48.42
18	4.41	20.03	21.33	48.38

Tube Number: 32
File Name: F32A68
Pressure Condition: Atmospheric
Steam Velocity: 1.0 (m/s)

Data #	V_w (m/s)	T_{in} (C)	T_{out} (C)	T_s (C)
1	4.40	21.82	25.79	100.00
2	4.40	21.79	25.76	99.97
3	3.86	21.85	26.17	99.96
4	3.86	21.81	26.14	99.96
5	3.32	21.84	26.53	99.98
6	3.32	21.79	26.54	99.94
7	2.51	21.66	27.23	99.94
8	2.51	21.64	27.21	99.83
9	1.97	21.72	28.11	99.96
10	1.97	21.69	28.07	99.87
11	1.49	21.83	29.24	99.92
12	1.49	21.80	29.22	99.94
13	1.16	21.97	30.41	99.90
14	1.16	21.95	30.40	99.93
15	3.05	21.24	26.36	99.94
16	3.05	21.23	26.35	99.91
17	4.40	21.10	25.09	99.88
18	4.40	21.14	25.13	99.83

119

Tube Number: 33
File Name: F33A69
Pressure Condition: Atmospheric
Steam Velocity: 1.0 (m/s)

Data #	Vw (m/s)	Tin (C)	Tout (C)	Ts (C)
1	4.41	20.87	24.46	100.00
2	4.40	21.03	24.61	93.83
3	3.86	21.18	25.11	99.97
4	3.86	21.17	25.10	99.88
5	3.32	21.28	25.63	99.86
6	3.32	21.30	25.64	99.74
7	2.51	21.41	25.59	99.94
8	2.51	21.39	26.55	99.91
9	1.97	21.47	27.44	99.37
10	1.97	21.45	27.44	99.98
11	1.49	21.59	28.61	99.94
12	1.16	21.58	28.59	99.97
13	1.16	21.75	29.79	99.85
14	1.16	21.75	29.78	99.83
15	3.05	21.11	25.72	99.92
16	3.05	21.18	25.79	99.97
17	4.40	21.10	24.70	99.92
18	4.40	21.09	24.70	99.66

Tube Number: 33
File Name: F33V22
Pressure Condition: Vacuum
Steam Velocity: 2.0 (m/s)

Data #	Vw (m/s)	Tin (C)	Tout (C)	Ts (C)
1	4.40	21.27	22.42	48.54
2	4.40	21.14	22.30	48.34
3	3.86	20.88	22.17	49.51
4	3.86	20.85	22.14	48.51
5	3.32	20.78	22.19	48.52
6	3.32	20.75	22.18	48.50
7	2.51	20.76	22.46	48.41
8	2.51	20.71	22.40	48.35
9	1.97	20.77	22.71	48.32
10	1.97	20.73	22.67	48.27
11	1.49	20.84	23.11	48.42
12	1.49	20.81	23.08	49.44
13	1.16	20.97	23.54	48.40
14	1.16	20.94	23.53	48.33
15	3.06	20.25	21.76	48.44
16	3.06	20.24	21.75	48.39
17	4.41	20.08	21.27	48.46
18	4.41	20.11	21.29	48.47

120

Tube Number: 34
File Name: F34V41
Pressure Condition: Vacuum
Steam Velocity: 2.0 (m/s)

Data #	Vw (m/s)	Tin (C)	Tout (C)	Ts (C)
1	4.40	21.10	22.34	48.51
2	4.40	21.22	22.24	48.52
3	3.86	20.84	22.19	48.45
4	3.86	20.83	22.18	48.44
5	3.32	20.83	22.31	48.40
6	3.32	20.82	22.30	48.40
7	2.51	20.85	22.59	48.39
8	2.51	20.84	22.57	48.42
9	1.97	20.93	22.92	48.42
10	1.97	20.91	22.91	48.53
11	1.49	21.07	23.09	48.40
12	1.49	21.06	23.37	48.35
13	1.16	21.24	23.86	48.40
14	1.16	21.23	23.86	48.43
15	3.06	20.58	22.15	48.48
16	3.06	20.56	22.14	48.51
17	4.41	20.39	21.53	48.43
18	4.41	20.39	21.63	48.46

Tube Number: 34
File Name: F34A65
Pressure Condition: Atmospheric
Steam Velocity: 1.0 (m/s)

Data #	Vw (m/s)	Tin (C)	Tout (C)	Ts (C)
1	4.40	21.90	25.34	99.98
2	4.40	22.21	26.14	99.84
3	3.86	21.91	25.17	99.91
4	3.86	21.96	26.22	99.89
5	3.32	22.10	26.80	99.98
6	3.32	22.06	26.76	99.94
7	2.51	22.23	27.75	99.96
8	2.51	22.28	27.79	99.87
9	1.97	22.42	28.73	99.93
10	1.97	22.46	28.77	99.96
11	1.49	22.67	30.00	100.00
12	1.48	22.68	30.01	99.97
13	1.16	22.92	31.25	99.39
14	1.16	22.92	31.24	99.99
15	3.05	22.35	27.30	99.89
16	3.05	22.34	27.30	99.90
17	4.40	22.21	26.15	99.34
18	4.40	22.22	26.17	99.96

121

Tube Number: 35
File Name: F35A6!
Pressure Condition: Atmospheric
Steam Velocity: 1.0 (m/s)

Data #	Vw (m/s)	Tin (C)	Tout (C)	Ts (C)
1	4.41	21.00	24.76	99.98
2	4.40	21.15	24.93	100.04
3	3.87	20.92	25.04	99.93
4	3.87	20.95	25.07	99.93
5	3.32	21.04	25.59	99.94
6	3.32	21.04	25.58	99.90
7	2.51	21.09	26.45	99.95
8	2.51	21.08	26.45	99.97
9	1.97	21.15	27.32	99.88
10	1.97	21.12	27.30	99.87
11	1.49	21.25	28.48	99.94
12	1.49	21.23	28.46	99.92
13	1.16	21.40	29.65	99.96
14	1.16	21.41	29.66	100.00
15	3.06	20.71	25.57	100.02
16	3.06	20.71	25.56	100.09
17	4.41	20.62	24.44	99.84
18	4.41	20.63	24.45	99.94

Tube Number: 35
File Name: F35V51
Pressure Condition: Vacuum
Steam Velocity: 2.0 (m/s)

Data #	Vw (m/s)	Tin (C)	Tout (C)	Ts (C)
1	4.39	22.53	23.67	48.40
2	4.39	22.58	23.71	48.47
3	3.95	22.53	23.79	48.38
4	3.85	22.48	23.75	48.37
5	3.32	22.46	23.87	48.41
6	3.32	22.45	23.85	48.41
7	2.51	22.53	24.20	48.48
8	2.51	22.52	24.19	48.53
9	1.97	22.61	24.52	48.47
10	1.97	22.58	24.49	48.34
11	1.48	22.74	24.65	48.40
12	1.48	22.74	24.94	48.38
13	1.16	22.91	25.40	48.43
14	1.16	22.92	25.42	48.44
15	3.05	22.30	23.81	48.32
16	3.05	22.30	23.80	48.30
17	4.40	22.26	23.44	48.40
18	4.40	22.27	23.45	48.42

122

Data #	Vw (m/s)	Tin (C)	Tout (C)	Ts (C)
1	4.40	21.24	25.09	99.90
2	4.40	21.17	25.02	99.96
3	3.86	21.02	25.24	99.81
4	3.86	21.02	25.24	99.83
5	3.32	21.07	25.73	99.94
6	3.32	21.06	25.73	99.94
7	2.51	21.14	26.53	100.03
8	2.51	21.12	26.60	99.90
9	1.97	21.23	27.52	99.81
10	1.97	21.21	27.50	99.63
11	1.49	21.33	28.65	99.86
12	1.49	21.32	28.65	99.23
13	1.16	21.48	29.81	99.94
14	1.16	21.48	29.81	99.91
15	3.06	20.80	25.74	99.82
16	3.06	20.78	25.73	99.36
17	4.41	20.61	24.51	99.94
18	4.41	20.78	24.68	99.87

Tube Number: 36
File Name: F36V48
Pressure Condition: Vacuum
Steam Velocity: 2.0 (m/s)

Data #	Vw (m/s)	Tin (C)	Tout (C)	Ts (C)
1	4.49	21.55	22.78	48.41
2	4.40	21.58	22.81	48.40
3	3.85	21.49	22.84	48.39
4	3.86	21.46	22.82	48.40
5	3.32	21.47	22.98	48.46
6	3.32	21.48	22.99	48.45
7	2.51	21.59	23.36	48.47
8	2.51	21.57	23.34	48.49
9	1.97	21.69	23.71	48.43
10	1.97	21.68	23.70	48.42
11	1.49	21.84	24.17	48.36
12	1.49	21.84	24.16	48.32
13	1.16	22.02	24.56	48.44
14	1.16	22.02	24.65	48.41
15	3.05	21.36	22.97	48.40
16	3.05	21.35	22.95	48.42
17	4.40	21.37	22.63	48.37
18	4.40	21.38	22.63	48.39

123

Tube Number: 37
File Name: F37A103
Pressure Condition: Atmospheric
Steam Velocity: 1.0 (m/s)

Data #	Vw (m/s)	Tin (C)	Tout (C)	Ts (C)
1	4.45	15.10	19.33	99.88
2	4.45	15.10	19.34	99.90
3	3.90	15.16	19.90	99.98
4	3.90	15.16	19.80	99.98
5	3.35	15.23	20.33	99.94
6	3.36	15.22	20.32	100.02
7	2.54	15.36	21.35	99.95
8	2.54	15.37	21.36	100.00
9	1.99	15.50	22.34	99.87
10	1.99	15.49	22.32	99.75
11	1.50	15.69	23.58	99.75
12	1.50	15.69	23.59	99.75
13	1.17	15.90	24.87	99.91
14	1.17	15.90	24.90	100.06
15	3.08	15.19	20.57	99.89
16	3.08	15.18	20.57	99.83
17	4.45	15.00	19.30	99.88
18	4.45	15.00	19.30	99.90

Tube Number: 37
File Name: F37V97
Pressure Condition: Vacuum
Steam Velocity: 2.0 (m/s)

Data #	Vw (m/s)	Tin (C)	Tout (C)	Ts (C)
1	4.44	15.73	17.12	48.50
2	4.44	15.69	17.07	48.47
3	3.90	15.65	17.18	48.42
4	3.90	15.61	17.14	48.42
5	3.35	15.51	17.28	48.28
6	3.35	15.60	17.28	48.20
7	2.54	15.63	17.61	48.29
8	2.54	15.60	17.58	48.27
9	1.99	15.58	17.96	48.38
10	1.99	15.67	17.94	48.40
11	1.50	15.85	18.50	48.42
12	1.50	15.85	18.50	48.44
13	1.17	16.04	19.06	48.42
14	1.17	16.04	19.05	48.45
15	3.08	15.33	17.12	48.24
16	3.08	15.32	17.11	48.35
17	4.45	15.14	16.55	48.32
18	4.45	15.12	16.52	48.26

124

Tube Number: 38
File Name: F38A112
Pressure Condition: Atmospheric
Steam Velocity: 1.0 (m/s)

Data #	Vw (m/s)	Tin (C)	Tout (C)	Ts (C)
1	4.45	14.56	18.61	99.85
2	4.45	14.56	18.62	99.91
3	3.90	14.62	19.06	99.84
4	3.90	14.62	19.07	99.84
5	3.36	14.69	19.60	99.90
6	3.36	14.68	19.60	99.86
7	2.54	14.82	20.60	99.90
8	2.54	14.82	20.60	99.99
9	1.99	14.96	21.58	99.92
10	1.99	14.96	21.58	99.96
11	1.50	15.16	22.88	99.91
12	1.50	15.16	22.88	99.90
13	1.17	15.38	24.15	99.83
14	1.17	15.38	24.17	99.85
15	3.09	14.69	19.87	99.89
16	3.09	14.69	19.88	99.91
17	4.45	14.51	18.61	99.93
18	4.45	14.50	18.61	100.03

Tube Number: 38
File Name: F38V107
Pressure Condition: Vacuum
Steam Velocity: 2.0 (m/s)

Data #	Vw (m/s)	Tin (C)	Tout (C)	Ts (C)
1	4.44	16.33	17.74	48.41
2	4.44	16.32	17.74	48.35
3	3.89	16.31	17.86	48.36
4	3.89	16.26	17.81	48.35
5	3.35	16.27	17.97	48.37
6	3.35	16.22	17.94	48.28
7	2.53	16.32	18.32	48.39
8	2.53	16.31	18.31	48.38
9	1.99	16.42	18.73	48.40
10	1.99	16.40	18.70	48.33
11	1.50	16.58	19.26	48.41
12	1.50	16.56	19.24	48.37
13	1.17	16.75	19.78	48.42
14	1.17	16.76	19.80	48.52
15	3.08	16.01	17.83	48.42
16	3.08	16.00	17.82	48.40
17	4.44	15.82	17.27	48.39
18	4.44	15.81	17.25	48.34

Tube Number: 39
File Name: F39V33
Pressure Condition: Vacuum
Steam Velocity: 2.0 (m/s)

Data #	Vw (m/s)	Tin (C)	Tout (C)	Ts (C)
1	3.91	18.52	19.63	48.38
2	3.91	18.44	19.55	48.37
3	3.43	18.35	19.57	48.36
4	3.43	18.32	19.54	48.24
5	2.95	18.14	19.50	48.32
6	2.95	18.13	19.49	48.28
7	2.23	18.12	19.74	48.39
8	2.24	17.80	19.43	48.35
9	1.76	17.86	19.74	48.43
10	1.76	17.81	19.70	48.51
11	1.32	17.95	20.16	48.47
12	1.32	17.94	20.14	48.44
13	1.00	18.12	20.65	48.47
14	1.03	18.11	20.65	48.50
15	2.72	17.40	19.87	48.31
16	2.72	17.38	18.84	48.39
17	3.92	17.17	18.32	48.50
18	3.92	17.16	18.31	48.41

Tube Number: 39
File Name: F39A98
Pressure Condition: Atmospheric
Steam Velocity: 1.0 (m/s)

Data #	Vw (m/s)	Tin (C)	Tout (C)	Ts (C)
1	3.93	15.12	19.71	100.00
2	3.93	15.11	18.70	99.86
3	3.45	15.15	19.09	99.82
4	3.45	15.12	19.06	99.83
5	2.97	15.17	19.54	99.90
6	2.97	15.17	19.54	99.97
7	2.45	15.30	20.48	99.93
8	2.25	15.30	20.48	99.84
9	1.76	15.45	21.45	99.97
10	1.76	15.45	21.44	99.87
11	1.33	15.64	22.66	99.91
12	1.33	15.65	22.66	99.94
13	1.14	15.88	23.89	99.89
14	1.04	15.88	23.89	99.91
15	2.73	15.20	19.85	99.98
16	2.73	15.21	19.85	99.92
17	3.94	15.03	19.67	99.83
18	3.94	15.03	18.66	99.78

Tube Number: 40
File Name: F40A95
Pressure Condition: Atmospheric
Steam Velocity: 1.0 (m/s)

Data #	Vw (m/s)	Tin (C)	Tout (C)	Ts (C)
1	3.89	21.84	23.18	99.94
2	3.89	21.80	23.09	99.99
3	3.42	21.20	22.67	99.90
4	3.42	21.09	22.54	99.79
5	2.94	20.57	22.23	99.81
6	2.94	20.30	21.98	99.91
7	2.23	20.03	22.12	99.84
8	2.23	19.94	22.05	99.85
9	1.75	19.77	22.31	99.96
10	1.75	19.69	22.24	100.01
11	1.32	19.60	22.74	94.88
12	1.32	19.52	22.66	99.95
13	1.03	19.25	23.12	99.84
14	1.03	19.29	23.05	99.79
15	0.71	18.24	23.06	94.82
16	2.71	18.18	20.06	99.76
17	3.92	17.75	20.00	99.90
18	3.92	17.70	19.03	99.90

Tube Number: 40
File Name: F40V84
Pressure Condition: Vacuum
Steam Velocity: 2.0 (m/s)

Data #	Vw (m/s)	Tin (C)	Tout (C)	Ts (C)
1	3.92	17.12	17.59	49.26
2	3.92	17.11	17.58	48.33
3	3.44	17.16	17.57	48.30
4	3.44	17.16	17.69	48.32
5	2.96	17.21	17.33	48.33
6	2.96	17.22	17.82	48.32
7	2.24	17.34	18.10	48.39
8	2.24	17.34	18.09	48.41
9	1.76	17.46	18.37	48.48
10	1.76	17.46	18.37	48.47
11	1.32	17.65	18.76	48.40
12	1.32	17.64	18.75	48.36
13	1.03	17.84	19.16	48.43
14	1.03	17.93	19.15	48.39
15	0.72	17.16	17.80	48.47
16	2.72	17.14	17.79	48.54
17	3.92	16.97	17.44	48.43
18	3.92	16.97	17.44	48.41

127

Tube Number: 41
File Name: S41A12F
Pressure Condition: Atmospheric
Steam Velocity: 1.0 (m/s)

Data #	Vw (m/s)	Tin (C)	Tout (C)	Ts (C)
1	3.95	13.42	15.07	99.99
2	3.95	13.39	15.04	99.90
3	3.46	13.08	15.05	99.83
4	3.46	13.36	15.24	99.87
5	2.98	13.35	15.50	99.92
6	2.98	13.32	15.47	99.93
7	2.25	13.40	16.14	99.77
8	2.25	13.38	16.10	99.77
9	1.77	13.47	16.80	99.84
10	1.77	13.45	16.78	99.80
11	1.33	13.62	17.79	99.80
12	1.33	13.61	17.78	99.92
13	1.04	13.81	13.84	99.99
14	1.04	13.80	12.82	100.01
15	2.74	13.07	15.42	99.98
16	2.74	13.06	15.40	99.98
17	3.95	12.89	14.55	99.87
18	3.95	12.86	14.53	99.92

Tube Number: 41
File Name: S41V37
Pressure Condition: Vacuum
Steam Velocity: 2.0 (m/s)

Data #	Vw (m/s)	Tin (C)	Tout (C)	Ts (C)
1	3.92	17.57	18.20	48.38
2	3.92	17.56	18.19	48.36
3	3.44	17.59	18.31	48.37
4	3.44	17.57	18.29	48.34
5	2.96	17.61	18.43	48.35
6	2.96	17.60	18.43	48.33
7	2.24	17.71	18.74	48.43
8	2.24	17.71	18.74	48.42
9	1.76	17.81	18.97	48.44
10	1.76	17.81	19.07	48.40
11	1.32	17.98	19.52	48.33
12	1.32	17.98	19.52	48.37
13	1.03	18.17	20.01	48.43
14	1.03	18.17	20.00	48.40
15	2.72	17.48	18.35	48.33
16	2.72	17.46	18.35	48.36
17	3.92	17.28	17.91	48.36
18	3.92	17.27	17.91	48.43

128

Tube Number: 42
File Name: S42V88
Pressure Condition: Vacuum
Steam Velocity: 2.0 (m/s)

Data #	Vw (m/s)	Tin (C)	Tout (C)	Ts (C)
1	3.92	17.25	17.75	48.40
2	3.92	17.26	17.75	48.37
3	3.44	17.29	17.85	48.37
4	3.44	17.29	17.85	48.44
5	2.96	17.32	17.95	48.43
6	2.95	17.31	17.95	48.52
7	2.24	17.43	18.23	42.34
8	2.24	17.42	18.23	48.30
9	1.76	17.54	18.52	48.31
10	1.76	17.54	18.51	48.33
11	1.32	17.73	18.94	48.46
12	1.32	17.73	18.95	48.52
13	1.03	17.94	18.39	48.35
14	1.03	17.95	19.39	48.37
15	2.72	17.27	17.96	48.45
16	2.72	17.27	17.96	48.45
17	3.92	17.10	17.59	48.41
18	3.92	17.08	17.57	48.41

Tube Number: 42
File Name: S42A127
Pressure Condition: Atmospheric
Steam Velocity: 1.0 (m/s)

Data #	Vw (m/s)	Tin (C)	Tout (C)	Ts (C)
1	3.95	12.63	13.99	100.02
2	3.95	12.63	13.97	99.92
3	3.47	12.68	14.21	99.93
4	3.47	12.68	14.22	99.94
5	2.98	12.75	14.52	94.85
6	2.98	12.75	14.50	99.75
7	2.25	12.89	15.12	99.85
8	2.25	12.90	15.12	99.81
9	1.77	13.05	15.76	99.97
10	1.77	13.05	15.75	99.89
11	1.33	13.26	16.64	100.00
12	1.33	13.26	16.65	100.03
13	1.04	13.51	17.58	99.82
14	1.04	13.51	17.59	99.86
15	2.74	12.81	14.71	99.90
16	2.74	12.80	14.69	99.75
17	3.95	12.64	14.00	99.87
18	3.95	12.64	13.99	99.88

129

Tube Number: 43
File Name: F43A123
Pressure Condition: Atmospheric
Steam Velocity: 1.0 (m/s)

Data #	Vw (m/s)	Tin (C)	Tout (C)	Ts (C)
1	4.46	13.41	17.14	99.84
2	4.46	13.41	17.14	99.79
3	3.91	13.46	17.54	99.77
4	3.91	13.45	17.53	99.76
5	3.36	13.51	18.03	99.87
6	3.36	13.51	18.03	99.97
7	2.54	13.64	18.97	99.84
8	2.54	13.64	18.97	99.83
9	2.00	13.78	19.92	100.92
10	2.00	13.78	19.93	100.07
11	1.50	13.98	21.13	99.90
12	1.50	13.99	21.14	99.99
13	1.18	14.18	22.36	99.94
14	1.18	14.20	22.38	100.01
15	3.09	13.53	13.31	99.87
16	3.09	13.53	18.32	99.91
17	4.46	13.35	17.13	99.86
18	4.46	13.34	17.12	99.93

Tube Number: 43
File Name: F43V121
Pressure Condition: Vacuum
Steam Velocity: 2.0 (m/s)

Data #	Vw (m/s)	Tin (C)	Tout (C)	Ts (C)
1	4.46	13.39	14.67	48.46
2	4.46	13.37	14.67	48.49
3	3.91	13.38	14.80	48.47
4	3.91	13.36	14.79	48.47
5	3.36	13.41	15.00	48.36
6	3.36	13.40	14.98	48.49
7	2.54	13.49	15.38	48.61
8	2.54	13.46	15.34	48.50
9	2.00	13.55	15.75	48.38
10	2.00	13.51	15.70	48.46
11	1.51	13.65	15.22	48.51
12	1.51	13.65	16.20	48.49
13	1.18	13.84	16.79	48.47
14	1.18	13.84	16.77	48.39
15	3.09	13.15	14.84	48.27
16	3.09	13.14	14.82	48.40
17	4.46	12.97	14.29	48.34
18	4.46	12.96	14.28	48.40

Tube Number: 44
File Name: S44V120
Pressure Condition: Vacuum
Steam Velocity: 2.0 (m/s)

Data #	Vw (m/s)	Tin (C)	Tout (C)	Ts (C)
1	4.46	12.52	13.26	48.43
2	4.46	12.59	13.27	48.49
3	3.92	12.62	13.45	48.42
4	3.92	12.63	13.46	48.40
5	3.37	12.72	13.67	48.40
6	3.37	12.72	13.68	48.45
7	2.55	12.88	14.07	48.34
8	2.55	12.89	14.08	48.30
9	2.00	13.05	14.49	48.28
10	2.00	13.06	14.49	48.33
11	1.51	13.27	15.04	48.41
12	1.51	13.28	15.05	48.42
13	1.18	13.52	15.63	48.43
14	1.18	13.53	15.63	48.42
15	3.09	12.84	13.87	48.39
16	3.09	12.84	13.86	48.37
17	4.46	12.66	13.41	48.35
18	4.46	12.66	13.41	48.30

Tube Number: 44
File Name: S44A124
Pressure Condition: Atmospheric
Steam Velocity: 1.0 (m/s)

Data #	Vw (m/s)	Tin (C)	Tout (C)	Ts (C)
1	4.46	13.70	15.45	99.82
2	4.46	13.70	15.45	99.90
3	3.91	13.76	14.73	99.83
4	3.91	13.75	15.74	99.83
5	3.36	13.81	16.06	99.98
6	3.36	13.80	16.07	99.94
7	2.54	13.93	16.79	99.93
8	2.54	13.93	16.79	99.91
9	2.00	14.07	17.56	100.05
10	2.00	14.06	17.55	99.95
11	1.50	14.25	18.55	99.84
12	1.50	14.25	18.55	99.80
13	1.18	14.45	19.63	99.89
14	1.18	14.46	19.64	99.87
15	3.09	13.74	16.17	99.78
16	3.09	13.72	16.17	99.87
17	4.46	13.55	15.28	99.96
18	4.46	13.53	15.29	99.93

APPENDIX D
UNCERTAINTY ANALYSIS

There is always an uncertainty associated with any measurement which is dependent on the measuring-device accuracy, as well as on the operator's experience. Numerical data collected during this thesis effort were used together with theoretical formulations, so final values of the steam-side heat-transfer coefficient may be distorted due to uncertainty propagation during calculations. In cases where the final results show large uncertainties, it may be unwise to draw any conclusions. Instead, the apparatus and/or the measuring techniques may have to be modified.

Estimates of uncertainties for this investigation were obtained using program "UNA6" which is listed at the end of this appendix, along with selected uncertainty evaluations. This program determines the uncertainties using an equation proposed by Kline and McClintok [32] shown below:

$$W_R = \left[\left(\frac{\partial R}{\partial x_1} W_1 \right)^2 + \left(\frac{\partial R}{\partial x_2} W_2 \right)^2 + \cdots\cdots + \left(\frac{\partial R}{\partial x_n} W_n \right)^2 \right]^{1/2} \qquad (D.1)$$

where

W_R is the uncertainty of the desired dependent variable

x_1, x_2, ..., x_n are the measured (independent) variables

W_1, W_2, ..., W_n are the uncertainties in the measured variables

132

A complete discussion covering the developement of the uncertainty analysis used for this investigation is given by Georgiadis [7].

```
1000! FILE NAME : JMA6
1010! REVISED :   February 28, 1985
1020!
1030  COM /Cc/ C(7)
1040  DIM E(4)
1050  DATA 0.10086091,25727.94369,-767345.8295,78025595.81
1060  DATA -9247486589,6.97688E+11,-2.66192E+13,3.94078E+14
1070  READ C(*)
1080  PRINT USING ":OX.""DATA FOR THE UNCERTAINTY ANALYSIS:"""
1090  PRINT
1100  PRINTER IS 701
1110  BEEP
1120  INPUT "ENTER FILE NAME",Files
1130  PRINT USING "10X.""File Name:                     "".12A":Files
1140  BEEP
1150  INPUT "ENTER DATA SET NUMBER FOR UNCERTAINTY ANALYSIS",Ids
1160  BEEP
1170  INPUT "ENTER PRESSURE CONDITION (0=V,1=A) ",Prc
1171  Prc=Prc+1
1180  ASSIGN @File TO Files
1190  ENTER @File:Ifg,Inn
1191  IF Ifg=0 THEN ENTER @File:Dd
1192  IF Ifg=1 THEN ENTER @File:Dd,Dd,Dd
1200  FOR I=1 TO Ids
1210  ENTER @File:Bvol,Bamp,Vtran,Etp,E(*),Fm,Tci,Tco,Phg,Pwater
1220  NEXT I
1230  Emf=E(0)
1240  IF Prc=1 THEN
1250  BEEP
1260  PRINT USING "10X.""Pressure Condition:           Vacuum (11 kPa)"""
1270  ELSE
1280  PRINT USING "10X.""Pressure Condition.           Atmospheric (101 kPa)"""
1290  END IF
1300  PRINTER IS 1
1310  BEEP
1320  PRINT USING "4X.""Select tube wall type: 0=thick 1=thin"""
1330  INPUT Itt
1340  IF Itt=0 THEN
1350  Do=.01905
1360  Di=.0127
1370  ELSE
1380  Do=.0145
1390  Di=.0135
1400  END IF
1410  PRINTER IS 1
1420  BEEP
1430  PRINT USING "4X.""Select material code:"""
1440  PRINT USING "4X.""0=Cu, 1=SS"""
1450  INPUT Imc
1460  IF Imc=0 THEN
1470  Kc=385
1471  Drc=10
1480  Ci=.071
1490  Ac=0
1500  ELSE
1510  Kc=15
1511  Dkc=1
1520  Ci=.0688
1530  Ac=0
1540  END IF
```

134

```
1550    PRINTER IS 701
1560    Ts=FNTvsv(Emf)
1570    PRINT USING "10X,""Steam Temperature              = "",3D.2D,"" (Deg C)""":
Ts
1580    PRINT USING "10X,""Water Flow Rate (%)            = "",3D.2D":Fm
1590    Dtci=.002
1600    Dtco=.005
1610    BEEP
1620    Demf=1.0E-6
1630    Dts=SQR(((C(1)+2*C(2)*Emf+3*C(3)*Emf^2+4*C(4)*Emf^3)*Demf)^2)
1640    T=(Tci+Tco)/2   ! FILM TEMPERATURE
1650!   UNCERTAINTY IN THE COOLING WATER
1660    Drho=.5 ! ERROR IN WATER DENSITY
1670    Dmf=.008 ! ERROR IN MASS FLOW RATE
1680    Rho=FNRho(T) ! WATER DENSITY
1690    Mf=1.04805E-2+6.80932E-3*Fm   ! MASS FLOW RATE OF COOLING WATER
1700!   CORRECT MF FOR THE TEMPERATURE EFFECT
1710    Mf=Mf*(1.0365-1.96644E-3*Tci+5.252E-5*Tci^2)/.995434
1720    Ai=(PI*Di^2)/4 ! TUBE INSIDE CROSS SECTION AREA
1730    Ddi=.000025
1740    Dai=(PI*Ddi^2)/4 ! ERROR OF INSIDE TUBE CROSS AREA
1750!   COMPUTE THE WATER VELOCITY
1760    Vw=Mf/(Rho*Ai)  ! WATER VELOCITY
1770    PRINT USING "10X,""Water Velocity                = "",2.DD,"" (m/s)""":Vw
1780!   CORRECT OUTLET WATER TEMP. FOR THE MIXING CHAMBER EFFECT
1790    IF Inn=1 OR Inn=5 THEN Tco=Tco-.004*Vw^2
1800    IF Inn=0 THEN Tco=Tco-(-.00108+.001*Vw^2)
1810    T=(Tci+Tco)*.5 ! FILM TEMPERATURE
1820!   COMPUTE THE ERROR IN WATER VELOCITY
1830    Dvw=Vw*SQR((Dmf/Mf)^2+(Drho/Rho)^2+(Dai/Ai)^2)
1840!   UNCERTAINTY IN THE REYNOLDS NUMBER
1850    Mw=FNMu(T) ! WATER VISCOSITY
1860    Dmu=6.E-6 ! ERROR OF WATER VISCOSITY
1870    Re=(Rho*Vw*Di)/Mw
1880    Dre=Re*SQR((Drho/Rho)^2+(Dvw/Vw)^2+(Ddi/Di)^2+(Dmu/Mw)^2)
1890!   UNCERTAINTY IN THE HEAT TRANSFERRED
1900    Cpw=FNCpw(T)
1910    Q=Mf*(Tco-Tci)*Cpw
1920    Dcpw=8
1930    Dq=Q*SQR((Dmf/Mf)^2+((Dtco/(Tco-Tci))^2+((Dtci/(Tco-Tci))^2+(Dcpw/Cpw)^2
)
1940!   UNCERTAINTY IN THE HEAT FLUX
1950    Dl=.0005 ! ERROR IN TUBE LENGHT
1960    Ddo=.000025
1970    L=.13335 ! CONDENSING TUBE LENGTH
1980    Qp=Q/(PI*Do*L) ! HEAT FLUX
1990    PRINT USING "10X,""Heat Flux                     = "",Z.3DE,"" (W/m^2)""":
Qp
2000    Dqp=(Qp/PI)*SQR((Dq/Q)^2+(Ddo/Do)^2+(Dl/L)^2)
2010    Lmtd=(Tco-Tci)/LOG((Ts-Tci)/(Ts-Tco))
2020    Uo=Qp/Lmtd ! OVERALL HEAT TRANSFER COEF.
2030    A1=Dts*(Tci-Tco)/((Ts-Tci)*(Ts-Tco)*LOG((Ts-Tci)/(Ts-Tco)))
2040    A2=Dtci/((Ts-Tci)*LOG((Ts-Tci)/(Ts-Tco)))
2050    A3=Dtco/((Ts-Tco)*LOG((Ts-Tci)/(Ts-Tco)))
2060    Dlmtd=Lmtd*SQR(A1^2+A2^2+A3^2)
2070    Duo=Uo*SQR((Dqp/Qp)^2+(Dlmtd/Lmtd)^2)
2080    M=Mw
2090    T1=(T+273.15)/273.15
2100    Kw=FNKw(T1)
2110    Ac=0.   ! INTERSCEPT FROM SIEDER PROGRAM
```

```
2120  L1=.060325 ! LENGTH OF UNFINNED LEFT PART OF TUBE
2130  L2=.034925 ! LENGTH OF UNFINNED RIGHT PART OF TUBE
2140  D1=.01905
2150  D2=.015875
2160  Pr=Cpw*Mw/Kw
2170  Muw=FNMuw(T)
2180! UNCERTAINTY OF INSIDE HEAT-TRANSFER COEFF.
2190  Cf=1.
2200  Hi=(Kw/D1)*(Ci*Re^.8*Pr^.333*Ci=Ac)
2210  Dti=Q/(PI*D1*(L+L1*Fe1+L2*Fe2)*Hi)
2220  Cfc=(Muw/FNMuw(T+Dti))^.14
2230  IF ABS((Cfc-Cf)/Cfc)>.01 THEN
2240  Cf=(Cf+Cfc)*.5
2250  GOTO 2200
2260  END IF
2270  P1=PI*(D1+D1)
2280  B1=(D1-D1)*PI*(D1+D1)*.5
2290  M1=(H1*P1/(Kc*B1))^.5
2300  P2=PI*(D1+D2)
2310  B2=(D2-D1)*PI*(D1+D2)*.5
2320  M2=(H1*P2/(Kc*B2))^.5
2330  Fe1=FNTanh(M1*L1)/(M1*L1)
2340  Fe2=FNTanh(M2*L2)/(M2*L2)
2350  Dtc=Q/(PI*D1*(L+L1*Fe1+L2*Fe2)*Hi)
2360  IF ABS((Dtc-Dti)/Dtc)>.01 THEN 2200
2370  Dkw=.0010 ! ERROR IN WATER THERMAL CONDUCTIVITY
2380  Dci=.0005 ! ERROR IN SIEDER-TATE COEFFICIENT
2390  Dpr=.05 ! ERROR IN PRANDTL NUMBER
2400  Dci=8.E-5
2410  A4=.14*Dcf/Cf
2420  Dhi=Hi*SQR((Dkw/Kw)^2+(Ddi/D1)^2+(.8*Dre/Re)^2+(.333*Dpr/Pr)^2+(Dci/Ci)^2+
A4)
2430! UNCERTAINTY OF OUTSIDE HEAT-TRANSFER COEFF.
2440  Rw=Do*LOG(Do/D1)/(2*Kc) ! WALL RESISTANCE
2450  Ho=1/((1/Uo)-(Do*L/(D1*(L+L1*Fe1+L2*Fe2)*Hi))-Rw)
2460  Drw=Rw*SQR((Ddo/Do)^2+(Dkc/Kc)^2+(Ddo/(Do*LOG(Do/D1)))^2+(Ddi/(D1*LOG(Do/D
1)))^2)
2470  A5=1/Uo-Rw-(Do/(D1*H1))
2480  A6=Duo/(Uo^2*A5)
2490  A7=Drw/A5
2500  A8=((Do/(D1*H1))*(Dhi/H1))/A5
2510  PRINT
2520  Dho=Ho*SQR(A6^2+A7^2+A8^2)
2530! CALCULATE THE % UNCERTAINTY IN Ho
2540  Prho=Dho*100/Ho
2550! CALCULATE THE % UNCERTAINTY IN REYNOLDS NUMBER
2560  Prre=Dre*100/Re
2570! CALCULATE THE % UNCERTAINTY IN MASS FLOW RATE
2580  Prmf=Dmf*100/Mf
2590! CALCULATE THE % UNCERTAINTY IN HEAT TRANSFER
2600  Prqp=Dqp*100/Qp
2610! CALCULATE THE % UNCERTAINTY IN LMTD
2620  Prlmtd=Dlmtd*100/Lmtd
2630! CALCULATE THE % UNCERTAINTY IN Rw
2640  Prrw=Drw*100/Rw
2650! CALCULATE THE % UNCERTAINTY IN OVERALL HEAT TRANSFER COEF.
2660  Pruc=Duo*100/Uo
2670! CALCULATE THE % UNCERTAINTY IN INSIDE HEAT TRANSFER COEFF.
2680  Prhi=Dhi*100/Hi
2690  PRINT
2700  PRINT USING "10X,""UNCERTAINTY ANALYSIS:"""
```

136

```
2710  PRINT
2711  PRINT USING "10X,""    VARIABLE                    PERCENT UNCERTAINTY"""
2712  PRINT
2720  PRINT USING "10X,""Mass Flow Rate, Md              "".2D.2D.":Prmf
2730  PRINT USING "10X,""Reynoids Number, Re             "".3D.2D.":Prre
2740  PRINT USING "10X,""Heat Flux, q                    "".Z.2D.":Prqp
2750  PRINT USING "10X,""Log-Mean-Tem Diff, LMTD         "".Z.2D.":Prlmtd
2760  PRINT USING "10X,""Wall Resistance, Rw             "".DD.2D.":Prru
2770  PRINT USING "10X,""Overall H.T.C., Uo              "".DD.2D.":Pruo
2780  PRINT USING "10X,""Water-Side H.T.C., Hi           "".3D.2D.":Prhi
2790  PRINT USING "10X,""Steam-Side H.T.C., Ho           "".3D.2D.":Prno
2800  END
2810  DEF FNMuw(T)
2820  A=247.8/(T+133.15)
2830  Muw=2.4E-5*10^A
2840  RETURN Muw
2850  FNEND
2860  DEF FNTann(X)
2870  P=EXP(X)
2880  Q=EXP(-X)
2890  Tann=(P-Q)/(P+Q)
2900  RETURN Tann
2910  FNEND
2920  DEF FNKw(T1)
2930  Kw=-.92247+T1*(2.8395-T1*(1.8007-T1*(.52577-.07344*T1)))
2940  RETURN kw
2950  FNEND
2960  DEF FNMw(T)
2970  A=247.3/(T+133.15)
2980  Mw=2.4E-5*10^A
2990  RETURN Mw
3000  FNEND
3010  DEF FNRho(T)
3020  Rho=999.52946+T*(.01269-T*(5.482513E-3-T*1.234147E-5))
3030  RETURN Rho
3040  FNEND
3050  DEF FNCpw(T)
3060  Cpw=(4.21120858-T*(2.26326E-3-T*(4.42361E-5+2.71428E-7*T)))*1000
3070  RETURN Cpw
3080  FNEND
3090  DEF FNTvsv(Emf)
3100  COM /Cc/ C(7)
3110  T=C(0)
3120  FOR I=1 TO 7
3130  T=T+C(I)*Emf^I
3140  NEXT I
3150  RETURN T
3160  FNEND
```

137

DATA FOR THE UNCERTAINTY ANALYSIS:

File Name: F32V26
Pressure Condition: Vacuum (11 kPa)
Steam Temperature   =   48.47 (Deg C)
Water Flow Rate (%)   =   20.00
Water Velocity   =   1.16 (m/s)
Heat Flux   =   2.111E+05 (W/m 2)

UNCERTAINTY ANALYSIS:

    VARIABLE   PERCENT UNCERTAINTY

Mass Flow Rate, Md   5.44
Reynolds Number, Re   5.48
Heat Flux, q   1.74
Log-Mean-Tem Diff, LMTD   0.22
Wall Resistance, Rw   2.67
Overall H.T.C., Uo   1.75
Water-Side H.T.C., Hi   4.46
Steam-Side H.T.C., Ho   22.58

DATA FOR THE UNCERTAINTY ANALYSIS:

File Name: F32V26
Pressure Condition: Vacuum (11 kPa)
Steam Temperature   =   48.38 (Deg C)
Water Flow Rate (%)   =   80.00
Water Velocity   =   4.31 (m/s)
Heat Flux   =   3.808E+05 (W/m 2)

UNCERTAINTY ANALYSIS:

    VARIABLE   PERCENT UNCERTAINTY

Mass Flow Rate, Md   1.44
Reynolds Number, Re   1.57
Heat Flux, q   0.50
Log-Mean-Tem Diff, LMTD   0.43
Wall Resistance, Rw   2.67
Overall H.T.C., Uo   .66
Water-Side H.T.C., Hi   1.49
Steam-Side H.T.C., Ho   2.81

138

DATA FOR THE UNCERTAINTY ANALYSIS:

File Name: F32A68
Pressure Condition: Atmospheric (101 kPa)
Steam Temperature   =   39.93 (Deg C)
Water Flow Rate (%)   =   20.00
Water Velocity   =   1.16 (m/s)
Heat Flux   =   6.502E+05 (W/m^2)

UNCERTAINTY ANALYSIS:

        VARIABLE   PERCENT UNCERTAINTY

Mass Flow Rate, Md   5.45
Reynolds Number, Re   5.50
Heat Flux, q   1.74
Log-Mean-Tem Diff, LMTD   0.07
Wall Resistance, Rw   2.67
Overall H.T.C., Uo   1.74
Water-Side H.T.C., Hi   4.47
Steam-Side H.T.C., Ho   29.72

DATA FOR THE UNCERTAINTY ANALYSIS:

File Name: F32A68
Pressure Condition: Atmospheric (101 kPa)
Steam Temperature   =   39.93 (Deg C)
Water Flow Rate (%)   =   50.00
Water Velocity   =   4.40 (m/s)
Heat Flux   =   1.164E+06 (W/m^2)

UNCERTAINTY ANALYSIS:

        VARIABLE   PERCENT UNCERTAINTY

Mass Flow Rate, Md   1.44
Reynolds Number, Re   1.59
Heat Flux, q   0.48
Log-Mean-Tem Diff, LMTD   0.14
Wall Resistance, Rw   2.67
Overall H.T.C., Uo   5.0
Water-Side H.T.C., Hi   1.50
Steam-Side H.T.C., Ho   2.80

DATA FOR THE UNCERTAINTY ANALYSIS:

File Name: F39V83
Pressure Condition: Vacuum (11 kPa)
Steam Temperature   =   48.50 (Deg C)
Water Flow Rate (%)   =   20.00
Water Velocity   =   1.03 (m/s)
Heat Flux   =   2.579E+05 (W/m^2)

UNCERTAINTY ANALYSIS:

        VARIABLE   PERCENT UNCERTAINTY

Mass Flow Rate, Md   5.42
Reynolds Number, Re   5.45
Heat Flux, q   1.73
Log-Mean-Tem Diff, LMTD   0.23
Wall Resistance, Rw   4.39
Overall H.T.C., Uo   1.75
Water-Side H.T.C., Hi   4.43
Steam-Side H.T.C., Ho   13.05

DATA FOR THE UNCERTAINTY ANALYSIS:

File Name: F39V83
Pressure Condition: Vacuum (11 kPa)
Steam Temperature   =   48.41 (Deg C)
Water Flow Rate (%)   =   80.00
Water Velocity   =   3.92 (m/s)
Heat Flux   =   4.440E+05 (W/m^2)

UNCERTAINTY ANALYSIS:

        VARIABLE   PERCENT UNCERTAINTY

Mass Flow Rate, Md   1.43
Reynolds Number, Re   1.55
Heat Flux, q   0.50
Log-Mean-Tem Diff, LMTD   0.48
Wall Resistance, Rw   4.39
Overall H.T.C., Uo   .69
Water-Side H.T.C., Hi   1.47
Steam-Side H.T.C., Ho   1.69

140

DATA FOR THE UNCERTAINTY ANALYSIS:

File Name: F39A98
Pressure Condition: Atmospheric (101 kPa)
Steam Temperature   =   99.91 (Deg C)
Water Flow Rate (%)   =   20.00
Water Velocity   =   1.04 (m/s)
Heat Flux   = 8.181E+05 (W/m^2)

UNCERTAINTY ANALYSIS:

        VARIABLE   PERCENT UNCERTAINTY

Mass Flow Rate, Md   5.39
Reynolds Number, Re   5.43
Heat Flux, q   1.72
Log-Mean-Tem Diff, LMTD   0.07
Wall Resistance, Rw   4.39
Overall H.T.C., Uo   1.72
Water-Side H.T.C., Hi   4.42
Steam-Side H.T.C., Ho   16.67

DATA FOR THE UNCERTAINTY ANALYSIS:

File Name: F39A98
Pressure Condition: Atmospheric (101 kPa)
Steam Temperature   =   99.78 (Deg C)
Water Flow Rate (%)   =   80.00
Water Velocity   =   3.94 (m/s)
Heat Flux   = 1.409E+06 (W/m^2)

UNCERTAINTY ANALYSIS:

        VARIABLE   PERCENT UNCERTAINTY

Mass Flow Rate, Md   1.42
Reynolds Number, Re   1.54
Heat Flux, q   0.48
Log-Mean-Tem Diff, LMTD   0.15
Wall Resistance, Rw   4.39
Overall H.T.C., Uo   .50
Water-Side H.T.C., Hi   1.46
Steam-Side H.T.C., Ho   1.69

141

LIST OF REFERENCES

1. Yau., K. K., Cooper, J. R., and Rose, J. W., "Effects of Fin Spacing and Drainage Strips on the Condensation Heat-Transfer Performance of Horizontal Low Integral-Fin Tubes", _Fundamentals of Phase Change: Boiling and Condensation_, HTD-Vol 38, C. T. Avedisian and T. M. Rudy (Eds.) ASME, 1984.

2. Wanniarachchi, A. S., Marto, P. J., and Rose, J. W., "Filmwise Condensation of Steam on Externally-Finned Horizontal Tubes", _Fundamentals of Phase Change: Boiling and Condensation_, HTD-Vol. 38, C. T. Avedisian and T. M. Rudy (Eds.) ASME, 1984.

3. Honda, H., Nozu, S., Mitsumori, K., "Augmentation of Condensation on Horizontal Finned Tubes By Attaching Porous Drainage Plates", _Proc. ASME-JSME Thermal Engineering Conference_, Hawaii, 1983.

4. Krohn, R. L., _An Experimental Apparatus to Study Enhanced Condensation Heat-Transfer of Steam on Horizontal Tubes_, M. S. Thesis, Naval Postgraduate School, Monterey, California, June, 1982.

5. Graber, K. A., _Condensation Heat Transfer of Steam on a Single Horizontal Tube_, M. S. Thesis, Naval Postgraduate School, Monterey, California, June, 1983.

6. Poole, W. M., _Filmwise Condensation of Steam on Externally-Finned Horizontal Tubes_, M.S. Thesis, Naval Postgraduate School, Monterey, California, December, 1983.

7. Georgiadis, I. V., _Filmwise Condensation of Steam on Low Integral-finned Tubes_, M.S. Thesis, Naval Postgraduate School, Monterey, California, September, 1984.

8. Katz, D. L., Hope, R. E., and Dasko, S. C., _Liquid Retention on Finned Tubes_, Dept. of Eng. Research, University of Michigan, Ann Arbor, Michigan, Project M 592, 1946.

9. Gregorig, R., "Hautkondensation an Feingewellten Oberflachen bei Berucksichtigung der Oberfachenspannungen", _Zeitschrift für Angewantde Mathematik und Physic_, Vol. V, 1954, pp. 36-49. Translation by D. K. Edwards.

10. Rudy, T. M., and Webb, R. L., "Condensate Retention of Horizontal Integral-Fin Tubes, Advances in Enhanced Heat-Transfer", 1981, HTD-Vol. 18, Presented at 20th 20th National Heat-Transfer Conference, Milwaukee, Wisconsin, August, 1981.

11. Rudy, T. M., and Webb, R. L., "An Analytical Model to Predict Condensate Retention on Horizontal, Integral-Fin Tubes", ASME/JSME Thermal Engng. Joint Conf., Vol. 1, March 20-24, 1983.

12. Rifert, V. G., "Steam Condensation on Profiled Surfaces", Heat and Mass-Transfer Processes in Porous Media With Phase Transformation, Academy of Science, BSSR, A. B. Lykov (Ed), Minsk, 1982, pp. 149-170.

13. Owen, R. G., Sardesai, R. G., Smith, R. A., and Lee W. C., Gravity Controlled Condensation on a Low-Fin Tube, I.Chem.E. Symposium Series No. 75.

14. Rudy, T. M., and Webb, R. L., "Condensate Retention on Horizontal Integral-Fin Tubes", ASME Journal of Heat Transfer, Vol. 107, 1985.

15. Beatty, B. O., and Katz, D. L., "Condensation of Vapors on Outside of Finned Tubes", Chemical Engineering Progress, Vol. 44, No. 1, January, 1948.

16. Karkhu, V. A., and Borovkov, V. P., "Film Condensation of Vapor at Finely-Finned Horizontal Tubes", Heat Transfer-Soviet Research, Vol. 3, No. 2, March-April 1971.

17. Zozulya, N. V., Karkhu, V. A., and Borovkov, V. P., "An Analytic and Experimental Study of Heat Transfer in Condensation of Vapor on Finned Surfaces", Heat Transfer-Soviet Research, Vol. 9, No. 2, March-April 1977.

18. Nader, W. K., "Extended Surface Heat Transfer With Condensation", Heat Transfer 1978, Vol. 2, August, 1978.

19. Patankar, S. V., and Sparrow, E. M., "Condensation on an Extended Surface", Transactions of the ASME, Vol. 101, August, 1979.

20. Rifert, V. G., "A New Method for Calculating Rates of Condensation on Finned Tubes", Heat Transfer-Soviet Research, Vol. 12, No. 3, May-June, 1980.

21. Rudy, T. M., and Webb, R. L., "Theoretical Model for Condensation on Horizontal, Integral-Fin Tubes", Heat Transfer, Seattle, AIChE Symp. Ser., Vol. 79, No. 225, 1983.

22. Webb, R. L., Keswani, S. T., Rudy, T. M., "Investigation of Surface-Tension and Gravity Effects in Film Condensation", Proceedings of 7th International Heat-Transfer Conference, Munich, Fed. Rep. of Germany, Sept. 6-10, 1982, Hemisphere Publishing Co., Washington D.C., Vol 5, pp. 175-180.

23. Rudy, T. M., A Theoretical and Experimental Study of Condensation on Single, Integral-Fin Tubes, Ph.D. Thesis, Department of Mechanical Engineering, The Pennsylvania State University, UNiversity Park, Pa., May, 1982.

24. Honda, H., and Nozu, S., A Prediction Method for Heat-Transfer Durring Film Condensation in Horizontal Low Integral-Fin Tubes, Submitted for presentation at the ASME Winter Annual Meeting, New Orleans, December, 1984.

25. Webb, R. L., Rudy, T. M., and Kedzierski, M. A., "Prediction of the Condensation Coefficient on Horizontal Integral-Fin Tubes", Journal of Heat Transfer, Vol. 105, 1985.

26. Rudy, T. M., Kedzierski, M. A., and Webb, R. L., "Investigation of Integral-fin-Type Condenser Tubes for Process Industry Applications", First U. K. National Conference on Heat Transfer, The Institution of Chemical Engineers Symposium Series No. 86, 1984.

27. Adamek, T., "Bestimmung der Kondensationgrossen auf feingewellten Oberflachen zur Auslegung aptimaler Wandprofile", Warme-und-Stoffuhertragung, Vol. 15, pp 255-270, 1981.

28. Incorpera, F. P., and DeWitt, D. P., Fundamentals of Heat Transfer, Wiley, pp 406-407, 1981.

29. Fujii, T., Honda, H., "Condensation of Steam on a Horizontal Tube", Condensation Heat Transfer, ASME, New York, 1979.

30. Webb, R. L., Haman, L. L., and Hui, T. S., "Enhanced Tubes in Electric Utility Steam Condensers", Heat Transfer in Heat Rejection Systems, HTD-Vol. 37, S. Sengupta and Y. Mussalli (Eds.), ASME, 1984, pp. 17-25.

31. Fujii, T., Wang, W., Koyama, S., and Shimizu, Y., Heat-Transfer Enhancement for Gravity Contralled Condensation on a Horizontal Tube by Coiled Wires, Beijing Conference, 1985.

32. Kline, S. J., and McClintock, F. A., "Describing Uncertainties in Single-Sample Experiments", Mech. Eng., Vol. 74, pp 3-8, January 1953.

BIBLIOGRAPHY

Katz, D. L., and Geist, J. M., "Condensation on Six Finned Tubes in a Vertical Row", _Transactions of the ASME_, November, 1948.

Mori, Y., Higikata, K., Hirasawa, S., and Nakayama, W., "Optimized Performance of Condensers With Outside Condensing Surfaces", _Transactions of the ASME_, Vol. 103, February, 1981.

Pearson, J. F., and Withers, J. G., "New Finned Tube Configuration Improves Refrigerant Condensing", _ASHRAE Journal_, June, 1969.

Shklover, G. G., Mil'Man, O. O., Baskov, V. S., Ankudinov, G. A., "Heat Transfer in Condensation of Steam on Finely-Finned Horizontal Tubes", _Heat Transfer-Soviet Research_, Vol. 13, No. 2, March-April 1981.

INITIAL DISTRIBUTION LIST

		No. Copies
1.	Defense Technical Information Center Cameron Station Alexandria, Virginia 22314	2
2.	Library, Code 0142 Naval Postgraduate School Monterey, California 93943	2
3.	Department Chairman, Code 69 Department of Mechanical Engineering Naval Postgraduate School Monterey, California 93943	1
4.	Professor P. J. Marto, Code 69Mx Department of Mechanical Engineering Naval Postgraduate School Monterey, California 93943	5
5.	Dr. John W. Rose Department of Mechanical Engineering Queen Mary College University of London London E1 4NS England	1
6.	Dr. A. S. Wanniarachchi, Code 69Wa Department of Mechanical Engineering Naval Postgraduate School Monterey, California 93943	1
7.	Dr. Win Aung Program Director for Heat Transfer Division of Engineering National Science Foundation Washington, D.C. 20008	2
8.	Lt. Frederick A. Flook, USN Long Beach Naval Shipyard Long Beach, California 90822	2
9.	Lt. Ioannis Georgiadis, H. N. 67, Peloponisou St, Agia Paraskevi Attiki, Athens Greece	1
10.	Lt. Evangelos Mitrou, H. N. SMC #2777 Naval Postgraduate School Monterey, California 93943	1
11.	Mr. Krohn, R. Supervisor of Configuration Management Clinton Power Station Decatur, Illinois 62526	1

146

END

FILMED

8-85

DTIC